Fibroblasts Promote Resistance to BRAF inhibition; The Role of Molecular, Signaling and Metabolic Changes in Melanoma

Anna Barkovskaya

Master's Thesis at the Department of Molecular Biosciences
Faculty of Mathematics and Natural Sciences

UNIVERSITETET I OSLO
May 2015

Fibroblasts Promote Resistance to BRAF inhibition;

The Role of Molecular, Signaling and Metabolic Changes in Melanoma

Anna Barkovskaya

Department of Biosciences

University of Oslo

May 2015

May 2015

Fibroblasts Promote Resistance to BRAF inhibition; The Role of Molecular, Signaling and Metabolic Changes in Melanoma

Anna Barkovskaya

http://www.duo.uio.no/

Trykk: Reprosentralen, Universitetet i Oslo

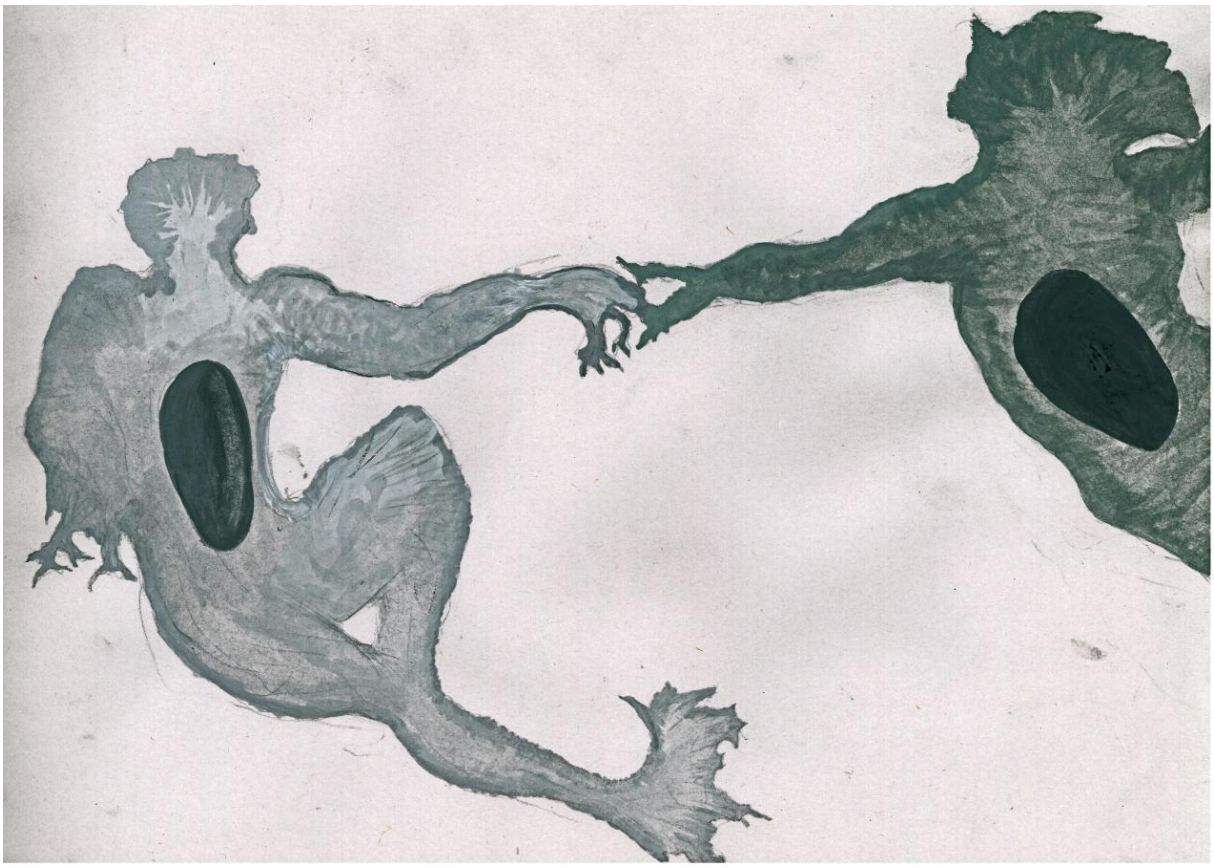

Abstract

Malignant melanoma is an aggressive type of skin cancer which urgently requires new and efficient treatment strategies. A novel targeted agent for advanced melanoma, vemurafenib, has shown high response rates among patients with BRAF mutation. However, relapses occur in almost all cases after a short period of progression-free survival. This project focused on the nature of vemurafenib resistance, specifically the role of the interaction between the cancer and the stromal cells. Here we used an extended melanoma cell panel to show that the stromal fibroblasts elicit strong protection of the melanoma cells against vemurafenib and do so via activation of mTORC1. We demonstrate that the fibroblast-mediated protection relies on direct cell-cell proximity and/or contacts. However, we could not find evidence of gap-junction involvement. We found that fibroblasts alter gene expression in the melanoma cells, inducing an invasive dedifferentiated molecular phenotype associated with resistance to vemurafenib. Melanoma cells which have been in contact with the fibroblasts also had altered expression of the energy metabolism regulators which suggested a decrease in the mitochondrial function. We further show that the altered cancer metabolism can serve as a target for therapeutic intervention since the melanoma cells in co-cultures were more vulnerable to the treatment with the mitochondrial stimulant, dicholoacetate, than in mono-cultures. Finally, we explored the changes in the energy metabolism of the melanoma cells induced by vemurafenib and the mTORC1 inhibitor, everolimus. We found a decrease in the mitochondrial activity triggered by both agents and a reduction of lactate production after the treatment with vemurafenib.

Our findings suggest lung fibroblasts as important regulators of melanoma response to vemurafenib. The results provide hints about potential targets for therapeutic intervention in order to overcome stroma-mediated protection.

Acknowledgements

This work was performed in the period from January 2014 to May 2015 at the Cancer Research Institute of the Oslo University Hospital Radium Hospital, department of Tumor biology, in the group led by prof. Gunhild M. Mælandsmo, PhD.

First of all, I would like to thank my main supervisor, Lina Prasmickaite. Your active participation in every aspect of this project, the scientific and methodological discussions, your help and support during the writing process were immensely important to me. The great experience that I enjoyed as a master student under your guidance has set a sky-high benchmark for anyone whom I may work with in the future.

Secondly, I am hugely grateful to Kotryna Vasiliauskaite - the PhD student whom I was lucky to work with and hope to continue working with further. I have met very few people with equally high standards of work ethics and diligence. You have been an inspiration to me throughout my whole master's.

I would also like to thank prof. Gunhild M. Mælandsmo and the entire department of tumor biology for introducing me to cancer research. I am also grateful to Edward Leithe for sharing his expertise concerning the gap-junctions.

One of the best parts of working on my master's project was having discussions, scientific or not, so I would like to thank my fellow master students - Marie, Karine and Galina as well as people from the department of molecular cell biology (former biochemistry) for listening to my presentation practices and making life a lot more fun. Special thanks to Kay Schink for taking time to go through the results of this study and provide useful comments.

Finally, I would like to thank the members of my family who have supported me the entire time from far away and made my education in Oslo possible.

Anna Barkovskaya

May 2015

List of Abbreviations

293HEK – 293 human embryonic kidney cells
Ab(s) – antibody (ies)
Acetyl-CoA – acetyl coenzyme A
ADP – adenosine-di-phosphate
AKT – protein kinase B
ARAF – rapidly accelerated fibrosarcoma protein kinase A
ATP – adenosine-tri-phosphate
AXL – tyrosine-protein kinase receptor UFO
BRAF – rapidly accelerated fibrosarcoma protein kinase B
BSA – bovina serum albumin
CAFs – cancer associated fibroblasts
CBX – carbenoxolone
cDNA – coding deoxyribonucleic acid
CM – conditioned medium
c-MET – hepatocyte growth factor receptor
COT – serine⁄threonine kinase MAP3K8
CRAF – rapidly accelerated fibrosarcoma protein kinase C
Ct value – cycle threshold number
CXCL12 – stromal cell-derived factor 1
DCA – dicholoacetate
DKK3 – dickkopf-related protein 3
DMSO – dimethyl sulfoxide
ECAR – extracellular acidification rate
EDTA – ethylenediaminetetraacetic acid
EGF – epidermal growth factor
EMEM – eagle's minimal essential medium
ERK – extracellular-signal-regulated kinase
FACS – fluorescence activated cell sorting
FAD – flavin adenine dinucleotide
FBS – fetal bovine serum
FCCP – carbonyl cyanide-*4*-(trifluoromethoxy)phenylhydrazone
FGF – fibroblast growth factor
GFP-luc – green fluorescent protein-luciferase
GTP-ase – guanosine triphosphate hydrolaze
HGF – hepatocyte growth factor
HRAS – transforming protein p21
IGF – Insulin-like growth factor
IMC – immature myeloid cell
KRAS – kirsten rat sarcoma viral oncogene homolog
LDH(A) – lactate dehydrogenase (A)
MLANA – Protein melan-A

MAPK – mitogen-activated protein kinases
MCT1 and MCT4 – monocarboxylate transporter 1 and 4
MEK – mitogen-activated protein kinase kinase
MES buffer – 2-(*N*-morpholino)ethanesulfonic acid buffer
MITF-M – microphthalmia-associated transcription factor isoform M
mRNA – messenger ribonucleic acid
mTORC1 – mammalian (mechanistic) target of rapamycin complex 1
MTS – tetrazolium dye
NAD – nicotinamide adenine dinucleotide
NRAS – neuroblastoma ras viral oncogene homolog
OCR – oxygen consumption rate
OxPhos – oxidative phosphorylation
PARP-1 – poly [ADP-ribose] polymerase 1
PBS – phosphate-buffered saline
PCR – polymerase chain reaction
PDH – pyruvate dehydrogenase
PDK – pyruvate dehydrogenase kinase
PFA – paraformaldehyde
PGC1-α – peroxisome proliferator-activated receptor gamma coactivator 1-alpha
PI3K – phosphoinositide3-kinase
PS6 – phospho S6
PVDF – polyvinylidene fluoride
ROS – reactive oxygen species
RPMI – Roswell Park Memorial Institute medium
RT – room temperature
RTK – receptor typosine kinase
S6K – S6 kinase
SEM – standard error of the mean
SMDR – stroma-mediated drug resistance
TBS1 – thrombosponsin 1
TBST – tris-Buffered Saline and Tween 20
TCA cycle – tricarboxylic acid cycle
TE buffer – Tris-EDTA buffer
TF – transcription factor
TGF-β – transforming growth factor beta
TYR - tyrosinase
Wnt – wingless-related integration site

Table of Contents

Introduction

Cancer and metastasis

Cancers are a group of diseases characterized by abnormal cell proliferation, multiple genetic and genomic alterations and tumor formation. Cancers are distinct from benign tumors in their ability to metastasize – migrate to and invade distant tissues and organs. Metastatic disease poses the biggest threat to a patient often resisting available therapies and spreading to the locations where it cannot be treated surgically, and may eventually lead to death. The biology of metastasis, therefore, is one of the most important as well as the most clinically significant areas of cancer biomedicine.

Metastasis during the late stages of cancer development occurs when a malignant cell leaves the primary tumor via blood or lymphatic vessels, travels to the other location in the body, docks to and establishes connections with the local microenvironment and begins to proliferate. The sheer complexity of this process means it has a very low success rate with only a few cancer cells being able to produce metastases. It is still debated whether this ability can be attributed to particular cells with certain characteristics or if it is an inherent property of all cancer cells, some of which encounter permissive conditions by chance [1]. It is clear, however, that the local non-malignant cells contribute greatly to metastasis development.

Metastatic niche

As the cancer progresses and spreads, it develops into a complicated structure where stromal cells are intertwined with the tumor, and, although not malignant themselves, engage in a complex molecular exchange with the cancer. The importance of stroma in cancer development and progression is difficult to overestimate with some studies suggesting that low cancer to stroma ratio in a tumor strongly correlates with the poor prognosis [2]. The composition of the tumor stroma depends on the anatomic location, but typically includes the extracellular matrix, fibroblasts, endothelial cells, cells of immune system and other locally present cells such as astrocytes in the brain (figure 1.1). Stromal

cells and the extracellular matrix at these sites respond to the presence of the cancer cells and create what is often referred to as the *metastatic niche*.

Numerous mechanisms involved in the metastatic niche formation have been described (reviewed in [3]). It may come as no surprise that many types of cancer favour metastatic locations resembling stem cell niches, such as the bone marrow, and/or settle near the blood capillaries which supply the growing tumor with nutrients and oxygen. A metastatic niche would support the state of cellular dedifferentiation and provide soluble chemical signals, stimulating proliferation and survival of the cancer cells [4-6]. In addition, cell-cell contacts and adhesion have been shown to play an important role [7].

There are also reports suggesting that formation of the pre-metastatic niche is initiated before the cancer cells even arrive to the location. The *pre*-metastatic niche is "primed" by secreted factors and vesicles produced by the primary tumor, which leads to recruitment of stromal cells [8]. Together they create a permissive environment able to receive the metastatic cells and allow them to survive and proliferate.

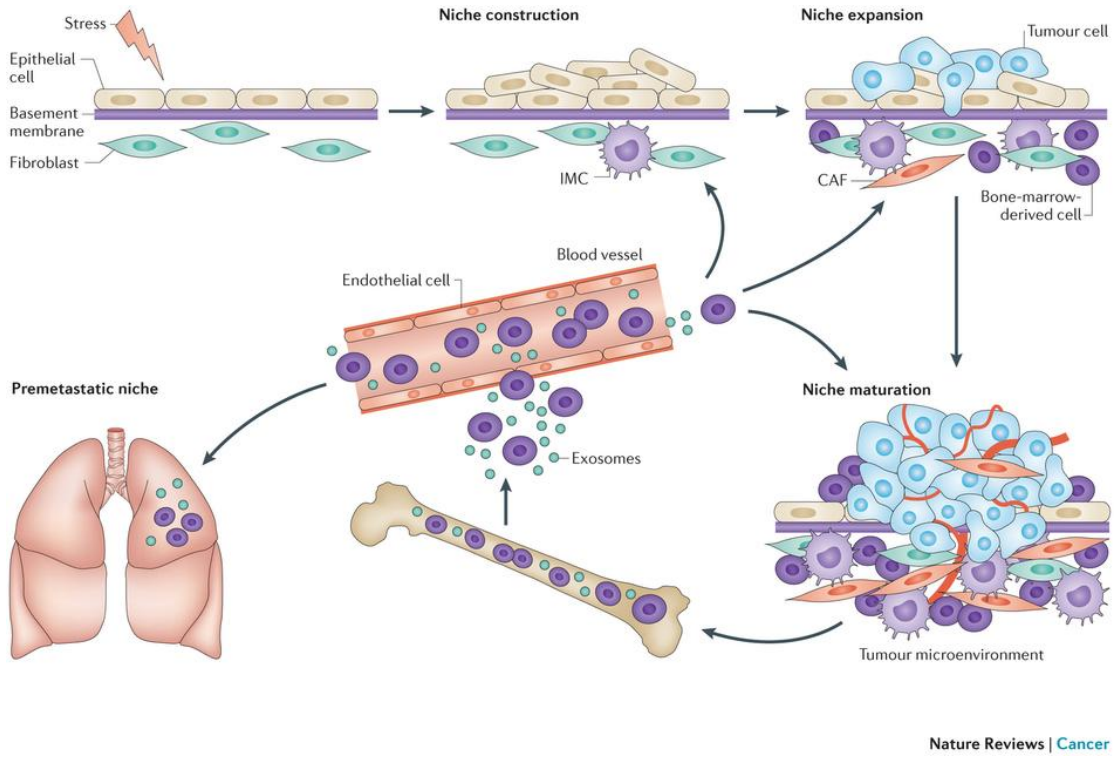

Figure 1.1 Formation of the metastatic niche in cancer. A niche is formed by the cells and the extracellular matrix of the local microenvironment. Tumor microenvironment stimulates cancer cell proliferation and evolves itself, leading to formation of reactive stroma, including cancer-associated fibroblasts (CAFs), which

promote conditions favouring malignancy and mutagenesis. Exosomes and bone-marrow derived cells released by a growing tumor initiate pre-metastatic niche formation at other secondary locations and prepare them to harbor circulating metastatic cancer cells. IMC - immature myeloid cells. Figure from Barcellos-Hoff MH. et.al [9].

Drug resistance in cancer and the role of stroma

In oncology, surgical intervention has the strongest potential for complete cure. Other treatments like chemotherapy, immuno-therapy and targeted therapy alone or in combination often shrink the tumors and prolong survival, but are mostly unable to fully eradicate cancer. This is often due to drug resistance which develops in the tumors or circulating cancer cells that have not been removed.

Drug resistance may be explained by a variety of mechanisms. These include existence of slowly dividing cancer cells (sometimes defined as cancer stem cells), which are not sensitive to anti-proliferation drugs (chemotherapy), increased drug metabolism and efflux, additional mutations and amplification of the mutated proteins, activation of the signaling pathways, which stimulate cell growth and survival, and other (reviewed in [10]).

Latest findings have implicated stroma in the drug resistance, showing that it helps create conditions, not only favourable of metastasis development, but also enabling cancer cells to avoid therapy. The mechanism of the stroma-mediated drug resistance (SMDR) is dual as it relies on both secretion of multiple soluble factors [11, 12] and direct intercellular connections [13, 14].

Soluble factors produced by the stroma cells include fibroblast-, hepatocyte-, insulin-like- and epidermal growth factors (FGF, HGF, IGF and EGF respecitvely), cytokines, transforming growth factor beta (TGF-β), stromal cell-derived factor 1α (CXCL12) and several others [15]. On the other side of the scale is SMDR mediated by intercellular adhesions, likely acting in concert with the soluble factor exchange.

Contact-dependent SMDR: gap junctions

In normal tissues, adhesion is crucial for cell survival as disruption of attachment to other cells and the extracellular matrix will lead to cell death by anoikis [16]. In cancer, docking to the local tissues enables metastasis and allows exchange of molecules and stimulation of

signaling in both the cancer cells and the stromal cells. There are several types of intercellular connections; however, in this project we focused our attention on the gap-junctions.

Gap junctions are composed of 6 connexin molecules arranged in a trasmembrane pore complex – connexon. Two connexons on the membranes of the two opposing cells bind to form a junction which allows transport of small molecules including ions, nucleic and amino acids and other, through a pore ranging from 11Å to 24Å in diameter (figure 1.2).

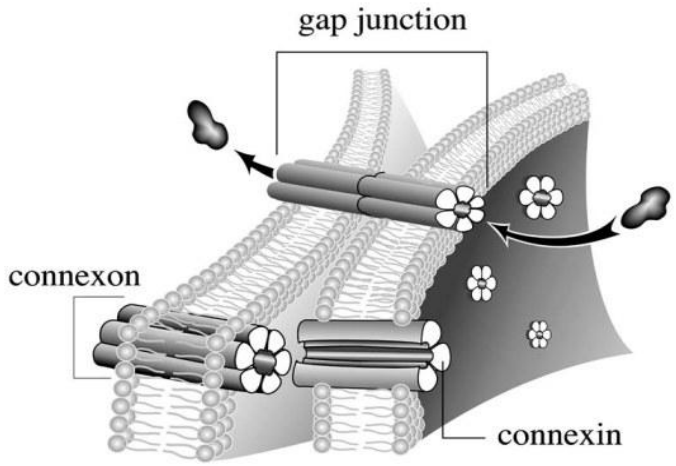

Figure 1.2 Gap junctions scheme. Picture from https://thesalience.wordpress.com/neuroscience/the-chemical-synapse/electrical-synapse/

In the nervous system connexons form electric synapses, which pass ions from neuron to neuron. In other tissues gap junctions directly transfer a wide variety of substances between the cells and have been shown to play a role in cellular proliferation and survival [17]. In cancer, gap junctions play a dual role either promoting or inhibiting tumor progression depending on the immediate circumstances. Connexon expression is often down-regulated in invasive malignancies suggesting that detachment from neighbouring cells is a requirement for metastasis [18]. At the same time, the cancer cells need to establish connections to the microenvironment of the metastatic niche which often involves formation of gap junctions [19]. Furthermore, it appears that gap junctions are also involved in SMDR. For instance, it was shown that gap-junctions between the astro-glial and the melanoma cells protect melanoma from chemotherapy by sequestering cytotoxic calcium ions out of the cancer cells [20, 21].

Other intercellular contacts are mediated via integrin and cadherin molecules, both of which can activate diverse signaling cascades in the participating cells [22, 23]. They may therefore be important for SMDR as well; however, we have not investigated this hypothesis further in the current project.

Malignant melanoma

Malignant melanoma is an aggressive cancer type which often spawns metastases, more rapidly than most of the other cancers. Malignant melanoma of the skin originates from the pigment producing cells called melanocytes, found in the basal skin layer. Melanocytes develop in the neuronal crest and migrate to the skin and hair follicles during embryogenesis [24]. After migrating to their final location, melanocytes differentiate into brunching cells with multiple protrusions. In the skin they make connections with up to 40 neighbouring keratinocytes to which they deliver a pigment called melanin [25]. Dark, non-transparent melanin, produced and transported in special organelles, melanosomes, surrounds the nuclei of keratinocytes, protecting them from the damaging ultra-violet radiation of the sun. Melanocytes are terminally differentiated, but occasionally begin to proliferate locally forming dark nevi on the skin. Most often, proliferation in the nevi is halted and they remain benign for the rest of the life. In rare cases, however, melanocytes undergo transformation and become malignant.

Melanomas are relatively uncommon, but their incidence is on the rise. In Norway, it has increased eight-fold over the last 60 years with approximately 1500 new cases registered every year [26]. The most afflicted population is the fair-skinned individuals with high sun light exposure, suggesting an important role of the ultra-violet radiation in melanoma development [27].

Melanomas may arise from an existing mole or appear *de novo*. They occur at different locations and affect people of all ages. Primary melanomas are often discovered on early stages as irregular-looking moles which can be completely removed with surgery. Melanomas are highly invasive, however, so it is extremely important that the primary tumor is removed entirely and on time.

Stages of melanoma progression

Melanoma development in can generally be divided into four stages (figure 1.3). It starts with formation of a dysplastic nevus on the skin which expands horizontally while still within the limits of the basal membrane. This early stage of radial growth is followed by vertical growth during which the basal membrane becomes impaired and the malignant cells expand into the derma. The thickness of a malignant nevus has a strong correlation with patient prognosis [28], however, at this point a melanoma may still be removed. If left untreated, the melanoma cells would migrate to the distant locations of the body via blood or lymphatic vessels, and establish secondary tumors. Most common sites of melanoma metastasis include the brain, the lymph nodes, liver, lung and distant locations on the skin. At the last stage of its development, melanoma is practically impossible to eradicate. 5-year survival rate of stage IV melanoma patients is approximately 6 percent with median survival period of only 7.5 months [29].

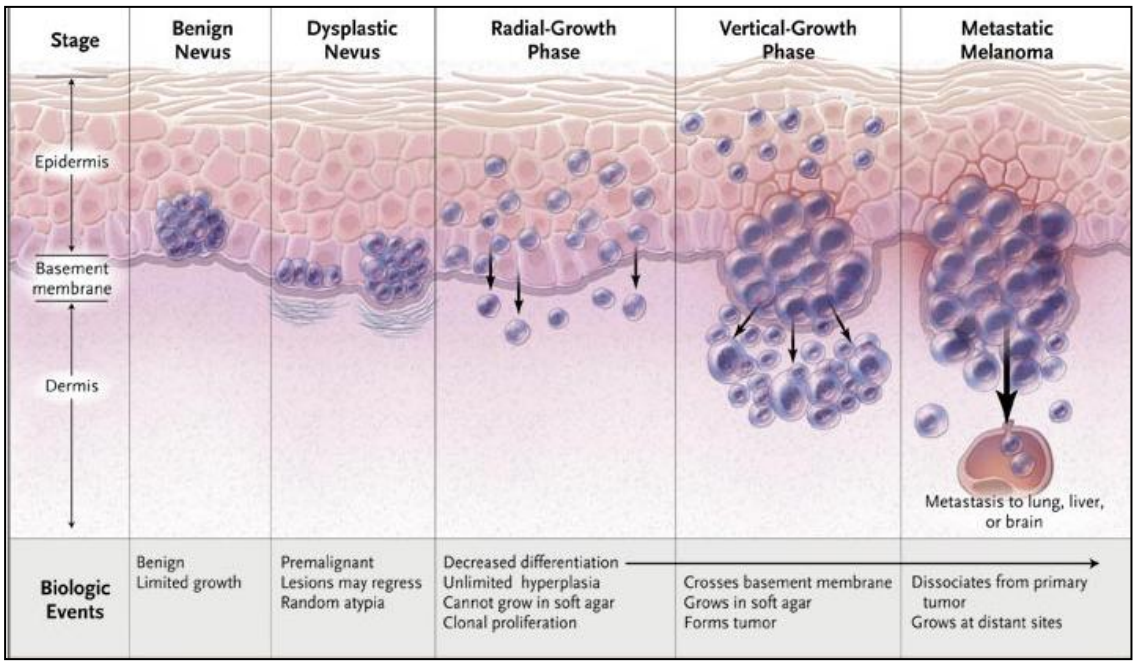

Figure 1.3 Stages of melanoma progression. Dysplastic nevus is characterized by abnormal shape, uneven colouring, blurred borders and diameter of >6mm. Melanocytes undergo malignant transformation at this stage, characterized by inhibition of tumor suppressors which leads to proliferation radial-growth. Progression to vertical-growth phase is defined by increased expression of invasion-associated molecules such as N-cadherin, matrix metalloproteinase-2 (MMP-2) and Vβ3 integrins. Thickness and ulceration of the melanoma during the vertical growth phase strongly correspond with the likelihood of metastasis. Finally, advanced

melanomas produce secondary tumors in the distant organs, most commonly lymph nodes, brain, lung and liver. Figure from Miller and Mihm; 2006 [30].

BRAF mutation

Melanoma cells carry a multitude of oncogenic mutations, the majority of which affect genes, encoding proteins of the proliferation supporting signaling, in particular, the mitogen-activated protein kinase (MAPK) pathway. The MAPK pathway normally regulates gene expression by conveying signals from the cell surface to the transcription factors through a chain of phosphorylation events performed by the MAPK kinases – RAF, MEK and ERK (figure 1.4). Each of the members of the MAPK pathway has several isoforms, some of which are frequently mutated in melanoma. These include NRAS [31] (HRAS and KRAS are mutated less often [32]), and BRAF [33] (oncogenic mutations in ARAF and CRAF have not been detected [34]). NRAS was shown to be mutated in approximately 15 percent of melanomas, while BRAF mutation is the most frequent, occurring in 60 percent of the patients [33].

Mutations in BRAF (rapidly accelerated fibrosarcoma protein kinase B) gene usually involve a single amino acid substitution at the residue 600 from valine to glutamic acid (denoted BRAF*V600E*) which dramatically up-regulates BRAF activity. This mutation renders BRAF constitutively active which leads to signal propagation in absence of extracellular stimulation.

Of note, BRAF*V600E* mutation in itself is not sufficient to induce melanocyte transformation and is often found in benign nevi [35]. In fact, constitutive activation of BRAF drives the cells to senescence, halting proliferation. However, additional mutations and activation of proliferation-related pathways can overcome the BRAF*V600E*-induced senescence and allow progression into a melanoma. One of the signaling events, implicated in this phenomenon is activation of mammalian target of rapamycin complex 1 (mTORC1). In the growth arrested melanocytes, its activity is normally suppressed [36]. In their recent publication, William Damsky et. al. have shown that reactivation of mTORC1 is necessary for BRAF*V600E* melanocytes' progression to melanoma [36].

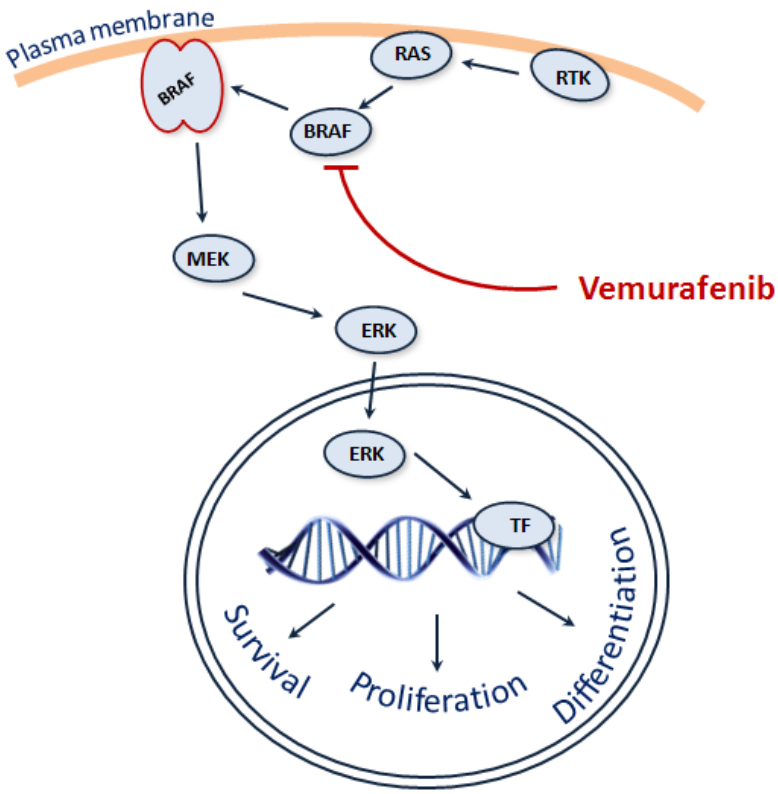

Figure 1.4 MAPK pathway. MAPK pathway is initiated by the activation of receptor tyrosine kinases (RTK). RTK ligands include growth factors, such as HGF, EGF and FGF. Ligand binding leads to phosphorylation of the RTK by its own kinase domain, which triggers GTP-binding and activation of a small GTPase – RAS. Activated RAS then binds to the RAF kinase, such as BRAF, inducing a conformational change which results in BRAF activation and dimerization. Activated BRAF phosphorylates the next kinase of the MAPK cascade - MEK, which then phosphorylates the extracellular signal-regulated kinase (ERK). Activated ERK translocates into the nucleus where it interacts with the transcription factors stimulating expression of genes involved in cellular proliferation and survival. Mutations in BRAF make it unable to adopt the inactive conformation rendering the MAPK pathway constitutively active even in absence of the upstream signals. A BRAF inhibitor vemurafenib inhibits BRAF activation by blocking its active site.

Vemurafenib and vemurafenib resistance

BRAF*V600E* can be selectively inhibited by novel targeted therapeutic agents, such as vemurafenib (figure 1.4). Introduced into the clinic in 2012, vemurafenib is one of the most efficient drugs available for the melanoma patients who carry a BRAF mutation, and has a response rate of around 60 percent leading to 5.3 months of progression-free survival [37]. This is a considerable improvement for the patients whose median survival prior to the vemurafenib discovery was only 7.5 months. Unfortunately, despite the strong initial

response, melanoma develops resistance to vemurafenib in almost all cases, leading to relapse within one year of treatment.

Mechanisms underlying vemurafenib resistance have been intensely investigated. It has been suggested that initial insensitivity to BRAF inhibition in melanoma, similarly to the absence of response in other cancer types with BRAF mutation, such as colorectal and thyroid cancer, may be explained by the loss of feedback inhibition of the RTK-mediated signaling by ERK [38-40]. This leads to increased activation of alternative signaling routes, such as the PI3K pathway, and sustained proliferation.

Resistance has also been attributed to mutational activation of NRAS [41], increased production of mutant BRAF after the end of the treatment period, activation of MEK via elevated levels of MAP kinase kinase kinase COT and activation of alternative signaling pathways through RTK, where stroma-produced chemical factors may play a role (reviewed in [42]) (figure 1.5).

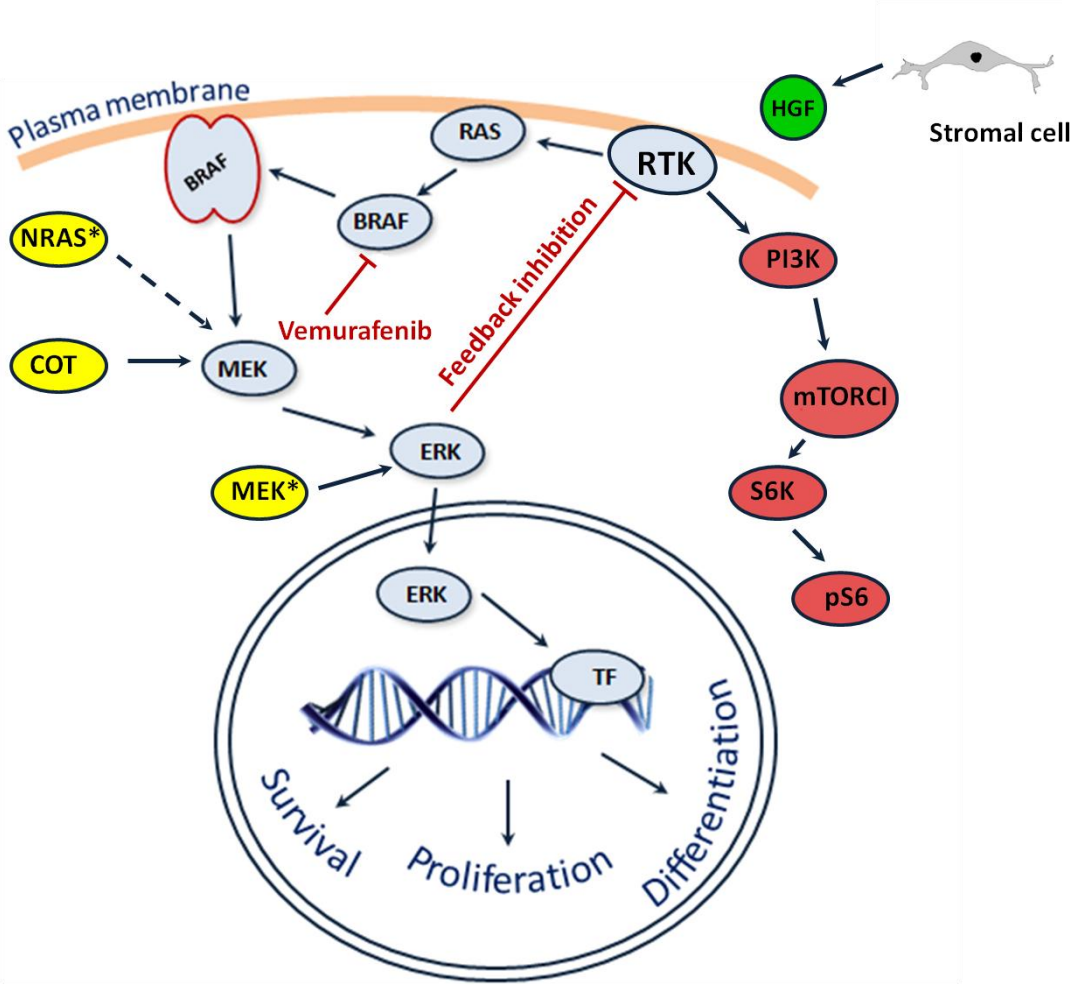

Figure 1.5 Vemurafenib resistance mechanisms. Resistance occurs when deactivation of the MAPK pathway (shown in blue) by vemurafenib abolishes the feedback inhibition of the RTK signaling. Other RTK-dependent cascades, such as the phospho-inositide-3-kinase (PIK3) – mTORC1 pathway then get activated and lead to continued proliferation (shown in red). Resistance depends on several mechanisms, including activation of the RTK by the stroma-produced growth factors (such as HGF), mutational activation of NRAS and MEK alongside up-regulation of COT all of which lead to reactivation of the MAPK activity. Modified from Holderfield M., et al, [42].

Vemurafenib resistance is often classified as either innate or acquired. Clinically, these are two distinct conditions depending on the disease progression state. Initial lack of response defines innate resistance, while patients who go through a period of disease regression and then relapse after several months appear to have acquired resistance during treatment. However, the cells that do not respond to vemurafenib, be it initially, or after prolonged

treatment with the drug, are very similar on the molecular level. As summarized in table 1.1, such cells can be characterized by several distinctive features.

Resistant phenotype feature	*Source*
Loss of feedback inhibition of RTK => activation of alternative signaling	[38, 41]
Overexpression of BRAF*V600E*	[43]
Up-regulation of COT	[44]
Stroma secreted factors stimulate proliferation-driving signaling	[45]
Low levels of the microphthalmia-associated transcription factor (MITF) expression	[46]
High expression of invasion-associated proteins	[46]

Table 1.1 Molecular alterations in the vemurafenib-resistant cells.

Resistance-associated properties may occur at any stage of the cancer progression, prior to the treatment, or after, in those cells where the MAPK inhibitors failed to induce cell death. It has been shown that in the sensitive cells, vemurafenib may either trigger apoptosis [47-49] or inhibit proliferation, driving the cells into a senescent state in which they do not divide [50-52]. This depends on the concentration of the drug that the cells are exposed to and *in vivo* may rely on vascularization of the tumor, among other factors. Those cells that halt proliferation, but do not undergo cell death, can be considered sensitive, but pose a hidden danger as the senescent state may be overcome. Over time mutations and phenotypic changes may accumulate and re-activate the proliferation-related signaling eventually resulting in development of the resistant phenotype (figure 1.6).

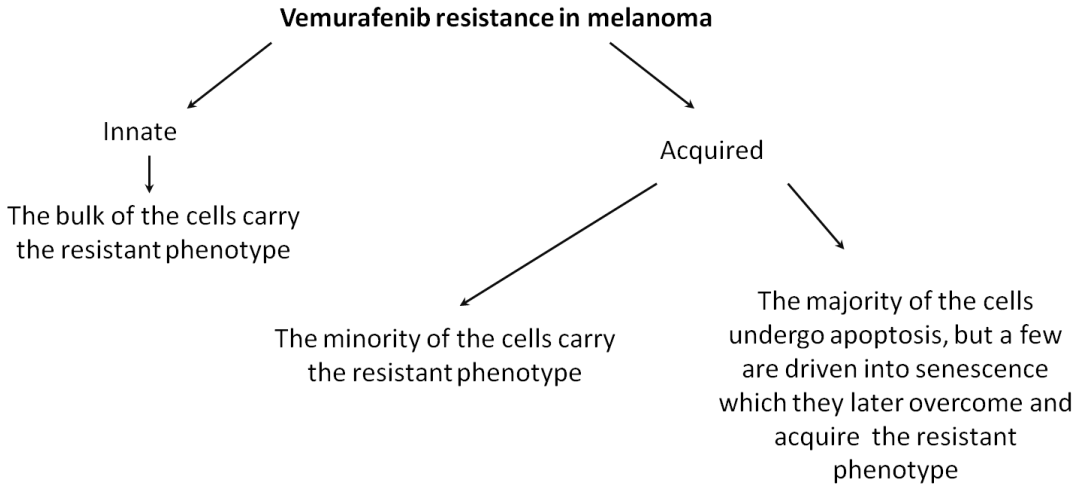

Figure 1.6 Potential scenarios underlying innate and acquired resistance to vemurafenib in melanoma.

To summarize, resistance relies on genetic instability and activation of oncogenic signaling. Stromal cells can contribute to both by creating aggressive pro-mutagenic environment within a tumor and by supplying proliferative signals which drive cancer growth. The extent to which the cancer cells interact with the stroma may define their sensitivity to therapy both before the drug is administered and afterwards during relapse of the disease. From this perspective, a better understanding of the tumor-stroma interactions may open opportunities for therapeutic interventions that could not only target rapidly proliferating cells, but prevent the SMDR.

The role of mTORC1 in SMDR against vemurafenib

One of the insights into stroma – mediated vemurafenib resistance in melanoma came from a comprehensive screening of multiple tumor and stroma cell lines cultured together and subjected to various therapeutic agents [45]. It was shown that the presence of stroma weakens drug response in cancer cells which was most apparent in the melanoma-fibroblast pairing treated with vemurafenib. In line with these observations, members of our group have shown higher viability of the melanoma cells in co-culture with the fibroblasts rather than alone after treatment with vemurafenib (figure 1.7).

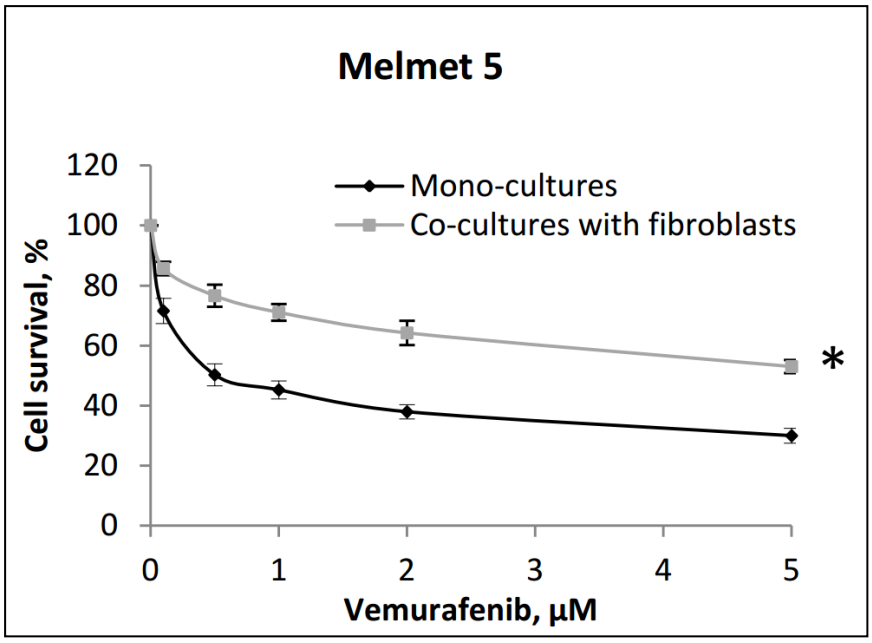

Figure 1.7 Improved relative viability of the melanoma Melmet 5 cells in co-culture with fibroblasts after 72h treatment with vemurafenib, measured by bioluminescence. Statistical significance. Data indicates average ± SEM ($n \geq 3$); *, $p \leq 0.05$. Vasiliauskaite K. *et al*., unpublished.

Ravid Straussman *et al.* have identified that fibroblast-induced protection occurs due to the HGF secreted by the fibroblasts [45]. HGF is a ligand of a RTK c-Met, located on the melanoma cellular surface, which is phosphorylated upon HGF binding.

c-Met phosphorylation leads to the activation of downstream cascades including MAPK pathway and PI3K (figure 1.5). One of the most prominent PI3K downstream targets is mTORC1 (figure 1.5). In cancer PI3K – mTORC1 signaling cascade is one of the frequently up-regulated pathways [53], whose activation helps the cancer cells bypass MAPK inhibition, i.e. by vemurafenib. Activation of mTORC1 signaling is associated with increased protein production and cell proliferation, among other effects [54].

mTORC1 activates S6 kinase (S6K), which phosphorylates the ribosomal protein S6 (figure 1.5). S6 is a component of the ribosomal 70S subunit and regulates protein translation. Dephosphorylation of S6 after vemurafenib treatment predicts strong response *in vitro* and *in vivo* [55]. Conversely, if S6 stays phosphorylated despite vemurafenib, it is likely that such

cells would not be affected by the treatment [55]. Members of our research group have previously shown that vemurafenib treatment results in reduced level of pS6 in BRAF*V600E* melanoma cells when they were cultured alone, indicating suppression of the mTORC1 activity. However, in the presence of fibroblasts, this suppression effect of vemurafenib on pS6/mTORC1 was abolished resulting in significantly higher levels of pS6 (figure 1.8). This implicates mTORC1 in the stroma-mediated resistance in melanoma (figure 1.8).

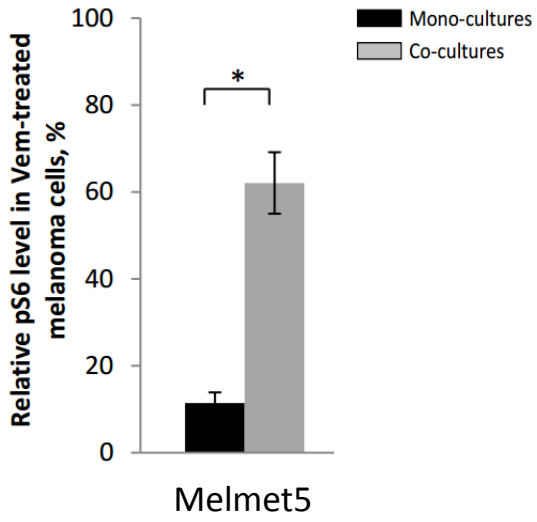

Figure 1.8 Phospho-S6 levels in Melmet5 melanoma cells either in mono-culture or in co-culture with stromal fibroblasts treated with vemurafenib, relative to untreated control. pS6 levels were strongly decreased in mono-culture samples, while co-culture with fibroblasts retained S6 phosphorylation. Data indicates average ± SEM (n=3); *, $p < 0.05$. Vasiliauskaite K. *et al*., unpublished.

Transcriptional state and sensitivity to vemurafenib

A growing tumor harbours increasingly diverse microenvironments with the centre of a tumor being entirely different from the periphery. Such difference in conditions coupled with genetic heterogeneity makes tumor architecture complex and uneven. Thus malignant cells in the same patient derived from different locations in the tumor may carry drastically different phenotypes. In 2008, Keith S. Hoek and colleagues suggested classification of the metastatic melanoma cells into proliferative and invasive phenotypes characterized by differential gene expression and distinct ability to migrate [56]. They proposed that melanoma cells are able to switch between the two phenotypes depending on the

surrounding microenvironment. Such plasticity allows cells to survive harsh conditions and travel to the secondary locations where they may switch their phenotype again. In their study, Hoek K. *et. al* [56] proposed a model for melanoma progression, according to which, the metastatic cells undergo several rounds of transition between the phenotypes so as to survive and proliferate in different contexts.

Cells of "proliferative" phenotype carry a distinct pattern of gene expression with high levels of melanocyte lineage genes, such as the MITF and its target genes. By contrast, the "invasive" cells have low expression of MITF and its targets, but high expression of "mesenchymal" genes, e.g. those involved in Wnt, TGF-β and Axl signaling [46, 57]. Importantly, several recent studies found an association between the molecular phenotype and sensitivity to vemurafenib. It has been shown that cells of the proliferative phenotype are sensitive to MAPK inhibitors, while the invasive phenotype cells are more resistant [57, 58]. The authors concluded that distinct molecular phenotype may be the cause of resistance to anti-MAPK therapy, and proposed MITF/AXL ratio as a "predictive indicator" of the treatment response [57, 58].

The role of energy metabolism in cancer

An aggressive resistant phenotype, also referred to as a state of de-differentiation, is associated with several functional changes. Among them, altered energy metabolism has been described as a distinct property of malignant cells and one of the hallmarks of cancer [59].

There are two metabolic pathways involved in ATP production in the cells (figure 1.9). The first involves generation of the proton gradient in the mitochondria using several substrates, including glucose-derived pyruvate. The proton gradient allows phosphorylation of ADP into ATP. This pathway is termed oxidative phosphorylation (OxPhos) because it requires the presence of oxygen as an electron acceptor. OxPhos generates up to 36 molecules of ATP per one molecule of glucose and thus is the most efficient way to produce energy for the cell. Most cells utilize this pathway if enough oxygen is present, however, under certain conditions, the other mechanism may be used.

The second pathway can be defined as glucose fermentation in the cytoplasm and results in production of lactate and two molecules of ATP. This pathway consists of two parts – glycolysis which ends with production of 2 pyruvate molecules, and conversion of pyruvate into lactate. This pathway does not require oxygen and is therefore mostly used in hypoxic conditions. In some cases, cells may utilize this pathway in presence of oxygen – a phenomenon termed aerobic glycolysis.

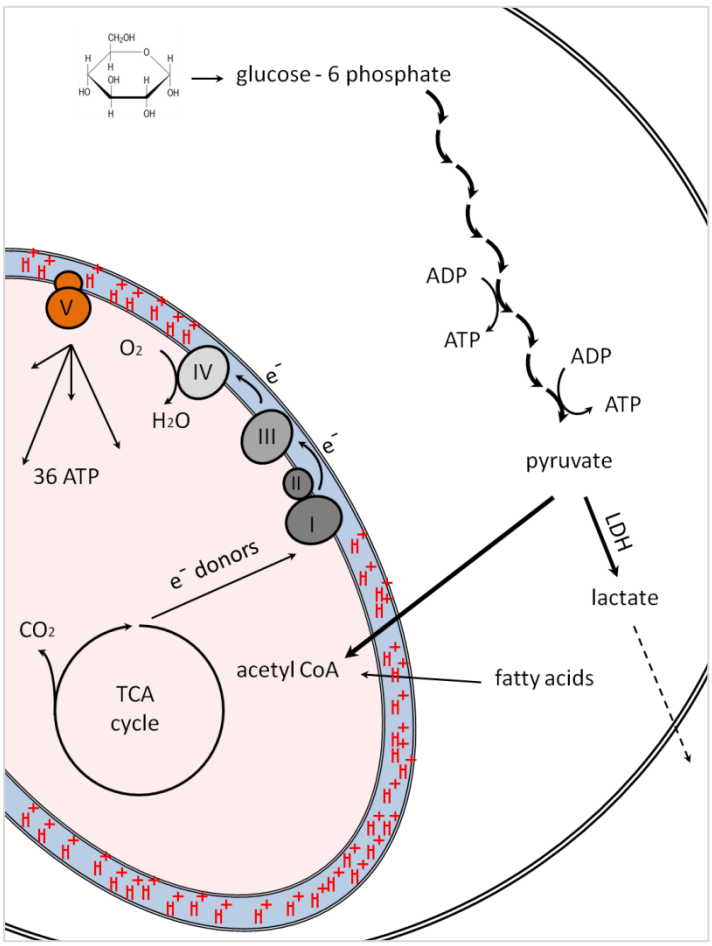

Figure 1.9 Intracellular energy metabolism. Glucose is imported into the cell via glucose transporters where it undergoes glycolysis. Glycolysis consists of ten chemical reactions that result in production of 2 ATP and 2 pyruvate molecules. Pyruvate can then either be converted into lactate by lactate dehydrogenase (LDH) and exported out of the cell, or uptaken by the mitochondria and converted into acetyl CoA. Other substrates, such as fatty acids can also be used to produce acetyl CoA which then enters the tricarboxylic acid (TCA) cycle. Consequent reactions of the TCA cycle result in reduction of 3NAD^+ and FAD^+ into NADH and FADH2. Together with NADH produced during glycolysis and conversion of pyruvate into acetyl CoA, NADH and FADH2 donate electrons to the complex I and complex II respectively. The electrons are then passed to complex III and to complex IV where they are accepted by oxygen with production of water. Complexes of the electron transport chain facilitate pumping of protons from the matrix of the mitochondrion into the intermembrane space. Abundance of protons between the mitochondrial membranes creates a gradient which allows protons to leave back into the matrix through the complex V (ATP-synthase). As the protons pass through it, the ATP-synthase phosphorylates ADP with production of up to 36 molecules of ATP per one molecule of glucose as an original substrate. Together all of the events in the mitochondria that result in production of ATP are termed oxidative phosphorylation (OxPhos). The output of OxPhos is adjusted to meet the current ATP demands of the cell.

Warburg effect

One of the first researchers to connect altered glucose metabolism and cancer progression was Otto Warburg, who observed that the cancer cells tend to utilize aerobic glycolysis to produce energy rather than rely on OxPhos [60]. This tendency to use glucose fermentation by cancer cells, termed the Warburg effect, has been traditionally linked to the rapid proliferation of the cancer cells. Growth and division require building blocks, however, in the process of OxPhos, many of the organic molecules are being degraded. On the contrary, aerobic glycolysis does not require additional substrates and can be more convenient for the dividing cells to use in case there is sufficient amount of glucose [61].

Most recently, it has been shown that the metabolic preference is dependent on a wide range of extra- and intracellular factors [62]. ATP production is acutely regulated by inhibition and activation of metabolic enzymes while long-term metabolic shifts occur through gene expression regulation. It has also been demonstrated that activation of proliferation-related signaling cascades in cancer cells can regulate energy metabolism [63]. Several studies have shown that up-regulated aerobic glycolysis is one of the manifestations of invasive phenotype in cancer [64-66]. Factors that contribute to such regulation have since been meticulously dissected.

It has also been shown that the MAPK pathway activation decreases the number and activity of the mitochondria [67]. With reduced use of the OxPhos pathway, the cancer cells are driven to up-regulated aerobic glycolysis. This creates an acidic environment which further promotes dedifferentiation and resistant phenotype in the cancer cells [68]. Studies have shown that vemurafenib as well as MEK inhibitors alone or in combination reduce this effect and stimulate expression of the OxPhos regulating genes, such as peroxisome proliferator-activated receptor gamma coactivator 1-alpha (PPARGC1A encoding PGC1-α) [67, 69, 70]. Three-day treatment with vemurafenib results in higher number and increased function of the mitochondria, which constitutes an evasion mechanism that allows cell survival in presence of MAPK inhibitors [67, 71]. Increase in OxPhos is accompanied by up-regulation in MITF expression, indicating that metabolic alterations are closely related to the phenotype shift.

Considering this connection between metabolism and malignant phenotype, using metabolism-regulating drugs in combination with MAPK inhibitors may improve response to therapy.

Cancer metabolism as a target for therapy

Recently, cellular metabolism has emerged as an attractive target for therapeutic intervention. Some studies suggest that inhibition of enzymes, such as poly (ADP ribose) polymerase-1 (PARP-1), involved in regulation of NAD-factor red-ox balance could be beneficial [72]. In addition, most cancers demonstrate increased capacity to sustain reactive oxygen species (ROS)-induced stress. This largely relies on antioxidant systems, which can also serve as targets to prevent increased cancer cell survival. This is particularly promising in melanoma, where the OxPhos pathway, and, as a consequence, the ROS production, are up-regulated after vemurafenib treatment as one of the compensation mechanisms [73]. Finally, inihibition of the lactate exporters, MCT1 and MCT4 proteins, which transport lactate accumulated during aerobic glycolysis out of the cells, may prove useful as well [74, 75].

A substantial body of research has described attempts to reverse the Warburg effect by blocking glycolysis [76, 77]. To that end, researchers used dichloroacetic acid (DCA), which blocks pyruvate dehydrogenase kinase (PDK). PDK inhibits pyruvate dehydrogenase (PDH), which mediates conversion of pyruvate into acetyl CoA. In other words, DCA stimulates OxPhos by inhibiting OxPhos inhibitor, PDK. DCA was shown to efficiently reduce cancer cell growth and invasion *in vitro* and *in vivo*, [78-80] and may therefore be considered for clinical use [81]. In the current project, we investigated whether DCA could be used to reverse stroma-mediated metabolic changes in the melanoma cells.

Aims of study

Previous studies in our group have revealed that the stromal cells can protect Melmet5 melanoma cells against targeted drug, vemurafenib, *in vitro*. The current project aimed to expand the melanoma cell line panel in order to verify this finding and investigate biological mechanisms involved at the molecular, signaling and metabolic levels.

Within the limits of this master's assignment, we defined the following sub-goals:

1. Verify the fibroblast-induced protection against vemurafenib in four melanoma cell lines.
2. Investigate whether the protection effect is mediated via stroma-secreted soluble factors or relies on the immediate cell-cell connections.
3. Investigate potential biological mechanisms involved in the protection by studying changes in the gene expression and signaling in melanoma under the influence of fibroblasts.
4. Study therapeutically induced alterations of the melanoma energy metabolism using novel technology provided by Seahorse Bioscience.

Materials and Methods

Cell lines

Four human malignant melanoma cell lines derived from distant metastases were used in this project: Melmet5, HM8, HM19 and Patient-3-pre. Human lung fibroblasts WI-38 were used as a stromal cell line.

	Tissue of origin	*Received from*
Melmet 5	Lymph node metastasis	Norway, Radiumhospitalet
HM8	Brain metastasis	Norway, Radiumhospitalet
HM19	Brain metastasis	Norway, Radiumhospitalet
Patient-3 pre	Lymph node metastasis	University of Sydney, Sydney, Australia
WI-38	Lungs	ATCC. Product number CCL-75, Lot number: 58483158

Table 2.1: Cell line sources

Cell culturing

All cancer cells were cultured as cell monolayer in tissue cultured flasks in RPMI medium supplemented with 10% FBS, 2mM Glutamax, and, in most cases, 1% Penicilin and 1% Streptavidin for protection against bacterial infections. The WI-38 fibroblasts were cultured in EMEM medium with the same supplements. All cells were kept at 37C° in an incubator with 5% atmospheric CO2 and were routinely tested for mycoplasma.

- Subculturing

  All cell lines were regularly split once the cell confluence approached 90-95%. EDTA 0.02% was used for detachment of all cancer cells, while WI-38 fibroblasts were detached with 0.05% Trypsin - EDTA solution. The cells were then collected, centrifuged and resuspended in fresh medium. 10µl of the cell suspension was stained with equal volume of trypan blue and used for counting. Automated cell counter *countess*™ was used to estimate the number of cells in suspension and their viability, based on the assumption that trypan blue only penetrates dead or dying cells with compromised membranes.

- Freezing

  To prepare frozen cell stocks, cells were detached, collected and counted as described above. One million cells per tube in medium containing 10% DMSO were frozen in a -80C° freezer before being transferred to liquid nitrogen tanks for long term storage.

- Thawing

  Frozen cells were rapidly thawed in a 37C° water bath and immediately transferred into tubes with pre-warmed medium. To remove remaining DMSO, the cell suspension was centrifuged and resuspended in fresh medium. The cells were then transferred to tissue culture flasks.

Virus production and transduction of cancer cells

For the majority of experiments, melanoma cell lines expressing green fluorescent protein and luciferase (GFP-luc) fusion protein have been used. Lenti-viral transduction was done to achieve stable expression. The virus was produced using 293HEK (human embryonic kidney) cells in several steps (figure 2.1).

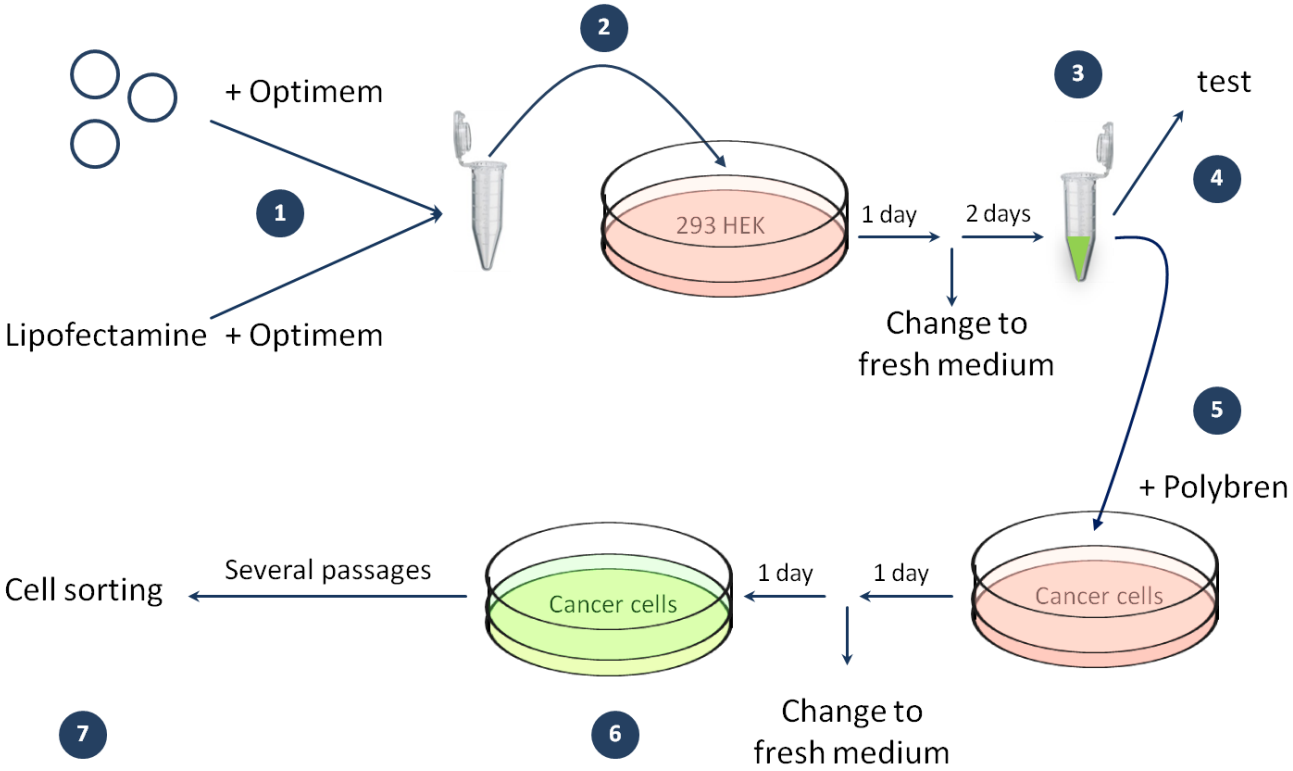

Figure 2.1 Lentivirus production and cancer cell transduction in steps

1. Three plasmids: pMD2.G encoding viral envelope proteins; psPAX.2 with packaging genes; and Luc-GFP #10-Neo plasmid carrying the genes of interest – luciferase and GFP under control of the ferritin promoter (a gift from prof. G Merlino [82]); were mixed using 1,5µg, 3,75µg and 5µg respectively. Optimem 479µl was added to the plasmid mix and, separately, 450µl of Optimem was mixed with 50µl of Lipofectamine-2000.

2. After 5min incubation at room temperature, the plasmid – Optimem mix and the lipofectamine-2000 in Optimem were combined and kept at room temperature for 20min. The resulting transfection solution was then applied to the semi-confluent HEK293 cells in a petri dish with 5ml of growth medium. 1.4mln 293HEK cells had been seeded out one day prior to transfection.

3. The medium was replaced with fresh RPMI 1 day later and 2 days after that, the medium was collected and centrifuged in order to remove the cell debris. The supernatant containing virus was collected, filtered through 0.45µm low-protein binding filter, aliquoted and frozen at -20C°.

4. 50000 293HEK cells/well were plated into a 24-well plate in supplemented RPMI medium and cultured for two days. 100µl, 50µl and 10µl of the virus stock solution were added to RPMI to the total volume of 500µl in each well. In addition, half of the wells received 10µg/ml polybrene. 18h later, the medium was replaced with fresh virus-free RPMI. 24h after that, successful transduction was verified using a fluorescent microscope. It was determined that the highest volume of the virus stock produced the strongest transduction efficacy. Polybrene did not influence the outcome of the test.

5. For transduction of cancer cells, 300µl of virus stock was combined with 10µg/ml polybrene in 500µl of RPMI medium and applied to the cells cultured in a well of a 6-well plate.

6. The medium was changed 1 day after transduction and a day after, the transduced cells were inspected for GFP with a fluorescent microscope.

7. After 5 passages, the cells were sorted by flow-cytometry in the cell sorting core facility of the Radium Hospital in order to purify cells with high levels of GFP-luc expression.

All of the steps involving virus production and transduction were performed at the specially designed biosafety level 2 laboratory which is used exclusively for this purpose and is equipped with neutralizing agents and protective clothing.

In vitro cancer cell viability assays

Testing drugs targeting oncogenic signaling pathways in cancer cell mono-cultures

To evaluate drug effects on cancer cell viability, cancer cells were plated in 100µl medium into 96-well plates, incubated overnight and treated with BRAF*V600E* inhibitor vemurafenib (stock solution 20mM in DMSO) dissolved in 100µl of fresh medium in concentrations of up to 10µM for 72 hours. The mTORC1 pathway inhibitor everolimus (stock solution 20µM in DMSO) was applied following the same protocol in concentrations from 5nM to 100nM. At

the end of the treatment, cell viability was measured using bioluminescence or MTS analyses described below.

Testing dichloroacetic acid in mono- and co-cultures

Dichloroacetic acid (DCA) was tested on melanoma cells in mono-culture and in co-culture with WI-38 fibroblasts in order to investigate tumor cells' sensitivity to metabolic alterations. Cells were seeded out in 100µl medium (cell numbers specified in table 2.2) and incubated for 72 hours in order to induce stroma-mediated phenotypic changes in the cancer cells. Freshly prepared DCA (2M stock solution in PBS) was then applied in 10mM, 20mM and 30mM concentrations, in 100µl of RPMI medium. The plates were incubated further for 48 hours after which, the viability of the cancer cells was measured using the bioluminescence assay, described below.

	Melmet 5	***HM8***
Mono-culture	5500	4000
Co-culture	1500	1000
WI-38 in co-culture	4000	4000

Table 2.2 Number of cells per well seeded for mono-culture and co-culture experiments on 96-well plates for testing DCA.

CellTiter 96® AQ_{ueous} Non-Radioactive Cell Proliferation Assay (MTS)

MTS is a tetra-zolium dye which is converted into a coloured formazan product by intracellular reductases found in metabolically active viable cells. The quantity of the formazan product and, therefore, colour intensity, is directly proportionate to the number of living cells in culture. MTS was diluted with medium 1:5 and added to the cells for approximately 1-hour long incubation at 37C°. Absorbance at 490nm was then measured using a 1420 Multilabel Counter Wallac® plate reader.

Cell viability measurement by bioluminescence analysis

All cancer cells lines in the current project were genetically modified to stably express GFP-Luciferase. Luciferase uses luciferin as a substrate in a reaction which results in light emission – bioluminescence. Reading the emission signal intensity allows tracking of the viable cancer cells and is proportional to their number. Luciferin (stock solution 20mg/ml) was mixed with medium at a ratio 1:200 and added to the cells for 10 minute incubation in the dark. The emitted bioluminescence was then measured by a 1420 Multilabel Counter Wallac® plate reader. Plates with opaque white walls specially designed for bioluminescence measurements were used in these experiments.

Co-cultures of cancer cells with WI-38 fibroblasts

Cell-cell contact-based cultures

To explore whether stromal cells influence cancer cells, we made use of co-cultures consisting of cancer cells and lung fibroblasts WI-38. For these experiments, both cancer cells and the WI-38 fibroblasts were detached, collected and counted in the similar manner as during cell splitting described above, to achieve the desired numbers of cells per well (table 2.3). Appropriate volumes of cell suspensions were then mixed and plated in 96-well plates in 100µl of medium to allow direct contact formation. RPMI medium was used in such experiments, which fibroblasts tolerated well. Drugs were applied in the same manner as on mono-cultures and the treatment lasted for 72 hours. Viability of the cancer cells by the end of the experiment was determined by measuring bioluminescence.

	Melmet 5	***HM8***	***HM19***	***Patient-3-pre***
Mono-culture	2500	4000	4000	2500
Co-culture	1250	2000	2000	1250
WI-38 in co-culture	1250	2000	2000	1250

Table 2.3 Number of cells per well seeded for mono-culture and co-culture experiments on 96-well plates.

Cultures on trans-well insert plates

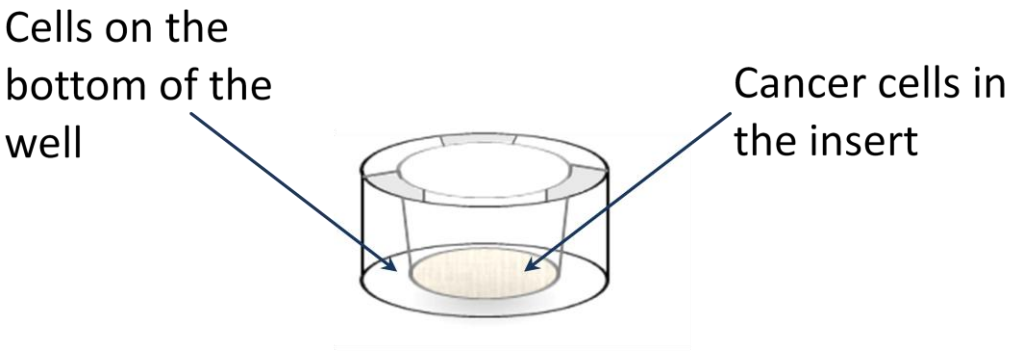

Figure 2.2: Scheme of a trans-well with an insert

To explore whether stromal cells have an influence on cancer cells via soluble factors, we used trans-well plates with inserts allowing separation of the cancer cells from stroma cells while simultaneously keeping them in shared conditions. 0.4 µm pores of the insert membrane eliminate direct cell-cell contacts but the medium containing soluble factors is exchanged freely.

- 24-well plates for viability analysis

8 000 melanoma cells were placed into the inserts, while the bottom wells had 15 000 fibroblasts (or 24 000 melanoma cells for control). When seeding, 700µl of medium was used in the bottom wells, and 100µl was applied to the cells in the inserts. The cells were incubated overnight before vemurafenib was added in different doses. When adding the drug, the inserts were temporarily removed and kept in a separate clean dish, while the medium was being changed in the bottom wells. The medium from the inserts was then removed and they were returned to the original plate. Finally, fresh medium containing drugs was placed into the inserts. This technique made it possible to avoid drying of the cells. After 72 hours of incubation with vemurafenib, MTS assay was performed on the cancer cells in the inserts to determine their viability.

- 6-well plates for molecular analyses

6-well plates with inserts were used to prepare samples for western blotting, flow cytometry and PCR. In a similar manner as for the experiments on 24-well plates described above, 200 000 melanoma cells were seeded in the inserts, while 250 000 fibroblasts (or 300 000 cancer cells for control) were placed in the bottom wells. 1 day after seeding, the medium was replaced with fresh RPMI with supplements containing 1µM Vemurafenib. After 24-hour incubation, cells in the inserts were thoroughly washed with PBS, detached with trypsin-EDTA and collected for further analyses.

	Melmet 5	***HM8***	***WI-38***
Bottom well	24000	24000	15000
Insert	8000	8000	-

Table 2.4: Number of cells per well seeded in 24-well plates with inserts.

	Melmet 5	***HM8***	***WI-38***
Bottom well	300 000	300 000	250 000
Insert	200 000	200 000	-

Table 2.5: Number of cells per well seeded in 6-well plates with inserts.

Adhesion assay

To evaluate how well cancer cells attach to the stromal cells, adhesion assay was performed. 15000 fibroblasts per well were seeded into a white-wall 96-well plate for bioluminescence measurement and incubated until full confluence. The wells were then washed with PBS to remove all serum. Melanoma cells, 25 000 per well, in 100µl serum-free medium were added to the fibroblasts and incubated for 1 hour. Half of the wells were then thoroughly washed with PBS to remove the non-attached cancer cells, while the other half was left for data normalization. Adhesion efficacy was evaluated by measuring bioluminescence produced by the adherent melanoma cells as compared to the signal from the wells which had not been washed and expressed in percent.

Western blotting

Western blotting is a semi-quantative method for protein separation from cell- or tissue-derived samples. It is used to determine if a certain protein is present, estimate its comparative amount in a sample and identify certain modifications such as phosphorylation. The results can be analyzed visually, however, it is also possible to quantify the intensity or the acquired signal with special software.

Although there is room for variation in western blotting, in general, the procedure consists of eight steps (Figure 2. 3).

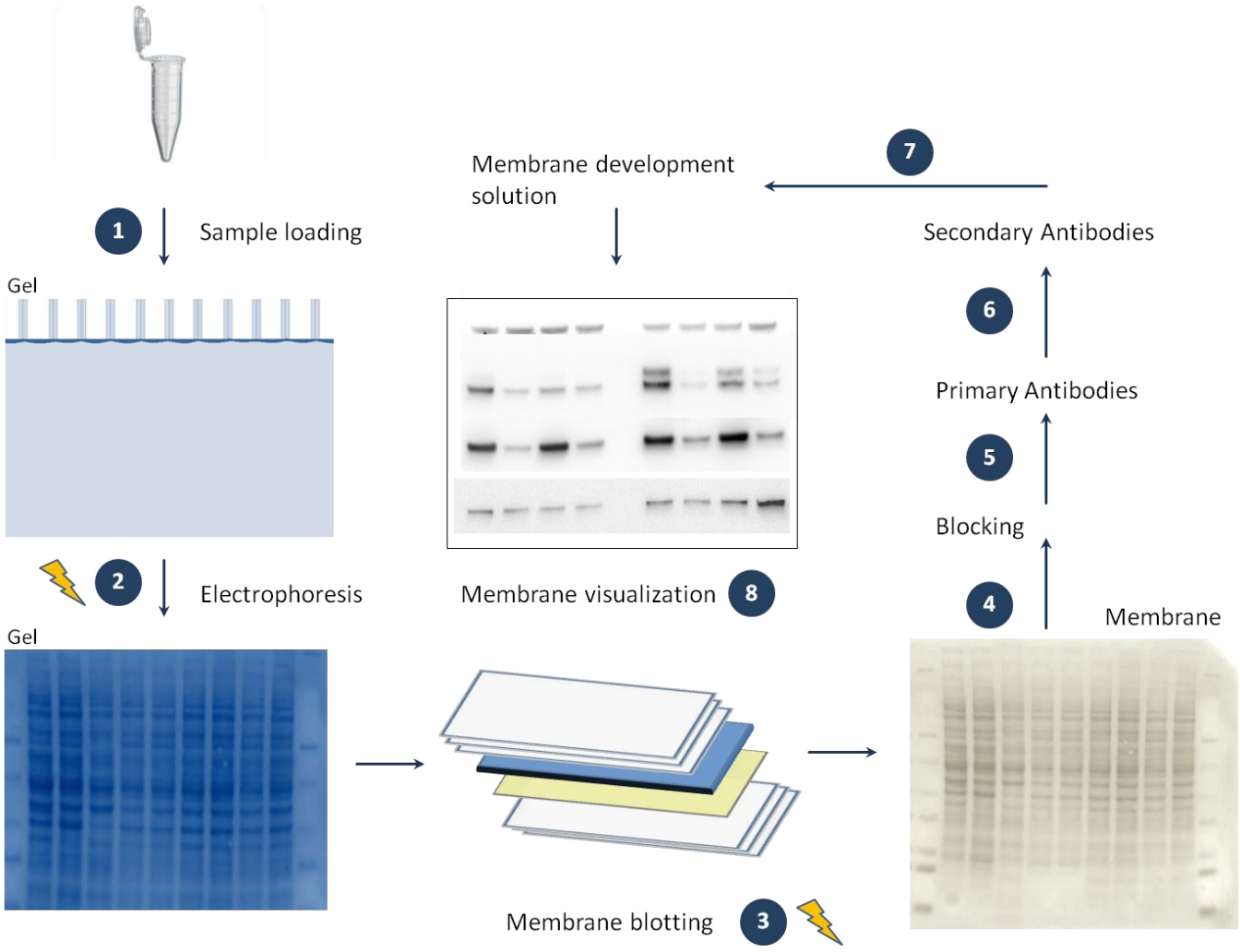

Figure 2.3 Scheme of a western blotting experiment

In this study, samples for western blot analysis were prepared from collected cells which were washed with PBS in order to remove remaining FBS. The cell pellets were lysed by sonication while being in the lysis buffer (150mM NaCl, 50mM Tris pH 7.5, 0.1% Nonidet P40) in the presence of phosphotase and protease inhibitors. Protein concentration was estimated in each sample with the use of Pierce™ BCA protein assay kit according to the supplied protocol. Prior to loading, the samples were kept at 75C° for 5 minutes in solution with reducing agent SDS, and loading buffer.

1. Samples, containing equal amounts or proteins, typically 20µg, were loaded into the gel pockets. Nu-PAGE 4-12% Bis-Tris 1.0mm x 12 well gels were used. In addition, at least two protein "ladders"- commercially available samples with coloured proteins of known sizes (See Blue®Plus 2 prestained standard, Invitrogen), were used in each western blotting experiment.
2. Electric charge of 150V was applied to the gel, making the proteins, all negatively charged by the reducing agent SDS, move downwards to the positive pole. Bigger proteins move slower than smaller ones, resulting in size-based separation in the process of electrophoresis. Current project involved 1-2 hour long electrophoresis performed in MES buffered solution.
3. The gel was pressed against the PVDF membrane and "sandwiched between" several layers of sponges and paper for semidry transfer. The "sandwich" was placed between two plates, which conduct electrical charge forcing the proteins out of the gel and onto the membrane. Transfer took 1 hour at 400mA.

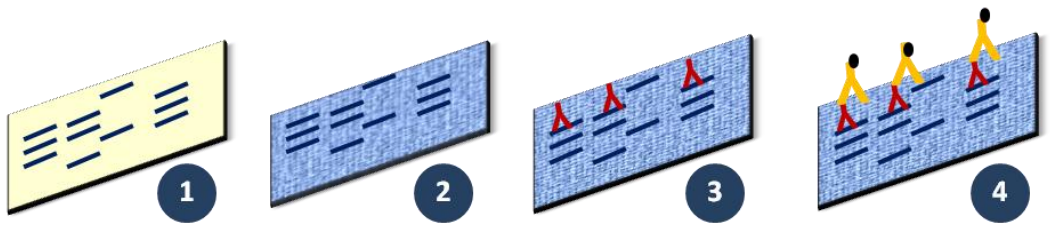

Figure 2.4 Membrane handling in western blotting. Step 1. The membrane strongly binds proteins from the gel. Step 2. Membrane blocking with dry milk or bovine serum albumin (BSA) to avoid unspecific binding of the Abs in the next steps. Step 3. Primary Abs are applied and bind very selectively to the protein of interest. Step 4. Secondary Abs conjugated with polyclonal horseradish peroxidase bind to the primary Abs.

4. Protein transfer onto the PVDF membrane was verified with Amido-Black staining, which unspecifically binds to the proteins. The membrane was then blocked with either 5% bovine serum albumin (BSA) or 5% dry milk in Tris-buffered saline Tween20 (TBST) solution. Blocking solution corresponded to the solution for the primary Abs recommended by the Abs' producer. Blocking was performed for 1 hour at room temperature (RT).
5. Primary Abs in recommended dilutions were applied in either 5% BSA or 5% dry milk solutions onto the membranes overnight at 4C°.
6. After being washed with TBST 3 times for 10 minutes, the membrane was incubated with appropriate secondary Abs in the same solution as the respective primary Abs for 1 hour at room temperature. Secondary Abs were diluted 1:3500 in either 5% BSA or 5% dry milk solution.
7. Finally, the membrane was washed 3 times and covered with Super Signal® West Dura Extended duration substrate.
8. The membrane was then immediately visualized in G:Box membrane visualization chamber at various exposures depending on protein signal intensity.

Real time polymerase chain reaction (PCR)

Real time PCR allows quantification of the gene expression levels in cells. mRNA is isolated from the cells and turned into cDNA by reverse-transcriptase. Using primers for genes of interest, a PCR reaction on the total cDNA is then initiated. Special probes, complementary to the sequences within the same genes are also added. They attach to the sequence and are then cleaved away by the moving DNA polymerase. Probes carry fluorescent tags which are inactive in the bound state, but turn fluorescent after being cleaved. As the PCR propagates, the fluorescent signal intensity grows exponentially. The number of the cycle during which the signal crosses the threshold is called the Ct value (figure 2.5). Ct value is

determined by how much of the target cDNA if any was present in the sample at the start of the PCR and is thus related to the expression levels of the corresponding gene.

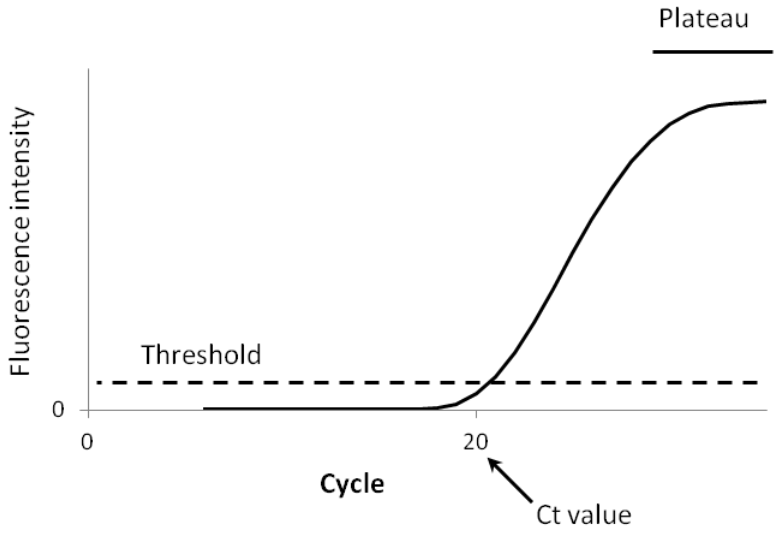

Figure 2.5 Illustration of a real time PCR experiment. The signal intensity crosses a threshold after several cycles. The number of the cycle reflects the amount of template DNA in the sample.

RNA isolation and cDNA synthesis

The cancer cells for the real time PCR were collected from the inserts of the 6-well trans-well plates. The inserts containing cancer cells were lifted and placed into a separate empty 6-well plate where they were treated with trypsin-EDTA. The cells were collected, centrifuged, resuspended in 500µl TRIzol® reagent and stored at -80C°. After thawing, 100µl chloroform was added to each sample, which were then centrifuged at 12000xg for 15min at 4C°. The colourless RNA-containing phase without TRIzol was removed and placed into RNAse-free test-tubes where RNA was precipitated using 250µl of isopropyl alcohol per sample. 3µl of acrylamide was also added to the mixture to make it easier to locate the RNA pellet in the following steps. The samples were transferred into -20C° freezers for overnight incubation. The samples were then centrifuged at 12000xg for 40min at 4C°. The supernatant was carefully removed and the RNA pellet was resuspended in 500µl of 75% ethanol and centrifuged at 12000xg for 15min at 4C°. The supernatant was removed; the pellets were briefly air-dried to remove all ethanol and resuspended in 50µl of RNAse-free water. Finally,

the samples were incubated at 55C° for 5-10min and placed on ice while the RNA concentration was measured using Nano Drop.

Biosciences qScript™ DNA synthesis kit was used to prepare 1000ng of cDNA according to the protocol supplied by the manufacturer. The following program was applied on the thermo-cycler GeneAmp® PCR system 9700:

- 22C° – 5min
- 42C° – 30min
- 85C°– 5min
- 6C° – ∞

Final cDNA concentration was brought to 12,5ng/µl in all samples.

Quantitative real-time PCR

Forward and reverse primers were mixed with the corresponding fluorescent probes and SuperMix (Quanta Biosciences, PerfeCTa™) containing nucleotides, $MgCl_2$ and DNA polymerase. 1µg/µl of cDNA was then added to each sample (table 2.6).

	x1 well	*x2 wells*
SuperMix	13.5	Mix 49.7
Primer forward	0.81	
Primer reverse	0.81	
Probe	0.54	
cDNA	2.16	4.32
Water	9.18	
Total	**27**	**54**

Table 2.6 Volumes of reagents used to prepare PCR samples

Every sample was divided into two wells using 25µl for each in a PCR plate to create two technical replicates. The PCR was then initiated using Bio-Rad CFX Connect™ Real Time System PCR machine. The following program was used:

- Cycle 1: (1x) Initial denaturation 95C°, 3min
- Cycle 2: (40x) Amplification 95C°, 15sec; 60C°, 1min;
- Cycle 3: (1x) 8C° - ∞

Having two technical replicates allows exclusion of technical inaccuracies. Every pair was compared to confirm that the difference in CT values did not exceed 0.5. PCR results were analyzed using CFX Manager™ Software. Expression levels of YARS - a control "house-keeping" gene, believed to be universally expressed in different cell lines, were used to normalize the expression of the genes of interest in the samples. Within the sample groups, relative expression was established by normalizing to an untreated control sample.

Flow cytometry

Flow cytometry is a method for molecular analysis of the single cells in suspension. It allows detection and quantification of biomarkers as well as separation of cell subpopulations based on set parameters. In a flow cytometer, a cell suspension is hydrodynamically focused into a one-cell wide stream of fluid which passes through a set of lasers. The extent to which the light is diffracted when passing through a cell reflects its size and granularity. These data are shown as forward and side scatter (figure 2.6). Lasers of different frequencies excite different fluorochromes producing a quantitative estimate of the fluorescent labeling on each cell.

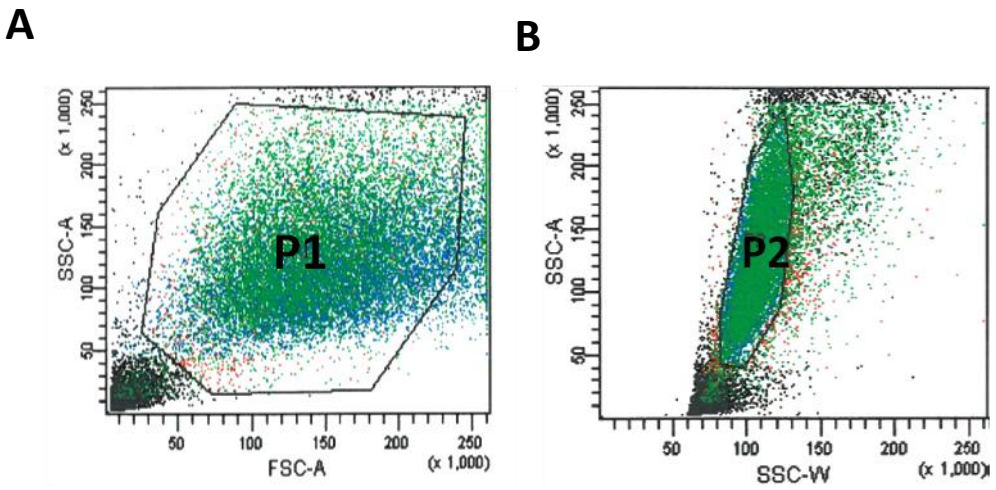

Figure 2.6 Illustration of cell gating strategy used in flow-cytometric analysis**. A.** Forward scatter vs side scatter gating defines the main cell population (P1) and excludes cell debris. **B.** Side scatter width vs side scatter area defines the single cell population (P2) and excludes duplets.

All of the analyzed parameters including size, granularity and the presence or absence of fluorescent labeling allow defining cell populations of interest using gating strategy. Using gating on the forward scatter versus side scatter makes it possible to exclude debris and most of the dead cells including only the main cell population for further analysis. Gating on the side scatter width versus side scatter area allows analysis of only single cells excluding duplets from the subsequent steps (figure 2.10). In the present study, flow cytometry has been used for detection of intracellular phosphoproteins, fluorescent dye transfer and cell cycle analysis.

Phospho-S6 detection by flow-cytometry

To prepare samples for intracellular flow cytometry, cells were grown as mono-cultures or co-cultures to full confluence in T25 cell culture flasks (table 2.7).

	Melmet5	***HM8***	***WI-38***
mono-culture	500 000	500 000	-
co-culture	250 000	250 000	250 000

Table 2.7 Cell numbers used for seeding for flow-cytometry analysis

In samples treated with Vemurafenib, 1µM final drug concentration was used. The drug was applied one day after cell seeding followed by the 24-hour incubation. All cells were detached using trypsin-EDTA, centrifuged and resuspended in 1:20 solution of 32% paraformaldehyde (PFA) and PBS. After 5min incubation at room temperature, the samples were centrifuged one more time and resuspended in 100% ice-cold methanol. Samples for phospho-S6 detection were stored at -80C° while samples for cell cycle analysis were stored at -20C°.

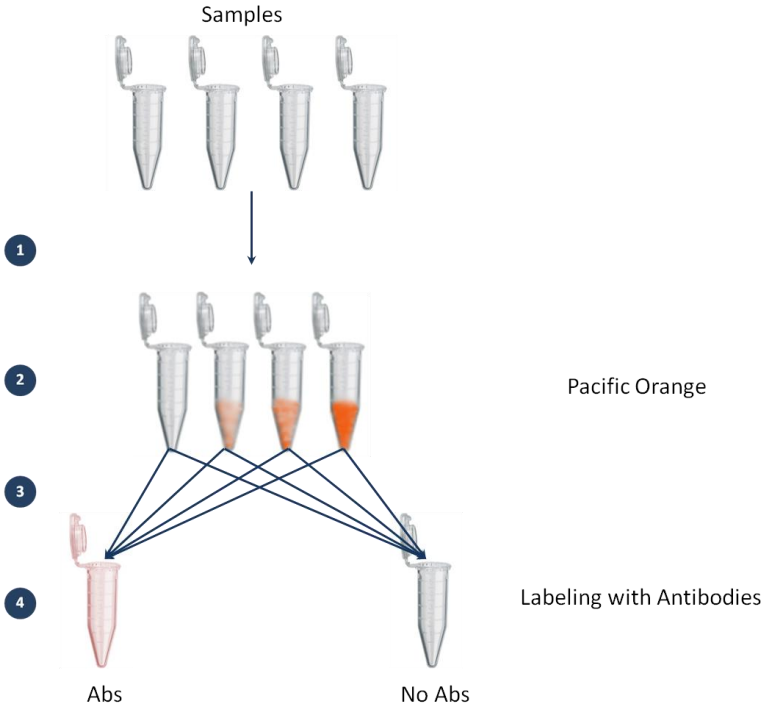

Figure 2.7 Sample preparation in intracellular flow cytometry. Ab – antibody, Abs – antibodies.

1. Samples were centrifuged at 2000rpm for 5min and resuspended in 1ml of PBS with 1%BSA to remove methanol.
2. Four samples from mono- and co-cultures with and without drug treatment, were then "barcoded" (as illustrated in figure 2.7) – labeled with a certain concentration of an unspecific, cell-binding fluorescent dye, pacific orange. This way, each cell from a sample carried a fluorescent tag, the intensity of which identified the sample. The cells were incubated with 5µl of pacific orange solution in four different

concentrations (0; 0.04ng/µl; 0.2ng/µl; 2ng/µl) for 30min at room temperature in the dark, centrifuged and resuspended in 1ml of PBS with 1%BSA.

3. "Barcoded" cells from four samples were placed into a tube containing fluorescently-labelled antibodies (Abs). In addition, the samples were added to a tube with no Abs for control.
4. After 30min incubation in the dark with the Abs, all samples were centrifuged and resuspended in 400µl of PBS with 1% BSA, filtered through a 35µm nylon mesh and analyzed on a BD LSRII flow-cytometer identifying the level of the Ab-binding phospho-S6 in each sample.

Dye transfer analysis

To determine whether the cancer cells and the stromal cells interact via direct connections, namely, intercellular gap-junctions, we analyzed how a small fluorescent dye, calcein, is exchanged between these two cell populations. Melanoma cells were labeled with calcein, fluorescent in green, while WI-38 fibroblasts were labeled with gap-junction impermeable DiL, fluorescent in red. The labeled cancer cells and fibroblasts were mixed and seeded into a 6-well plate overnight in a very dense co-culture. If the gap junctions were indeed present, calcein was transferred from cancer cells into the stromal cells, creating a double-positive population of fibroblasts, which could be identified by flow-cytometry. To verify the presence of gap-junctions, a gap-junction inhibitor, Carbenoxolone (CBX) was used to selectively block dye transfer (figure 2.8).

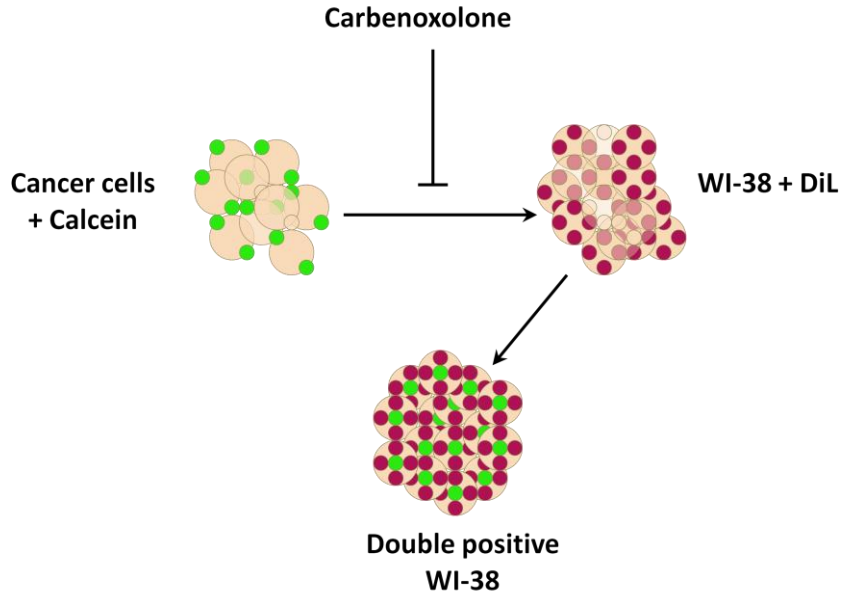

Figure 2.8 Dye transfer experiment scheme

For this analysis, 2mln cancer cells and 2mln WI-38 fibroblasts were labeled separately with 5µM fluorescent green calcein and 2,65µg/ml fluorescent red DiL respectively for 30min in the dark at 37C°. After repeated centrifugation to remove residual dye, 500 000 cells of each cell type were co-cultured in 6-well plates overnight to allow gap-junction formation. 500 000 of WI-38 stained with DiL and 500 000 of either Melmet5 or HM8 cancer cells stained with calcein were also seeded out separately in the same plate for gating control. 50µM freshly prepared Carbenoxolone was added to co-cultures when seeding for gap junction inhibition.

All samples were detached with trypsin-EDTA, washed with PBS and resuspended in 400µl of PBS with 1% BSA directly before the flow cytometry analysis.

Cell cycle analysis

To evaluate the DCA effect on Melmet5 and HM8 cells when cultured alone or with the WI-38 fibroblasts, cell cycle status of the cancer cells following the treatment was analyzedby flow cytometry. Melanoma cells and fibroblasts were plated into T25 cell culture flasks using 1:5 ratio, and incubated for 3 days to induce stroma-mediated phenotypic changes in the cancer cells. The cell cultures were then treated with 10mM and 30mM final dose of DCA for 48 hours. All samples were detached with trypsin-EDTA, washed with PBS and fixed with

100% ice-cold methanol in -20C° for at least 20min. The samples were then centrifuged to remove methanol, washed with PBS and resuspended in 400µl of PBS containing 0.15µl/1ml Hoechst 33258 for fixed cells. Hoechst 33258, fluorescent in blue, binds to DNA. The intensity of the signal acquired from a Hoechst-labelled cell depends on the total DNA amount and allows distinguishing cells that are undergoing G1/G0, S phase or G2/mitosis stage of the cell cycle. After 30min incubation at 37C° in the dark, the samples were filtered through a 35µm nylon mesh and analyzed.

Seahorse® metabolic analysis

Figure 2.9 The Seahorse® equipment used in the current study: an XFe 96 and an XFe 24 analyzer which were used with 96- and 24-well cell culture plates respectively. (picture adapted from http://www.seahorsebio.com/)

Seahorse® metabolism analyzers are designed to measure metabolic activity of the cells *in vitro* in normal culture conditions and under chemically induced stresses.

The Seahorse® analyzers measure oxygen concentration and pH of the media with sensitive fluorescence probes in close proximity to adherent cells *in vitro*. The results are presented as oxygen consumption rate (pmol O_2/min) (OCR) and exctracellular acidification rate (mpH/min) (ECAR). Each parameter reflects the extent to which the cells are utilizing either of the ATP-producing pathways: oxidative phosphorylation (OxPhos) taking place in the mitochondria or glycolysis in the cytoplasm. Oxygen is consumed in OxPhos, while glycolysis results in production and secretion of lactate into the media and decrease in pH.

The measurement is done when a cartridge which carries the fluorescent probes is lowered into the cell culture plate inside the machine and hangs only 7µm above the cells. The fluorescent probes are then excited and the emitted signal is recorded and interpreted by the software. In addition to measuring normal OCR and ECAR, seahorse analyzers offer a possibility to stress the cellular metabolic pathways with chemicals injected at predefined intervals of time into the media from 4 injection ports. Injected chemicals as well as oxygen are distributed evenly in the media when the probes move up and down between the measurements.

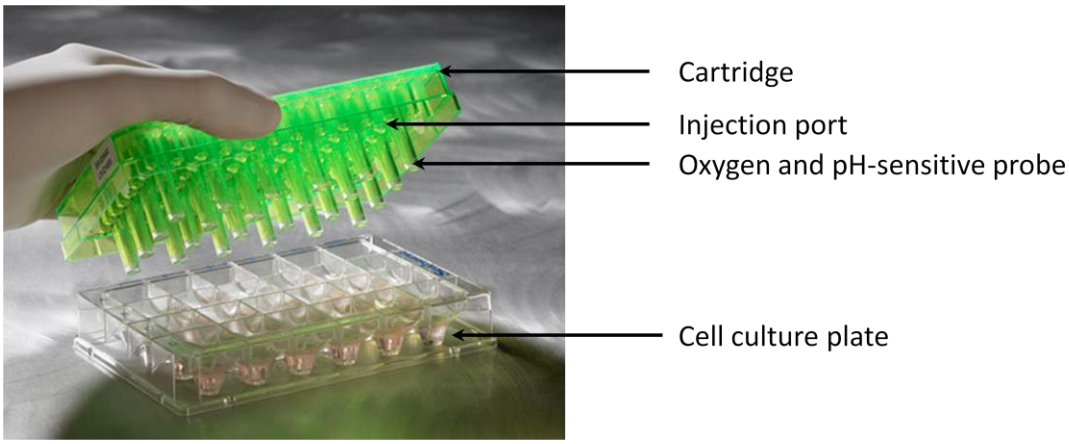

Figure 2.10 Cartridge with sensitive probes comes in close proximity with the cells in the culture plate (picture adapted from http://www.seahorsebio.com/).

Both OCR and ECAR are measured in every well of the plate making it possible to compare these two parameters and detect the "metabolic switch" – shift in the preference of either glycolysis or OxPhos under certain conditions.

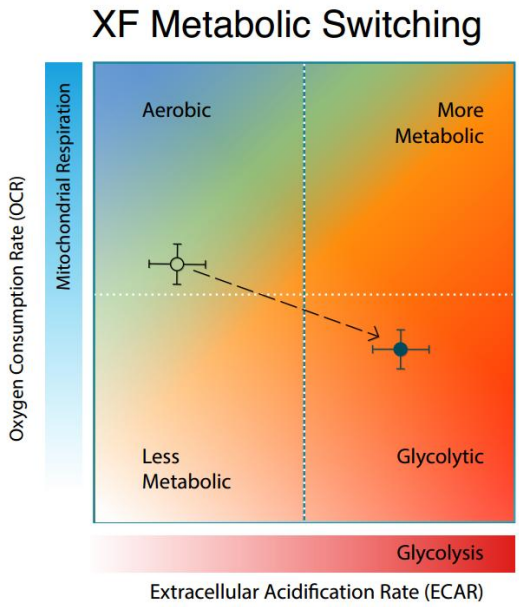

Figure 2.11 OCR versus ECAR shows metabolic preference of a cell population (picture adapted from http://www.seahorsebio.com/).

Media preparation for the analysis

Non-buffered DMEM medium with no supplements is used for the Seahorse® assays. On the day of the analysis, the medium is warmed up to 37C° and supplemented with appropriate nutrients (table 2.8) depending the stress-test that is being performed (described below). The pH is then measured and adjusted to 7.4. The medium is filtered through a 0.22µM filter before being applied to the cells.

	Final Concentration
Mito-stress test	
Glucose	10mM
Pyruvate	1mM
L-Glutamine	2mM
Glyco-stress test	
L-Glutamine	2mM

Table 2.8 Final concentrations of the nutrients added to the medium prior to analysis

Evaluation of ECAR and OCR in response to metabolic stress

Seahorse® provides two stress kits which contain a set of drugs most suitable for stressing a particular metabolic pathway: a mito-stress kit and a glycolysis stress kit. Each kit contains three drugs.

Mito-stress kit

The mito-stress kit consists of chemicals which inhibit the functions of the main components of the mitochondrial electron transport chain. This makes it possible to establish cellular stress responses and define a set of metabolic parameters (figure 2.12).

The standard setup usually includes measurements under “basal” conditions in pH-adjusted media supplemented with glucose, glutamine and pyruvate. The first injection then introduces oligomycin at an optimized concentration. Oligomycin inhibits ATP-synthase, greatly decreasing OCR. Second injection contains uncoupler FCCP at a cell-line specific concentration. Uncoupling of the electron transport chain leads to the leakage of protons from the intermembrane space of the mitochondria into the matrix and rapid reduction of oxygen. FCCP triggers dramatic increase in oxygen uptake and OCR. Finally, the third injection is a mixture of rotenone and antimycin which inhibit the first and the third complexes of the electron-transport chain respectively. As a result, the OCR is decreased to a minimum.

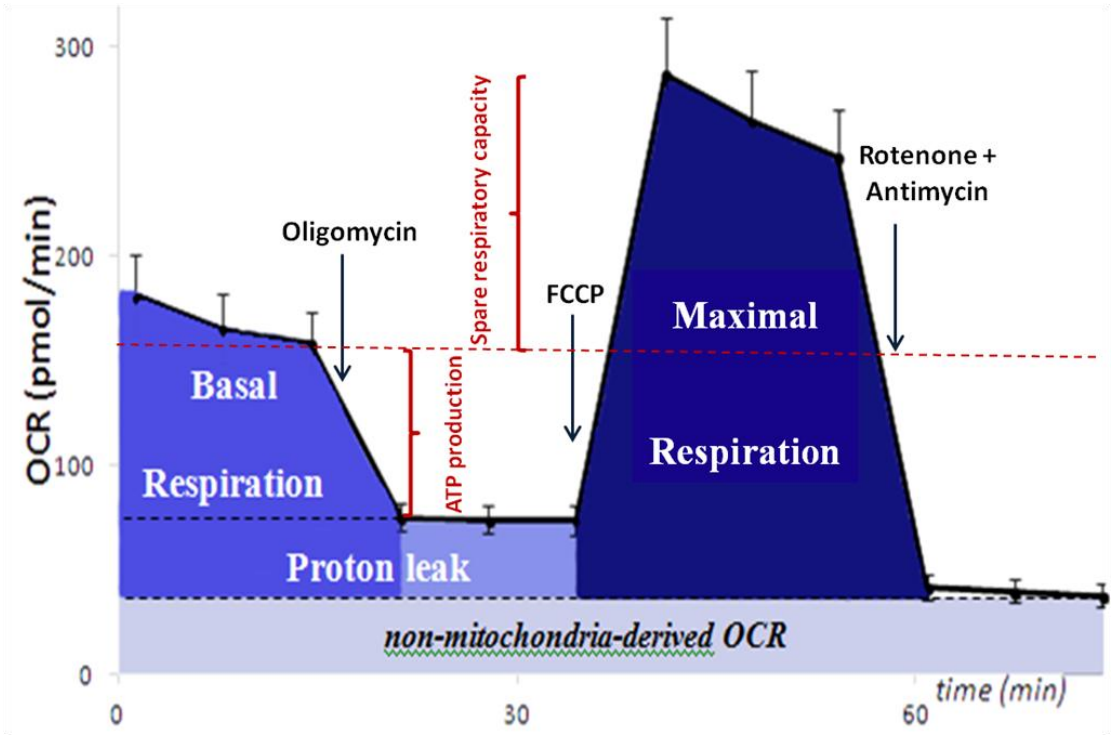

Figure 2.12 OCR in a mito-stress test. The first 3 measurements show OCR levels in normal conditions. Oligomycin decreases OCR revealing how much of the consumed oxygen is used for ATP production. FCCP increases OCR to the maximal level demonstrating maximal respiration rates. The difference between Maximal and basal respiration is defined as spare respiratory capacity. Rotenone an antimycin decrease OCR to the level of non-mitochondria-derived OCR. The difference between that level and the decrease after oligomycin injection shows proton leak.

Glycolysis-stress kit

The glycolysis stress kit is designed to create perturbations of cellular glycolysis system and determine basal and maximal rate of glycolysis of the cells. At the start of the test, the growth media is replaced with non-buffered DMEM medium supplemented with 2mM L-Glutamine, but no other nutrients (see table 2.8). After one hour incubation in such conditions cells exhaust their reserves and therefore the starting levels of ECAR are very low. The first injection introduces glucose into media which immediately increases ECAR. The second injection contains Oligomycin at the same concentration as in the mito-stress test. The resulting decrease in OCR leads to increased ECAR as a compensation mechanism which keeps the ATP production at a stable level. ECAR after oligomycin injection shows glycolytic

capacity while the difference with the basal glycolysis level reveals glycolytic reserve. The last injection introduces 2-deoxyglucose which competes with glucose molecules for the first enzyme of the glycolytic pathway – glucose hexokinase. As a result, ECAR is brought down to the minimal level of non-glycolytic acidification.

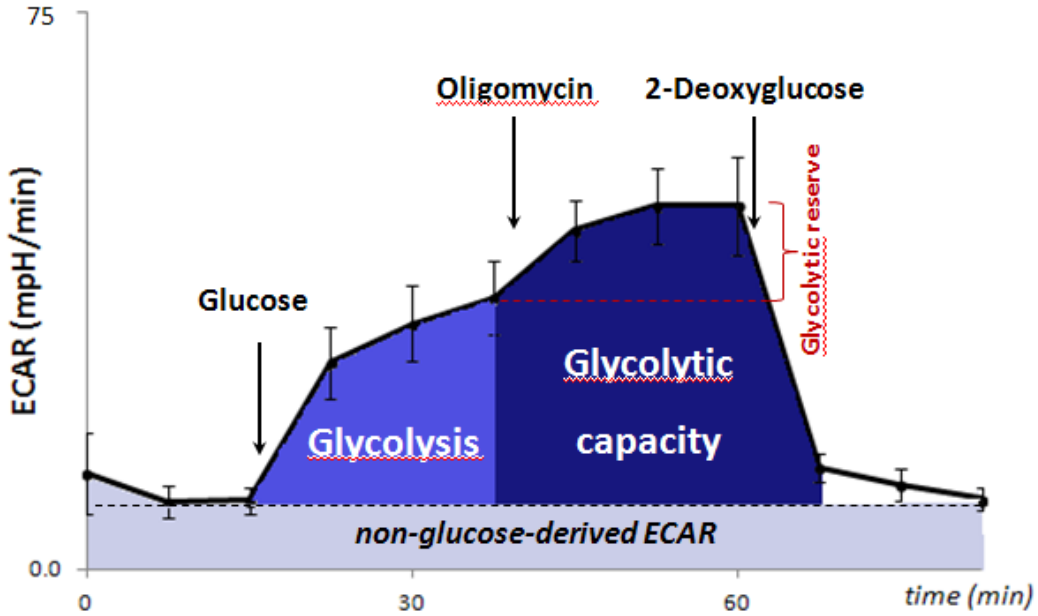

Figure 2.13 ECAR in glycolysis-stress test. Injection of glucose shows basal rate of glycolysis in absence of glutamine and pyruvate as media supplements. Oligomycin diverts cells towards glycolysis further increasing the ECAR. 2-deoxyglucose reduces ECAR to the minimal level demonstrating ECAR's dependence on glycolytic pathway and verifies non-glucose-derived ECAR.

Experimental work flow

Melmet5 were seeded in the Seahorse® plates in normal growth medium (table 2.9).

	XFe24 2 day incubation	***XFe96; 1 day incubation***	***XFe96; 2 day incubation***
Melmet5	10000 - 20000	10000 - 12000	7000

Table 2.9 Cell numbers used for seeding in metabolism assays.

Vemurafenib was added to the cells 1 day after seeding at 1μM and 4μM concentration for 24-hour incubation. For several experiments, fibroblast-derived factor rs100A4 was used to modulate metabolism of the Melmet5 cells. rs100A4 added to the cells 1 day after seeding at 2μg/ml for 48-hour incubation. 1 hour prior to analysis, the media was replaced with non-buffered DMEM medium with adjusted pH. Medium used for the mito-stress test was supplemented with glucose, pyruvate and glutamine, while medium used in the glyco-stress test did not have supplements. For two of the tests on the XFe24 analyzer, non-buffered RPMI medium was used as it was much better tolerated by the cells. However, the results produced with the use of the two different media were very similar.

Drug solutions were loaded into the injection ports of the cartridge at the following concentrations (table 2.10):

	Final Concentration
Oligomycin	1μM
FCCP	0.5 μM
Antimycin	1 μM
Rotenone	1 μM
Glucose	10mM
2-deoxyglucose	100mM
DCA	10mM

Table 2.10 Final concentrations of injected drug solutions. DCA was applied in the first injection in some of the experiments.

Optimal FCCP concentration and cell density were optimized following the guidelines provided by Seahorse® in separate experiments.

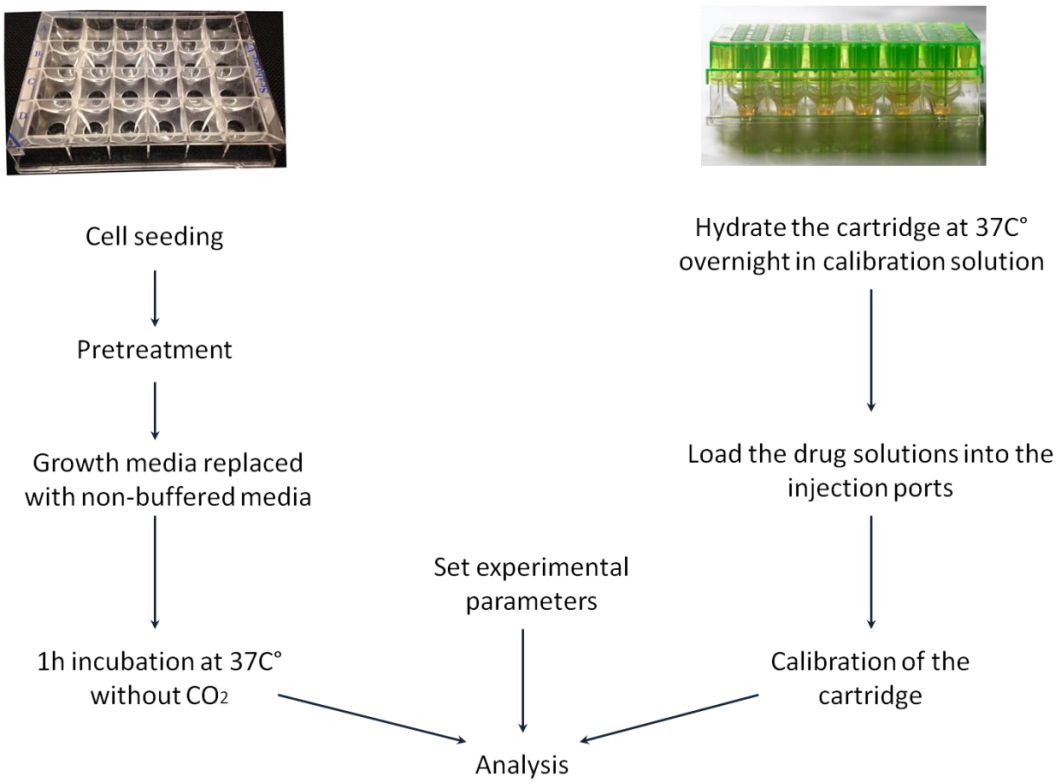

Figure 2.14 Experimental work flow in Seahorse® metabolism essays

Normalization

In 96-well plates

After analysis was completed, cell number was estimated for normalization using a double-stranded DNA intercalating fluorescent dye, pico-green. All medium was removed from the plates and replaced with 50µl per well of 4.12µl/ml solution of pico-green in TE buffer. The plates were then incubated for 30min at 37C° and the signal was measured in a plate reader using excitation of 485nm and emission of 528nm.

In 24-well plates

After the analysis was completed, cell number was estimated for normalization by measuring total protein amount. Medium was removed immediately after the end of the test. The plate was then rapidly frozen in -80C°. After thawing, cells were lyzed in each well with a mixture of lysis buffer and protease inhibitor. After 30min incubation on ice, samples were collected by vigorous pipetting and centrifuged for 15min. The protein concentration in the supernatant was assessed by nano-drop analyzer.

Results

1. Generation of the GFP-luc labeled melanoma cell lines.

Previously in the group, the effect of stromal cells on vemurafenib respose was investigated in one melanoma cell line, Melmet5 (figure 1.7). To expand the panel of cell lines, three additional melanoma cell lines, HM8, HM19 and Patient-3-pre were genetically modified to stably express green fluorescent protein (GFP) and luciferase (Melmet5 was modified previosuly in the group). Luciferase allowed evaluation of the melanoma cell viability in co-culture with the non-labeled WI-38 fibroblasts. GFP expression made it possible to separate melanoma cells from the stromal cells in flow-cytometric studies and to purify them using fluorescence-activated cell sorting (FACS) for further analysis.

Stable expression of GFP-luciferase fusion protein (GFP-luc) was achived by lentiviral transduction of melanoma cells as described in materials and methods. Subsequently, the cells with the strongest expression of GFP-luc were sorted by FACS (figure 3.1, A) and used to establish the cell cultures (figure 3.1, B).

A **B**

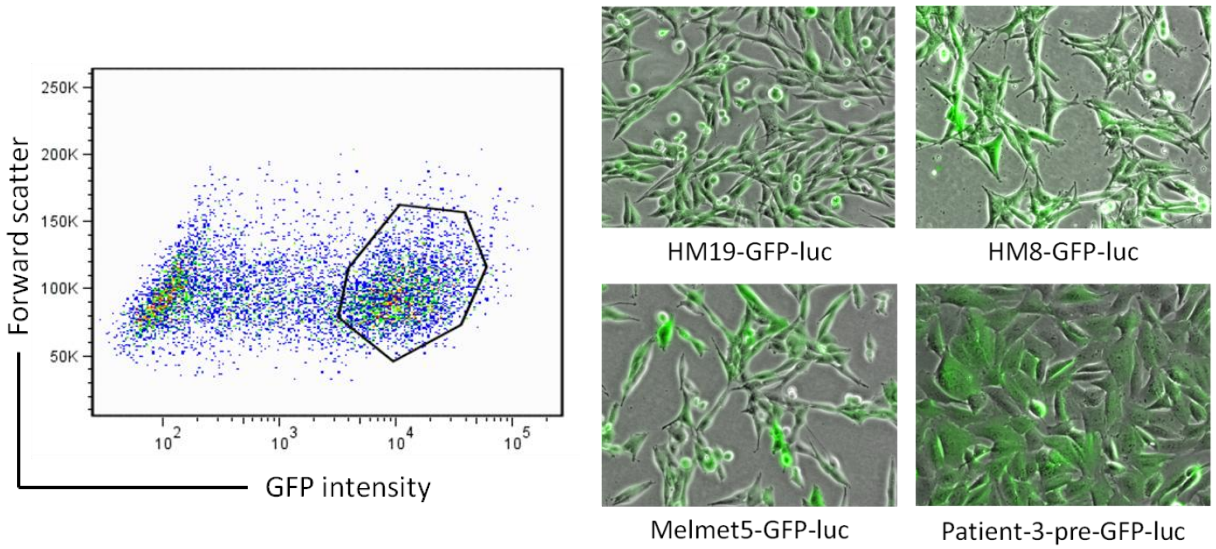

Figure 3.1 FACS of the GFP-positive melanoma cells. **A.** HM8 green positive cells (gated), separated from GFP-negative cells based on fluorescence intensity. **B.** Overlaid phase contrast and green fluorescent pictures of the four GFP-luc labeled melanoma cell lines involved in the study.

2. Lung fibroblasts reduce sensitivity to vemurafenib in melanoma cells

In the present study, 3 different culturing systems were used to explore the effect of lung fibroblasts on melanoma cell response to vemurafenib. 1) contact-based co-cultures, where melanoma cells and the fibroblasts were able to adhere to each other and establish cell-cell contacts; 2) trans-well inserts, where melanoma cells in the inserts were separated from the fibroblasts by a semi-permeable membrane, limiting interactions to soluble factor exchange; 3) conditioned media, which was collected from the densely populated culture flasks with fibroblasts, filtered and applied to the melanoma cells in combination with vemurafenib.

Co-cultures with fibroblasts are less sensitive to vemurafenib

All of the melanoma cell lines involved in the current study carry a BRAF*V600E* mutation which makes them sensitive to BRAF inhibition. In order to investigate whether the presence of stromal cells alters melanoma cells' response to vemurafenib, the cancer cells were grown either in mono-cultures or co-cultures with the WI-38 fibroblasts and treated with increasing doses of vemurafenib. As shown in figure 3.2, in all of the melanoma mono-cultures, the viability was strongly decreased after 72 hours of vemurafenib treatment. However, in co-cultures, the viability of the cancer cells was higher, reflecting their lower sensitivity to the drug. This indicates that the fibroblasts induce partial protection of the melanoma cells against targeted therapy. This was particularly obvious in the HM8 cell line where the presence of fibroblasts almost completely abolished effects of the vemurafenib treatment.

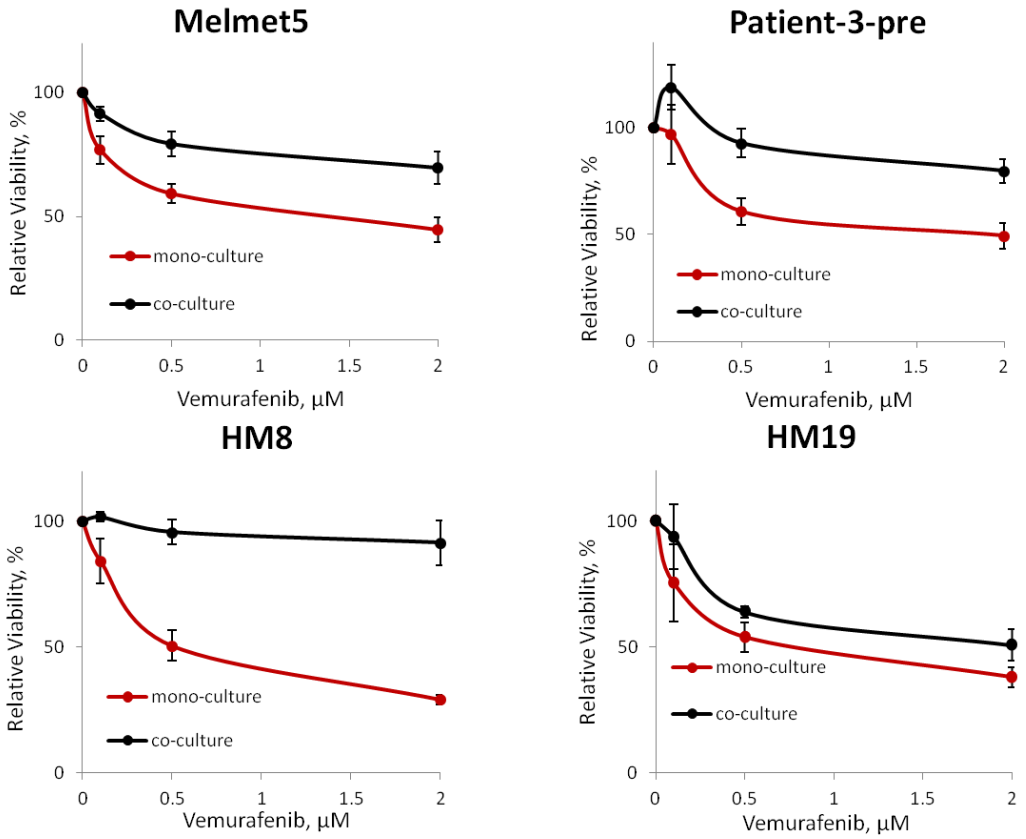

Figure 3.2 Viability of the melanoma cell lines in mono-cultures or co-cultures with the WI-38 fibroblasts after 72h treatment with vemurafenib as measured by the bioluminescence assay. Error bars represent SEM from three independent experiments. Significant at 0,5 and 2µM doses, p≤0.05 in all, apart from HM19, where p=0.1; unpaired t-test.

Absence of the tumor-stroma cell contacts eliminates protection against vemurafenib

To investigate whether a similar protection effect could be observed in the absence of direct contacts between tumor and stromal cells, we used the trans-well culturing system with inserts. A permeable membrane eliminates direct connections between melanoma and stromal cells, however, the 0.4µM large pores allow free exchange of the medium and secreted growth factors. We selected two melanoma cell lines for this analysis: Melmet5 and HM8. After 72h incubation with different doses of vemurafenib, both Melmet5 and HM8 showed almost no difference in viability between wells that did and did not contain fibroblasts (figure 3.6). This indicates that the partial protection, which we have observed

previously in co-cultures, relies heavily on cell-cell contacts between the tumor and the stromal cells.

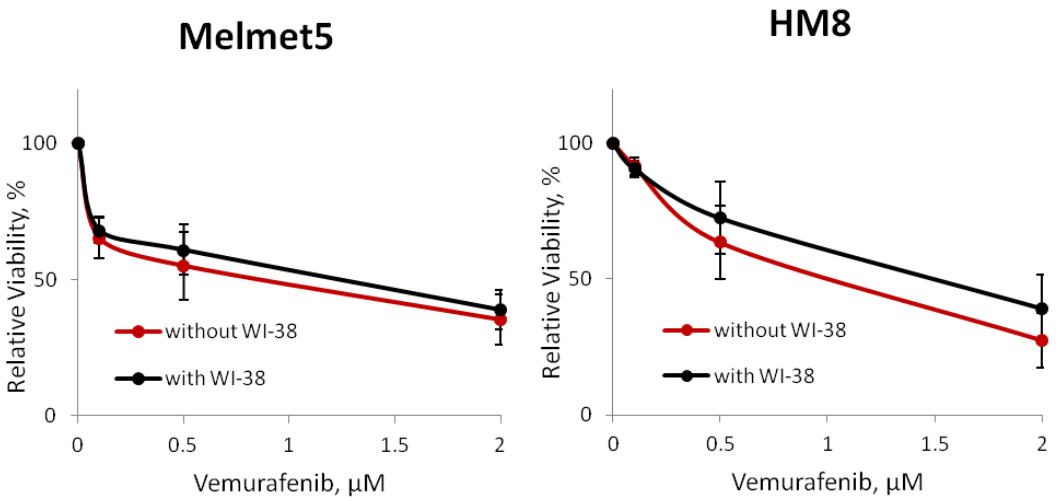

Figure 3.3 Viability of the Melmet5 and HM8 cells in the inserts of the transwell-plates after 72h treatment with vemurafenib measured by the MTS assay. The bottom wells contained either respective melanoma cells (without WI-38) or the WI-38 fibroblasts (with WI-38). Error bars represent SEM from 4 independent experiments. Non-significant in all doses; unpaired t-test.

Fibroblast-conditioned media (CM) induced partial protection

It has been shown that the fibroblast-derived soluble factors in the medium elicit protection of melanoma cells against vemurafenib [45]. We verified those findings in our system by treating mono-cultures of the HM8 cells with vemurafenib in 1:1 diluted CM collected from a densely populated flask with WI-38 fibroblasts. We consider that such CM contains highly concentrated fibroblast-derived soluble factors. Fresh RPMI and HM8-conditioned media were used as controls. 72h treatment resulted in higher viability of the HM8 cells which have received WI-38 conditioned medium compared to the controls (figure 3.4). However, the resulting viability of approximately 50% was lower than observed in the contact-based co-cultures, where the viability was close to 100% (figure 3.2).

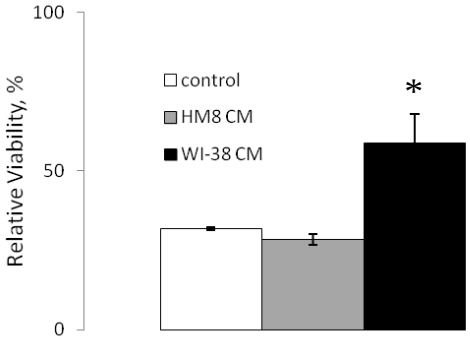

Figure 3.4 Viability of the HM8 cells after 72h treatment with 2μM vemurafenib in the conditioned medium (CM) from WI-38 fibroblasts or HM8 diluted 1:1 with the RPMI growth medium in which the HM8 cells had been seeded. Fresh RPMI medium was used for control. Error bars represent SEM from three individual experiments. *- significant, p=0.04; unpaired t-test.

3. Biological mechanisms involved in the fibroblast-mediated protection against vemurafenib

The role of HGF-c-Met signaling

The first published study that reported fibroblast-mediated protection from vemurafenib, revealed the role of HGF, secreted by the fibroblasts, that stimulates the c-Met receptor on the melanoma cells [45]. We therefore investigated whether cMet signaling is potentiated in Melmet5 and HM8 cells upon their interaction with the fibroblasts. For a positive control, we stimulated the MDA-MB-231 breast cancer cells, which are known to express the c-Met receptor [83], with recombinant HGF. We were able to see weak phosphorylation of the c-Met in the MDA-MB-231 cells in response to HGF (figure 3.4 A, red arrow). In Melmet5 and HM8 cells, however, no visible bands corresponding to the phospho-cMet were present either with or without HGF stimulation (figure 3.4 A). Analysis of the Melmet5 and HM8 cells collected from the inserts, in which they were exposed to the fibroblast-secreted factors with and without vemurafenib, did not show an increase in phospho-cMET. On the contrary, the phospho-cMET bands seemed to be weaker in the samples where the fibroblasts were present (Figure 3.4 B), although the intensity of the bands was very low. These results do not conclusively demonstrate c-Met receptor activation in the melanoma cells in response to the HGF or the fibroblast-derived soluble factors under tested conditions.

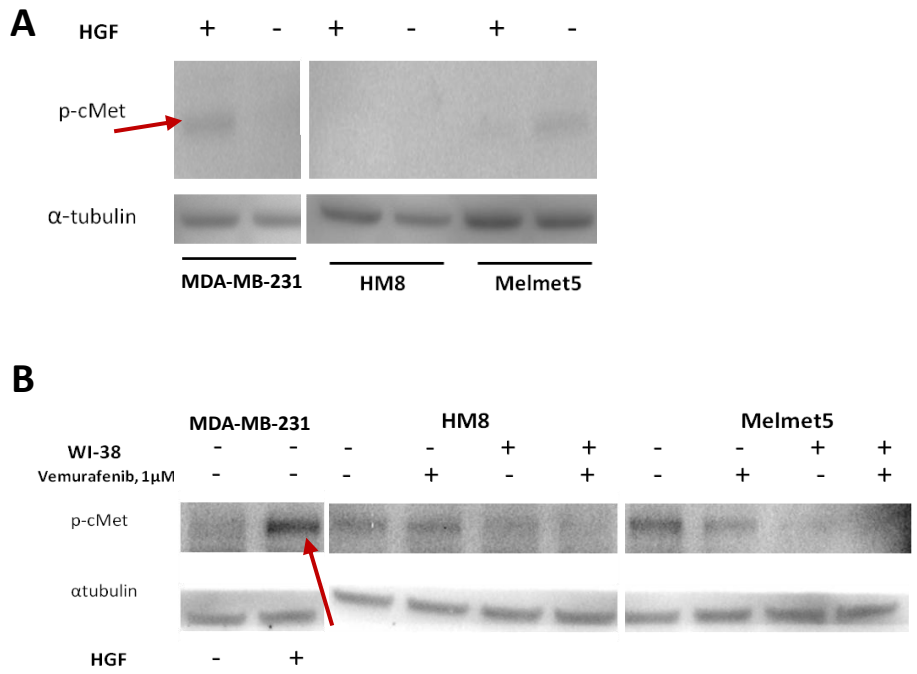

Figure 3.4 Phosphorylation of the c-Met receptor in Melmet5 and HM8 in response to either A) HGF, or B) WI-38 derived soluble factors. Breast cancer cell line (MDA-MB-231 stimulated with HGF was used as a positive control (red arrows). **A.** The level of phospho-c-Met after 10min treatment with 100ng/ml HGF following 28h starvation with serum-free medium. **B.** The level of phospho-c-Met in HM8 and Melmet5 cells collected from the inserts of the transwell-plates containing either WI-38 fibroblasts or the respective melanoma cells in the bottom well and cultured for 48h. 1μM vemurafenib was applied for 24h.

Fibroblasts activate the mTORC1-regulated pathway in melanoma cells via cell-cell contacts

Activation status of the mTORC1 pathway has been shown to predict response of the melanoma cells to vemurafenib. It was reported that mTORC1 is inactive in the melanoma cells which have a strong response, while resistant cells keep mTORC1 active despite the treatment with vemurafenib [55]. To explore the mTORC1 status in melanoma cells cultured with and without the fibroblasts we measured the level of phosphorylated ribosomal protein S6 (pS6) that is positively regulated by mTORC1 using flow-cytometry. As shown previously in the group (see figure 3.5), the level of pS6 was significantly reduced after treatment with vemurafenib in both Melmet 5 and HM8 mono-cultures, but not in co-cultures, where the pS6 level was significantly higher. As seen from figure 3.5 A (produced by Vasiliauskaite K.),

in the treated monocultures, the peak corresponding to pS6 level shifted to the left compared to the peak representing the non-treated cells. In the treated co-cultures, however, there were two melanoma cell subpopulations (two peaks in pink filled histogram): those with the reduced level of pS6 and those that maintained high level of pS6. In the Melmet 5 and HM8 cells collected from the inserts, however, the level of phospho-S6 was significantly reduced in all treated melanoma cells, despite the presence of fibroblasts (figure 3.5 B). This can be seen from the two overlapping peaks (filled histograms, clearly shifted to the left from the non-treated controls) representing the pS6 levels in the treated melanoma cells with and without the fibroblasts in the bottom. (figure 3.5 B). This was confirmed by western blotting (figure 3.5 C), where the intensity of the pS6 bands was equally low in all treated samples compared to non-treated controls. We also analyzed the levels of phospho-ERK, a downstream kinase of the MAPK pathway. As expected, ERK phosphorylation was reduced in the treated samples. Interestingly, the presence of fibroblasts in the untreated samples led to the reduction in pERK compared to the control sample. This was not further investigated.

Taken together, these findings indicate that in absence of the direct cell-cell contacts with the fibroblasts, the level of pS6/mTORC1 activity is reduced by vemurafenib. In contrast, in the contact-based co-cultures, the level of pS6/mTORC1 activity remains high in a big fraction of cells. This further compliments the observation that the cell-cell contacts have a more pronounced influence on the melanoma cells with respect to the mTORC1 pathway than the soluble factors.

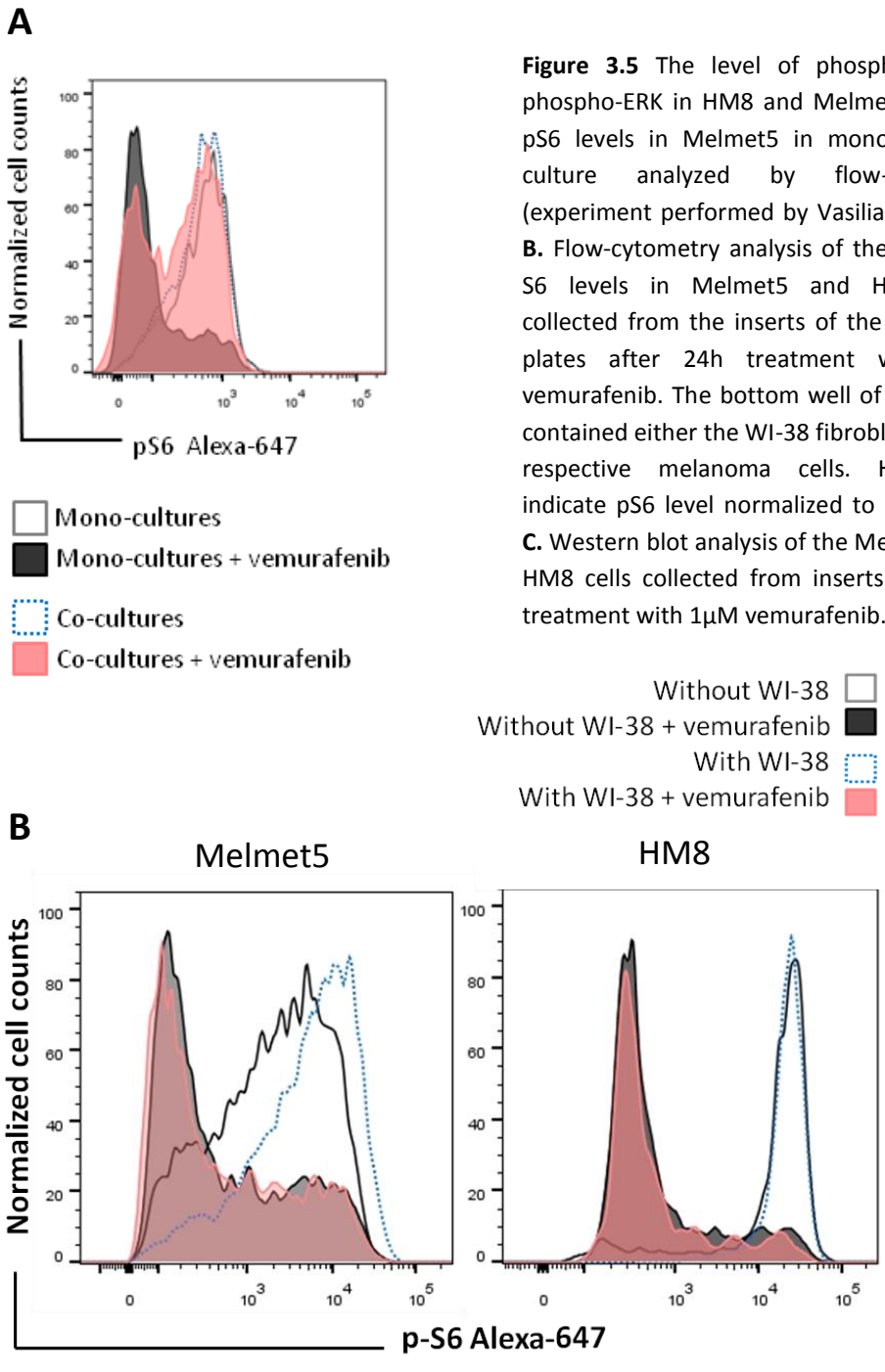

Figure 3.5 The level of phospho-S6 and phospho-ERK in HM8 and Melmet5 cells **A.** pS6 levels in Melmet5 in mono- and co-culture analyzed by flow-cytometry (experiment performed by Vasiliauskaite K.) **B.** Flow-cytometry analysis of the phospho-S6 levels in Melmet5 and HM8 cells, collected from the inserts of the trans-well plates after 24h treatment with 1µM vemurafenib. The bottom well of the plates contained either the WI-38 fibroblasts or the respective melanoma cells. Histograms indicate pS6 level normalized to cell count. **C.** Western blot analysis of the Melmet5 and HM8 cells collected from inserts after 24h treatment with 1µM vemurafenib.

The role of mTORC1 in the stroma-mediated protection

To validate involvement of the mTORC1 in the stromal protection, we applied an mTORC1 inhibitor, everolimus, together with vemurafenib and measured the viability of the melanoma cells in mono- and co-cultures. As shown in figure 3.5, the protection induced by the stromal cells (highlighted with red lines next to the bars) was either reduced (in HM8 and Patient-3-pre cells) or completely abolished (in Melmet5 and HM19 cells) when vemurafenib was used in combination with everolimus. This demonstrates that mTORC1 suppression combined with vemurafenib treatment, reduces melanoma cell survival.

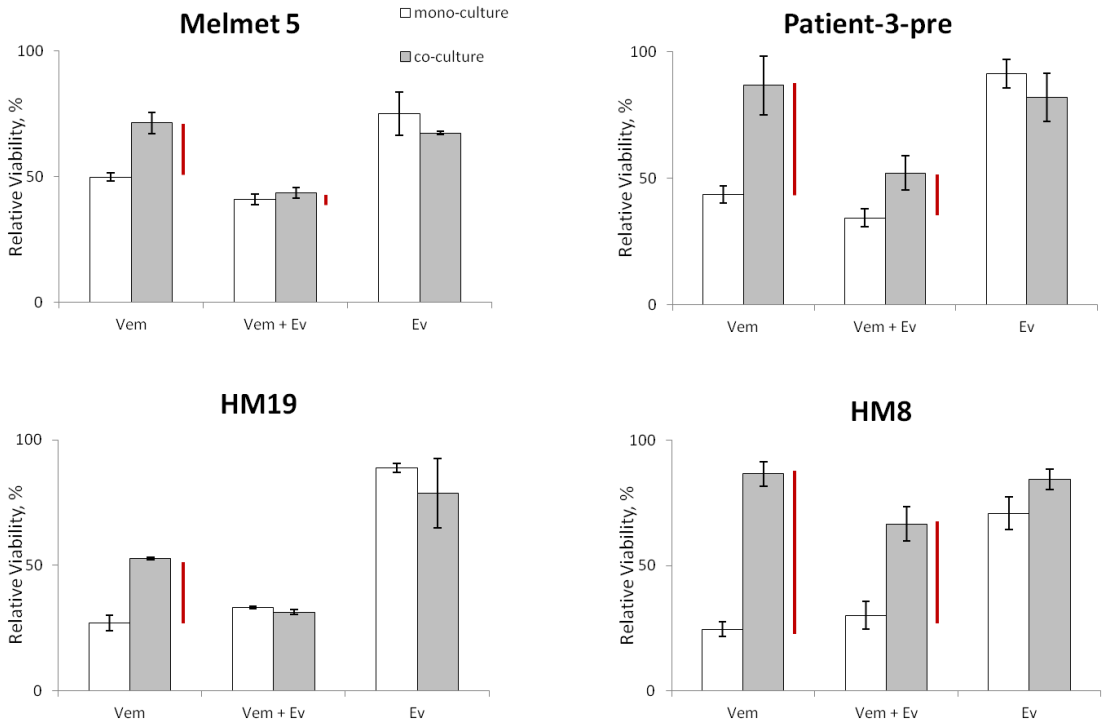

Figure 3.6 Viability of the four melanoma cell lines in mono-cultures versus co-cultures with WI-38 fibroblasts after 72h treatment with either 2µM vemurafenib (Vem), 5nM everolimus (20nM for Melmet5) (Ev), or a combination (Vem + Ev), measured by the bioluminescence assay. The red lines show the fibroblast-mediated protection effect, i.e. difference in viability of the melanoma cells in co-cultures compared to the mono-cultures. Error bars indicate standard deviations from 3 technical replicates in a single experiment.

Melanoma cells adhere to the fibroblasts in co-culture

Given the importance of direct cell-cell contacts for stromal protection, we characterized the capacity of the four melanoma cell lines to adhere to fibroblasts. In order to analyze this, we added melanoma cells to the confluent layer of fibroblasts, incubated them for 1h, washed

away non-adherent melanoma cells and scored the adherent fraction. We observed that 60 to 90% of the melanoma cells were adherent to the fibroblasts (figure 3.7), which shows that the melanoma cells are able to attach to the lung fibroblasts. The adhesion capacity, however, did not correlate with the stromal protection efficacy seen in figure 3.2.

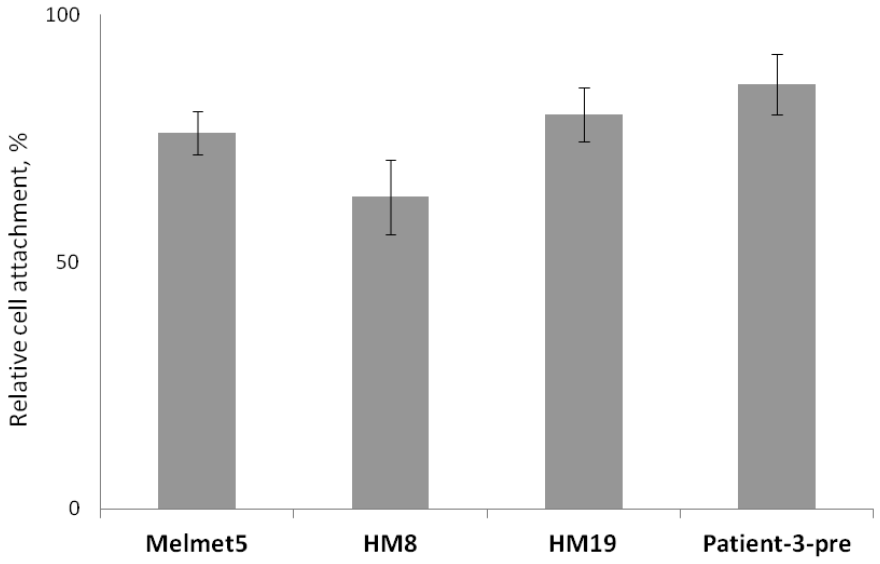

Figure 3.7 Attachment of the melanoma cells to the WI-38 fibroblast monolayer after 1h incubation as measured by the bioluminescence assay. Error bars represent standard deviation from 6 technical parallels in a single experiment.

The role of gap-junctions in the stroma-induced protection

The observation that the melanoma cells physically interact with fibroblasts via adhesion prompted further investigation into the role of the intercellular connections, specifically gap junctions that have been previously linked to SMDR [20]. Here we investigated whether gap-junctions contribute to the communication between melanoma cells and the WI-38 fibroblasts. First, we tested whether the Melmet5 and HM8 cells establish gap-junction connections to the fibroblasts in co-culture, using the dye-transfer method. We stained the melanoma cells and the fibroblasts with two different fluorescent dyes – calcein, fluorescent in green, and DiI, fluorescent in red. We then incubated the cancer cells together with the fibroblasts overnight and observed transfer of the gap-junction permeable calcein from melanoma cells to the fibroblasts by flow-cytometry. The presence of gap junctions was demonstrated by a population of red fibroblasts which gained green colour i.e. was double

positive. Both Melmet5 and HM8 showed a degree of dye transfer (figure 3.8), however it was a lot more pronounced in the co-culture with HM8 cells, rather than Melmet5, as can be seen from a large population of green fibroblasts in the case of HM8 (figure 3.8)

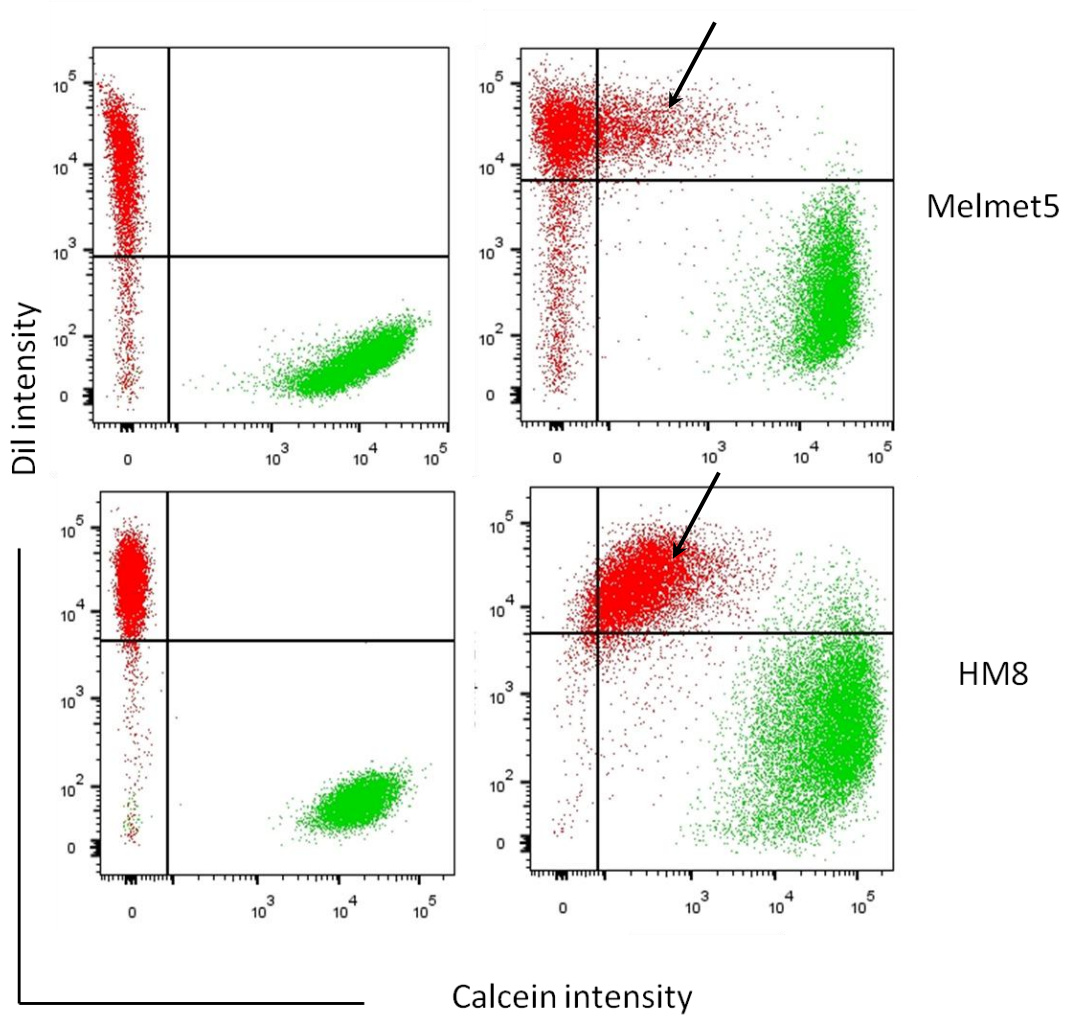

Figure 3.8 Evidence of gap junctions between fibroblasts and melanoma cells. Dot blots illustrating dye transfer from calcein-labeled melanoma cells (green dots) to Dil-stained fibroblasts (red dots) after over-night co-incubation. **Left panel**: Overlay of the separately stained and incubated melanoma cells with high calcein intensity (green) and fibroblasts with high Dil intensity (red), used for setting the gates. **Right panel**: transfer of calcein from the melanoma cells resulted in a shift of the red fibroblast population to the right, indicating the presence of double-positive cells (black arrows).

Having found evidence of gap-junctions between the melanoma cells and the fibroblasts, we next attempted to block them using two available gap-junction inhibitors – carbenoxolone (CBX) and chlordane. We tested them to find out the dose which does not impair cell viability. Both inhibitors showed little to no toxicity in small doses (figure 3.9 A). We chose to proceed with 50μM CBX in order to block gap-junctions. To validate CBX effect on gap junction inhibition, we cultured calcein-labeled melanoma cells with the red fibroblast as described above, in the presence of CBX. Comparing the size of the double-positive population of fibroblasts with and without the CBX, we found a considerable reduction after incubation with both Melmet5 and HM8. This can be seen from comparison of green and red histograms in figure 3.9 B), where a clear shift to the left in the presence of CBX was observed. However, gap junction inhibition was incomplete, since some of the fibroblasts retain calcein, i.e. some of the fibroblasts were double positive after inhibition with CBX. This can be seen in co-cultures with HM8 in particular, where cells treated with CBX (red peak) still had considerably stronger calcein intensity than in the control mono-cultures (black peak).

Finally, we set out to examine whether the inhibition of gap-junctions with CBX would diminish the stroma-mediated protection in the melanoma co-cultures with the fibroblasts. We were unable to perform the experiment on Melmet5 cells due to technical difficulties. The difference in viability between HM8 cells in mono- versus co-cultures was unaffected by the presence of CBX, and the same stroma-induced protection was observed (figure 3.9 C). Taken together these data do not exclude a possibility that the melanoma cells and the fibroblasts communicate via gap-junctions. However, in a non-toxic concentration, gap junction inhibitor CBX failed to reduce the stoma-mediated protection.

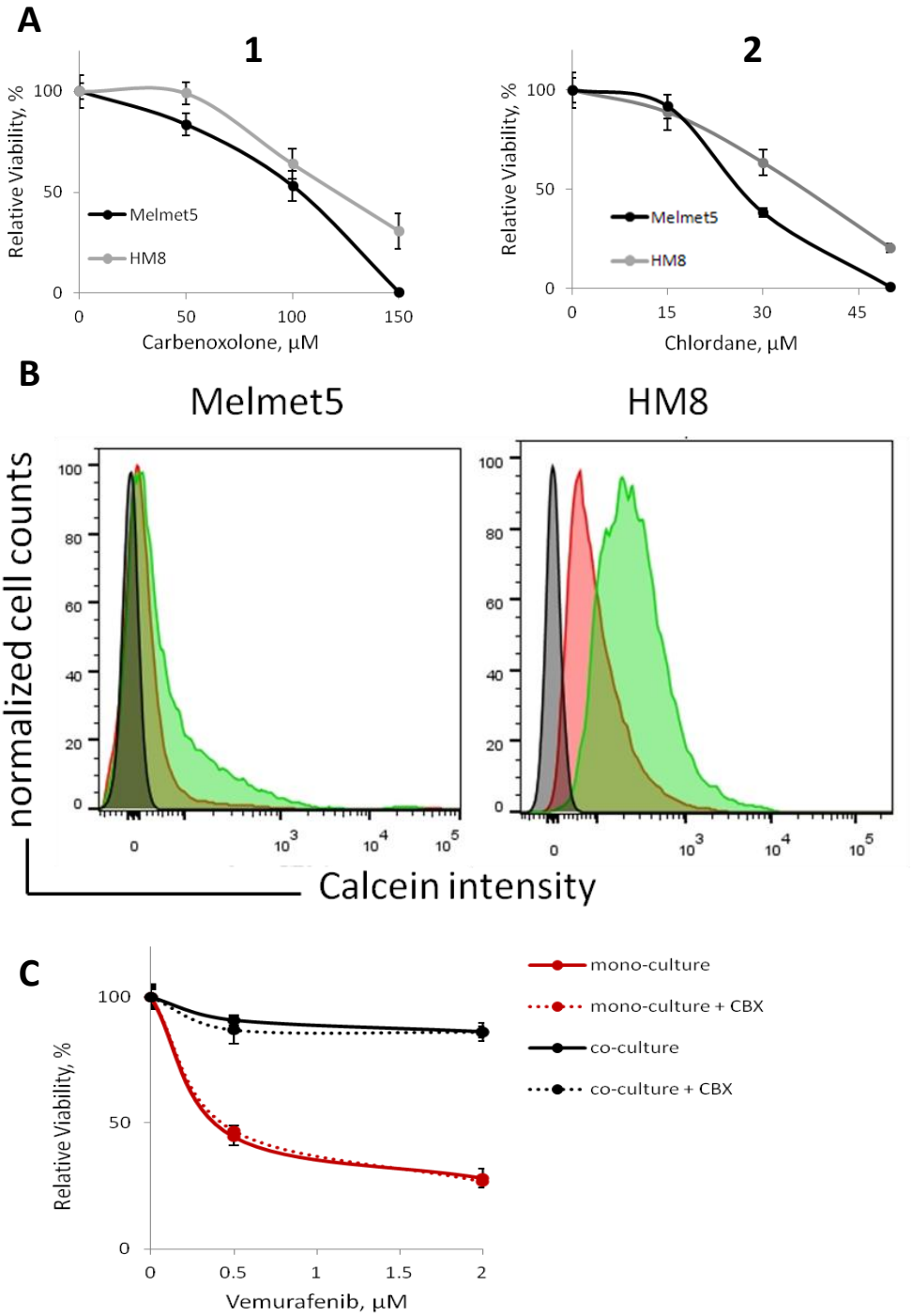

Figure 3.9 Effect of gap-junction inhibition by CBX **A.** Viability of the Melmet5 and HM8 cells following 72h incubation with gap junction inhibitors 1) carbenoxolone (CBX) or 2) chlordane measured by the bioluminescence assay **B.** Dye-transfer inhibition by CBX demonstrated as a shift in the calcein intensity of the fibroblasts, where black peak represents control Dil-labeled cells in mono-culture; green peak represents fibroblasts in co-culture with no CBX; and red – fibroblasts in co-culture treated with CBX. **C.** Viability of the HM8 cells either in mono-culture or co-culture with the WI-38 fibroblasts after 72h treatment with vemurafenib with or without 50µM CBX measured using the bioluminescence assay. Error bars represent standard deviations from 5 technical parallels in a single experiment.

4. Fibroblasts modulate transcriptional phenotype in melanoma cells

To evaluate how fibroblasts influence the molecular phenotype of the melanoma cells, we measured expression of genes previously shown to be associated with the so-called proliferative differentiated and invasive de-differentiated phenotype [46]. It has been recently discovered that the invasive phenotype (defined as $MITF^{high}/AXL^{low}$) is associated with resistance to vemurafenib [57, 58]. Expression levels of DKK3, THBS1 and AXL, which encode the Dickkopf-related protein 3, Thrombospondin 1 and Tyrosine-protein kinase receptor respectively, were used as markers of the invasive i.e. resistant phenotype [56]. Conversely, expression of the melanocyte-specific transcription factor MITF-M and its targets MLANA and TYR, was used as a label of the differentiated i.e. vemurafenib sensitive phenotype.

Melanoma cells derived from the co-cultures with fibroblasts and purified by FACS had decreased expression of the differentiation genes, particularly in Melmet 5 (figure 3.10 A). At the same time, the invasive signature genes were strongly up-regulated (figure 3.10 B).

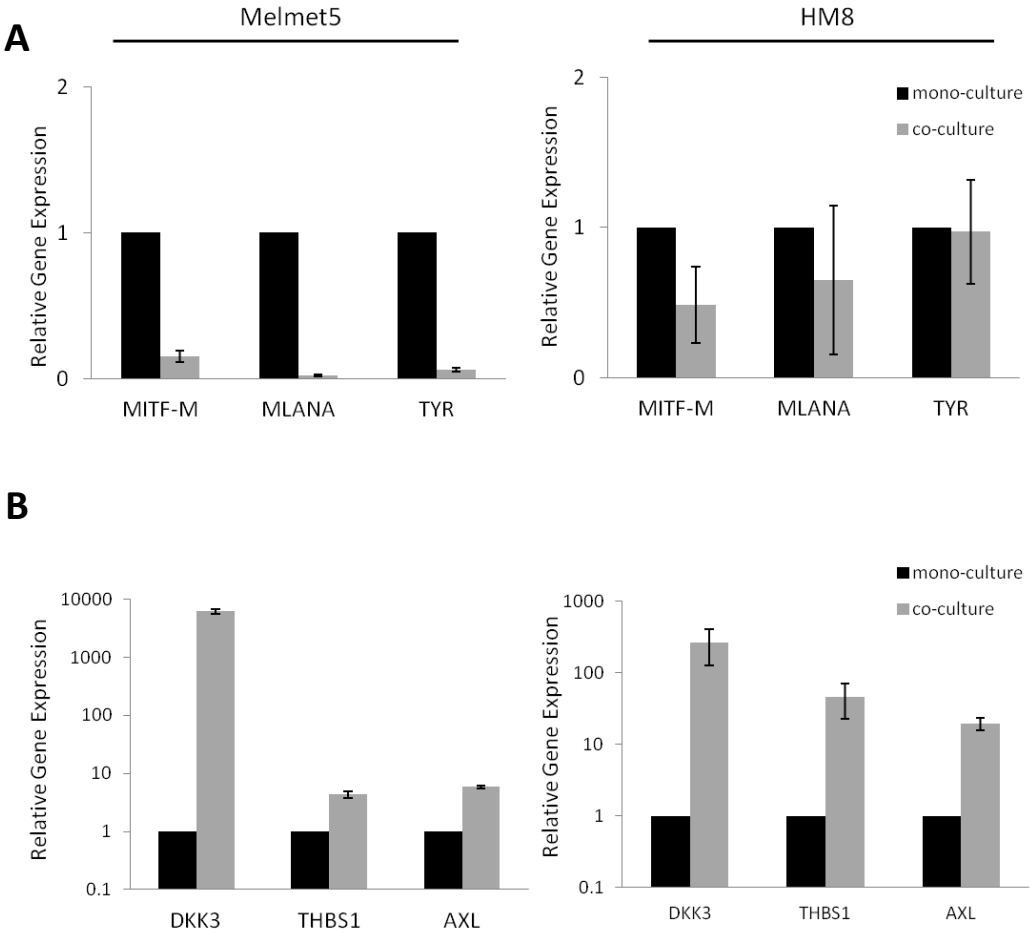

Figure 3.10 Relative gene expression levels in Melmet5 (left panel) and HM8 (right panel) cells in mono- and co-cultures, separated from fibroblasts by FACS, and analyzed by real time PCR. **A.** Relative expression of the melanocyte-specific differentiation genes in cancer cells derived from co-cultures compared to mono-cultures, where the expression levels were set to 1. **B.** Relative expression of the invasion-phenotype genes in melanoma cells derived from co-cultures compared to mono-cultures, where the expression levels were set to 1. Error bars in A and B represent standard error from three replicates. Significant in all Melmet5 samples and AXL in HM8. $p \leq 0.01$; unpaired t-test.

For comparison, we measured expression levels of the same genes in the melanoma cells collected from the inserts with or without the fibroblasts in the bottom. As shown in the figure 3.11, the fibroblast-induced gene expression changes in the melanoma cells were minimal in the absence of cell-cell contacts. Together, these data indicate that the WI-38 fibroblasts induce an invasive, de-differentiated phenotype in melanoma cells when cell-cell contacts are established. Fibroblast-derived soluble factors failed to induce such a phenotypic shift, which highlights the importance of cell-cell contacts in this context.

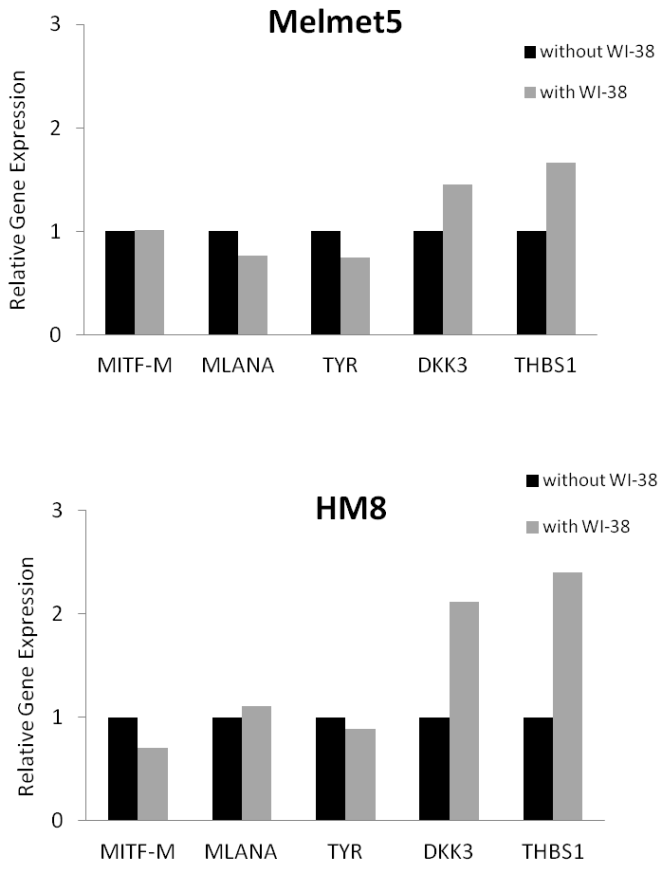

Figure 3.11 Relative gene expression levels in Melmet5 and HM8 cells collected from the inserts of the trans-well plates. The bottom well contained either respective melanoma cells (without WI-38) or the fibroblasts (with WI-38). Gene expression was normalized to the expression in samples without WI-38.

WI-38 fibroblasts alter expression of metabolism-related genes in melanoma cells via cell-cell contacts

Given an association between invasive phenotype, MITF and glycolysis, as described in the literature, [67, 69], we aimed to determine whether contact based-co-culture with the WI-38 fibroblasts modified expression of metabolism-associated genes. We evaluated the expression of PGC1α – the main regulator of mitochondrial activity in the cells, and LDHA – a critical enzyme involved in the final step of glycolysis. We observed that melanoma cells from the co-cultures strongly down-regulated PGC1α, while LDHA expression was up-

regulated (figure3.12). Both Melmet5 and HM8 cells demonstrated minimal changes of PGC1α and LDHA after being cultured in the inserts, however. This indicates that the presence of fibroblasts induces alterations in the expression of metabolism-related genes in melanoma cells, but this largely relies on direct cell-cell contacts.

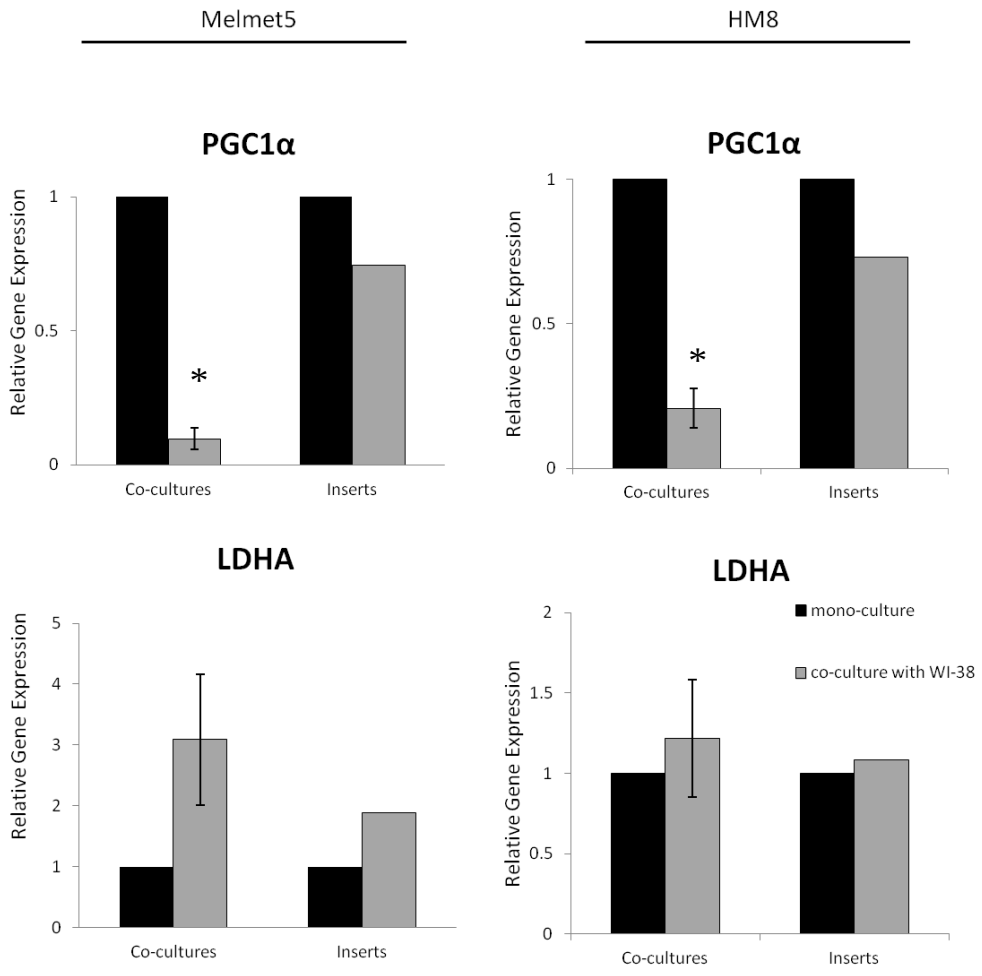

Figure 3.12 Relative expression levels of PGC1α and LDHA genes in Melmet5 and HM8 as measured by real-time PCR. Melmet5 and HM8 cells were cultured either as mono-cultures or co-cultures with the WI-38 fibroblasts for 72h and then separated using FACS (labeled co-cultures). Melanoma cells collected from the inserts of the trans-well plates, which contained either respective melanoma cells (without WI-38), or WI-38 fibroblasts (with WI-38) in the bottom well (labeled inserts). The error bars in the co-cultures group represent standard error from three independent experiments. *- significant. p≤0.05; unpaired t-test.

5. Using DCA to target the melanoma cells with altered metabolism

Changes in metabolism can be best studied by the Seahorse™ technology, which allows precise evaluation of the cellular metabolic activity *in vitro* in real time (see materials and methods for detailed protocol). It can be applied to the melanoma cells in order to establish their metabolic preference as well as reactions to various stimuli.

DCA induces strong metabolic shift from glycolysis to OxPhos in Melmet5

As we have observed previously, contact-based co-culture with the WI-38 fibroblasts induced invasive phenotype associated with increased expression of glycolysis-regulator LDHA in melanoma cells (figure 3.10). We proposed that this phenotypic switch makes the melanoma cells rely more heavily on glycolysis for ATP production, which may result in greater sensitivity to glycolysis inhibition. To test this, we employed DCA, which is a potent metabolic modulator that strongly up-regulates the use of the OxPhos pathway by blocking its inhibitor.

First, we validated the DCA effect on melanoma cell metabolism. To this end we acutely treated the Melmet5 cells with DCA and scored OCR and ECAR using the Seahorse™ technology. DCA injection led to a rapid increase of oxygen consumption (figure 3.19 A) while simultaneously down-regulating aerobic glycolysis as measured by the extracellular acidification rate (figure 3.13 B).

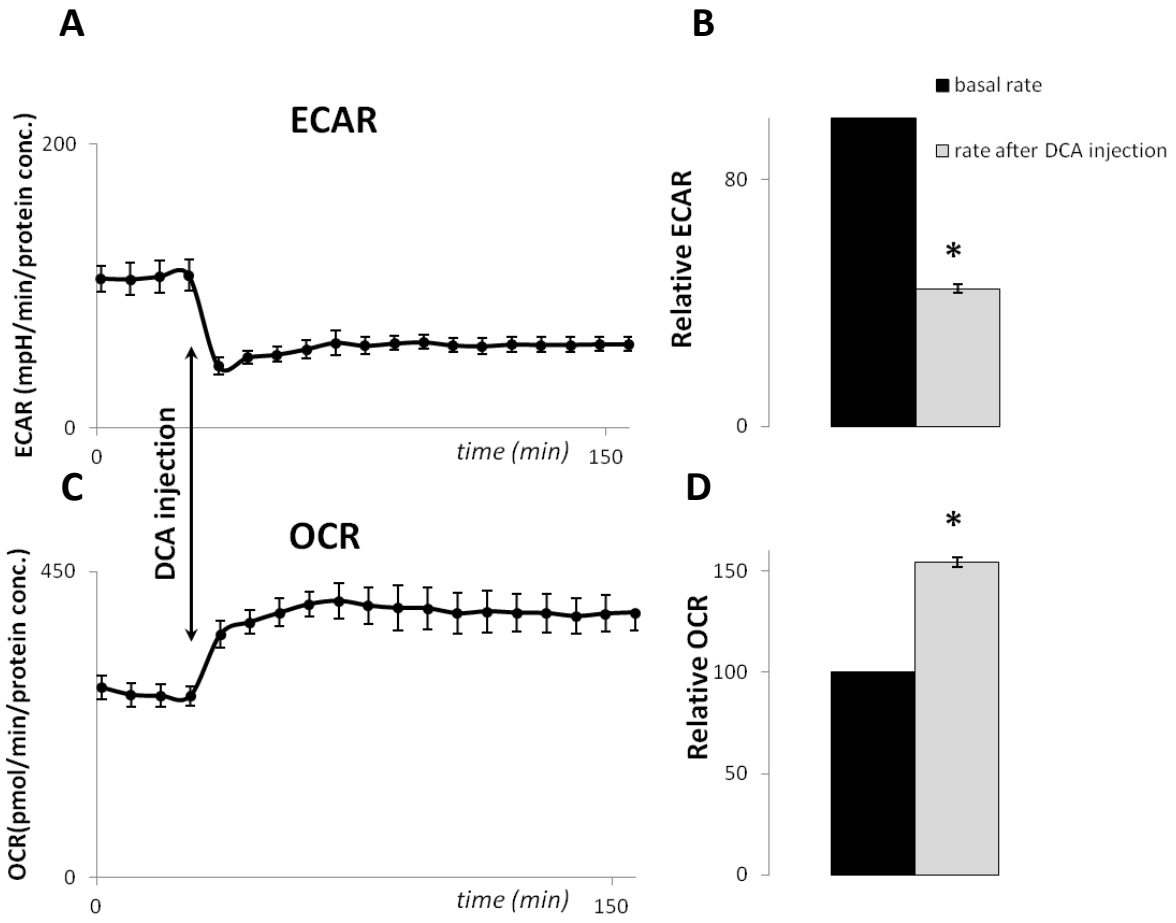

Figure 3.13 DCA treatment modulates metabolic profile of Melmet5. **A.** ECAR prior to and after the DCA injection. Graph from a representative experiment. **B.** ECAR in Melmet5 after acute treatment with 10mM DCA compared to the basal ECAR. **C.** OCR prior to and after the DCA injection. Graph from a representative experiment. **D.** OCR in Melmet5 after acute treatment with 10mM DCA compared to the basal respiration rate. The data were normalized to the basal respiration rate of control sample which was set as 100%. In A and C the error bars stand for standard deviations in 4 technical parallels. In B and D the error bars represent SEM in 4 separate experiments. *- significant. p≤0.0005; unpaired t-test.

Next, we cultured the melanoma cells alone and together with the WI-38 fibroblasts for a period of 72 hours to induce the stroma-mediated phenotypic switch. We then treated the cultures with increasing doses of DCA for 48 hours. HM8 cells did not demonstrate any differences in viability between mono- and co-cultures under these conditions. The Melmet5

cells, however, showed a dramatic difference where the viability in co-cultures was greatly reduced (figure 3.14).

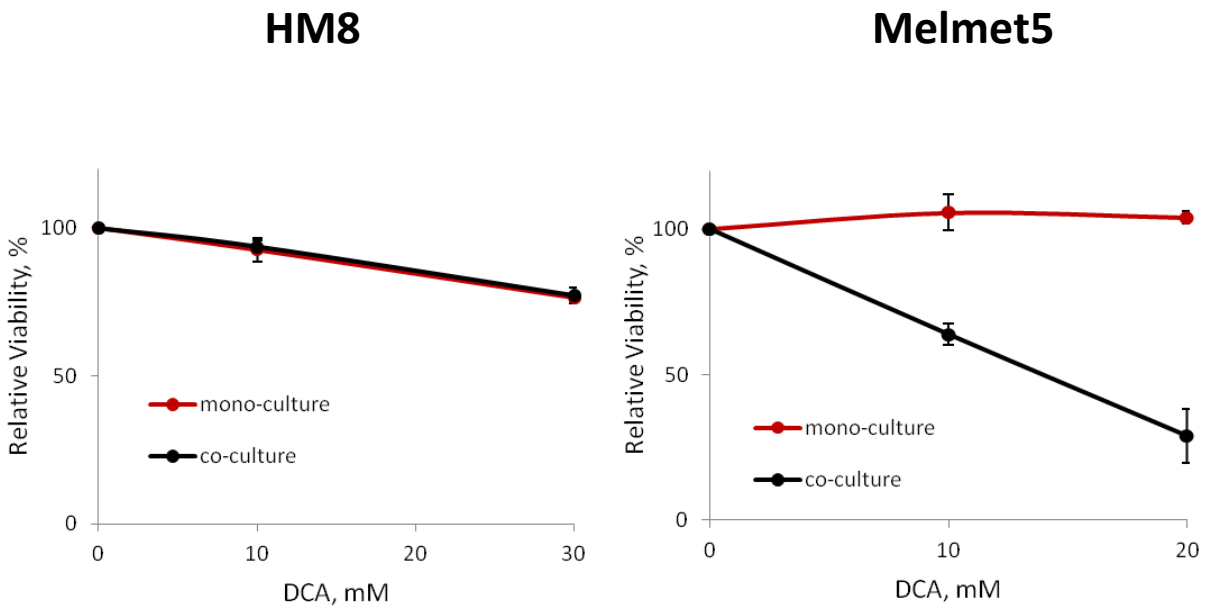

Figure 3.14 Viability of the HM8 and Melmet5 cells in mono-cultures or co-cultures with WI-38 fibroblasts after 72h followed by 48h of treatment with DCA measured by the bioluminescence assay. Error bars represent SEM from the four separate experiments. Significant in Melmet5, both doses. p=0.001; unpaired t-test.

We further verified increased sensitivity of cells in co-culture to DCA by analyzing cell cycle progression in Melmet5 and HM8. The cells were cultured for 72 hours prior to the 48hrs-DCA treatment, when the cells were collected, stained with the DNA-binding dye Hoechst 33258 and analyzed by flow cytometry. We found that in Melmet5, DCA treatment induced cell cycle arrest at G2 phase, which was more pronounced in co-cultures than in mono-cultures (figure 3.15). We performed three separate experiments which showed a similar trend, however here we include the one in which the difference was the strongest. This verifies that melanoma cells from co-cultures are more vulnerable to metabolic disruptions by DCA.

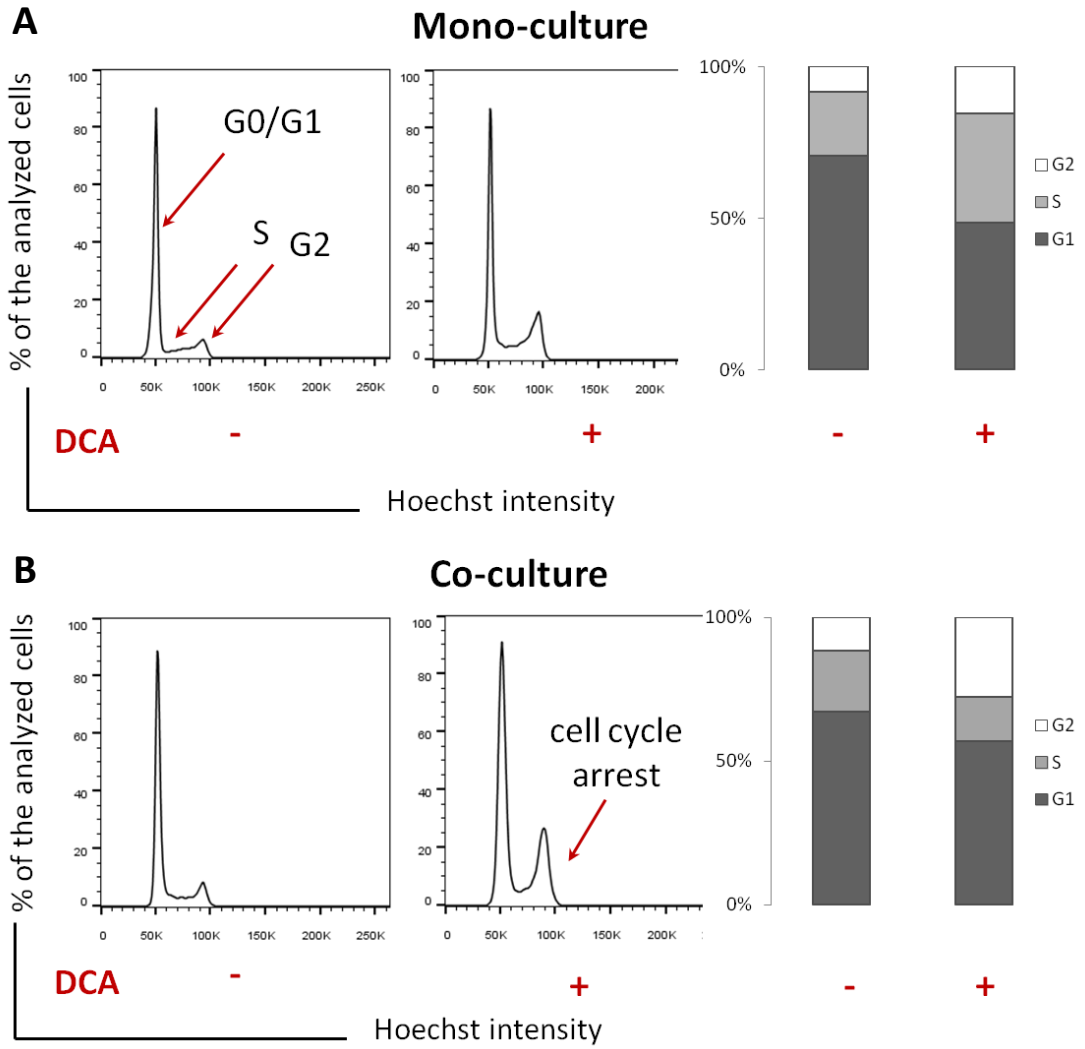

Figure 3.15 Cell cycle analysis in the Melmet5 cells in mono- and co-culture treated with DCA. Cells were cultured for 72 hours before being treated with 30mM DCA for 48 hours. **A.** Cell cycle in the mono-cultures. **B.** Cell cycle in the co-cultures. Increase in the second peak corresponds to the cell cycle arrest, which is more evident in co-cultures. Bar graphs in A and B show fractions of the analyzed cells undergoing different stages of the cell cycle (data from the analyzed histograms).

6. Vemurafenib and everolimus induce metabolic changes in the melanoma cells

It has been shown by others that therapeutic agents influence cancer cell metabolism [67]. Based on that, we tried to evaluate changes in the energy metabolism triggered by vemurafenib and everolimus in the Melmet5 melanoma cells.

Vemurafenib treatment modifies expression of metabolism-related genes

To explore how vemurafenib affects expression of metabolism-related genes, we measured expression of the previously mentioned PGC1α and LDHA in Melmet 5 and HM8. We discovered that in both cell lines, PGC1α expression was strongly up-regulated, suggesting increased preference of the OxPhos pathway in the vemurafenib treated cells. In contrast, expression of the LDHA was not significantly changed in either Melmet5 or HM8 cells (figure 3.16).

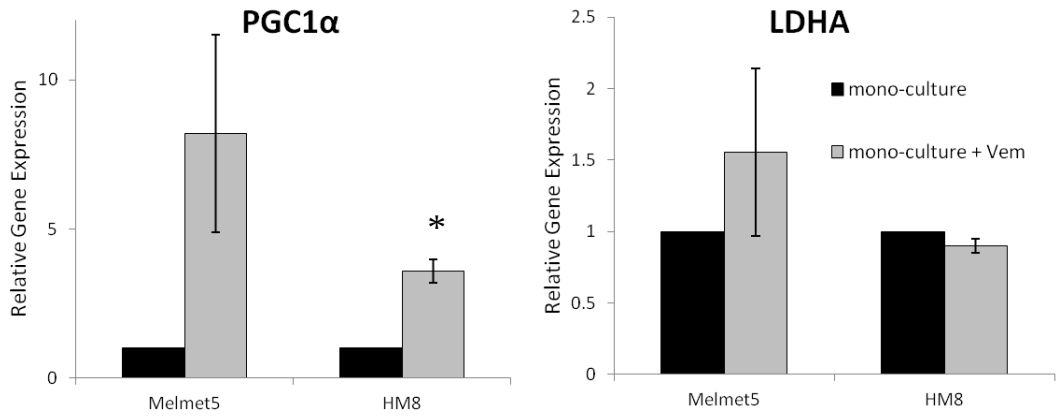

Figure 3.16 Expression levels of PGC1α and LDHA in Melmet5 and HM8 cells after 1μM Vemurafenib treatment for 24h. Error bars indicate standard errors from three parallels. *- significant. p=0.002; unpaired t-test.

Vemurafenib decreased lactate production and oxygen consumption rates in the Melmet5 cells

We further used Seahorse™ analyzers to test whether treatment with vemurafenib affects the metabolic functions – extracellular acidification rate (ECAR) and oxygen consumption rate (OCR), reflecting glycolytic and mitochondrial activity, respectively. Vemurafenib was applied for one day prior to the test and led to a decrease in basal ECAR, as well as ECAR after glyco-stress (described in materials s and methods) indicating down-regulation of the aerobic glycolysis (figure 3.17). The decrease in ECAR was not dose-dependent.

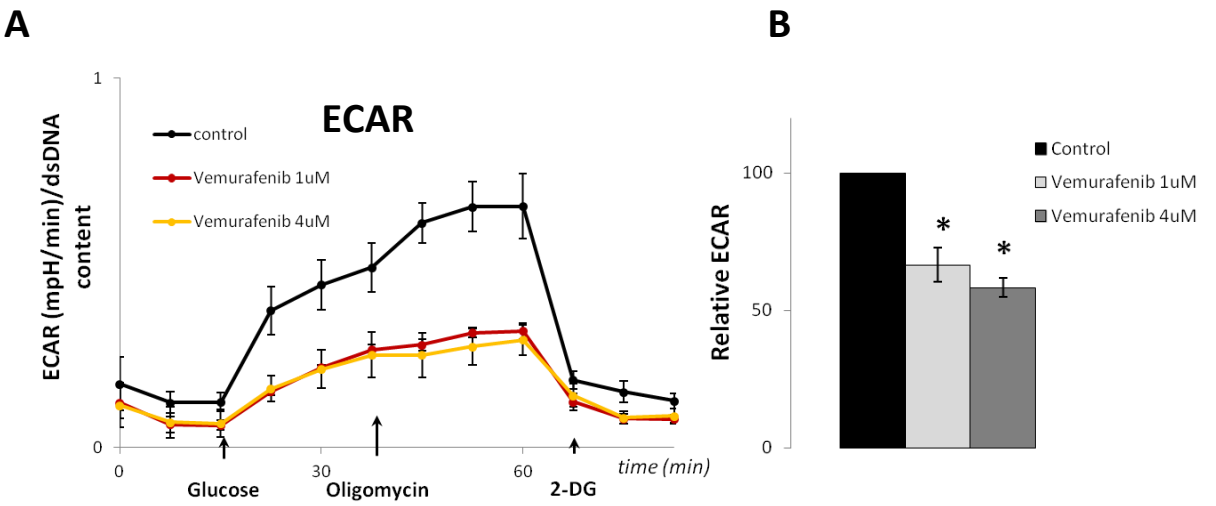

Figure 3.17 Metabolic parameters reflecting glycolytic activity in Melmet5 cells with and without treatment with 1µM and 4µM vemurafenib for 24h. **A.** Graphs from a representative experiment showing changes in ECAR in the control and vemurafenib-treated Melmet5 cells during the glyco-stress test. Error bars stand for standard deviations from 6 technical replicates in the representative experiments. **B.** Basal ECAR. Error bars represent SEM in three separate experiments, normalized to the untreated control, which was set as 100%. *- significant. p≤0.005; unpaired t-test.

In addition to triggering a reduction in aerobic glycolysis, vemurafenib also down-regulated basal OCR (figure 3.18 A, B), indicating a decrease of the mitochondrial activity. Vemurafenib-triggered reduction in both ECAR and OCR indicates an overall shift to a less metabolically active state.

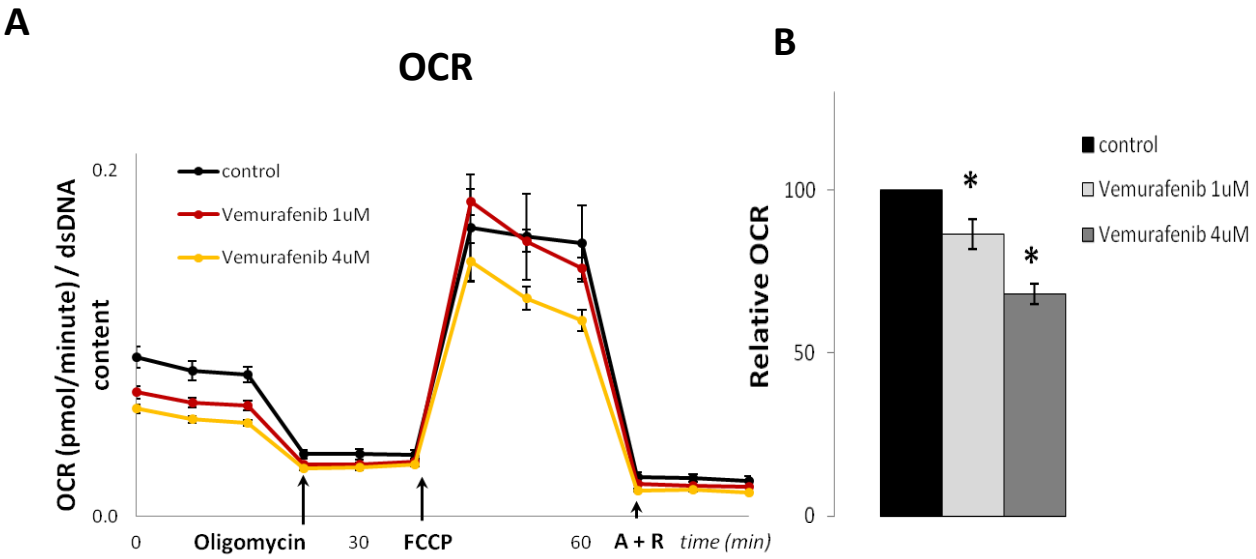

Figure 3.18 Metabolic parameters reflecting mitochondrial activity in Melmet5 cells with and without treatment with 1µM and 4µM vemurafenib for 24h. **A.** Representative experiment showing changes in OCR in the control and vemurafenib-treated Melmet5 cells in response to the chemically induced mitochondrial stress. Error bars stand for standard deviations from 6 technical replicates in the representative experiment. **B.** Basal OCR prior to the oligomycin injection. Error bars represent SEM in three separate experiments, normalized to the untreated control, which was set as 100%. *- significant. $p \leq 0.05$; unpaired t-test.

Despite the basal OCR reduction in Melmet5 cells (figure 3.18), the vemurafenib treatment resulted in a strong increase of the spare OCR, after addition of the uncoupler FCCP (figure 3.19). This effect was reproduced in three independent experiments and may indicate that BRAF inhibition leads to increased ability to utilize the OxPhos pathway in the treated cells.

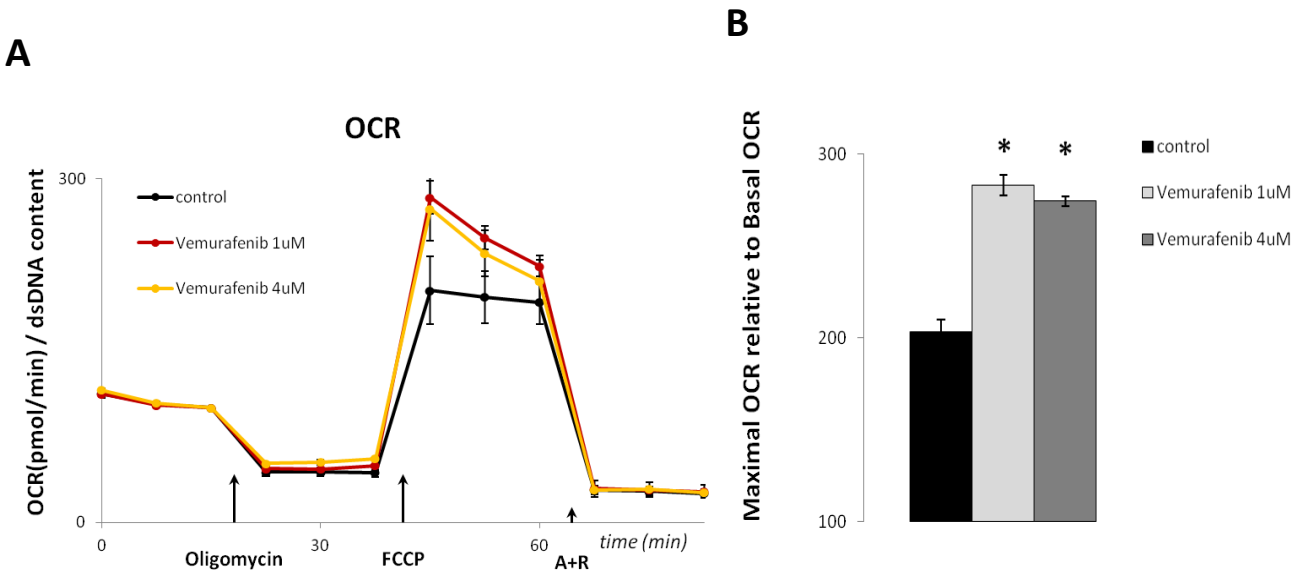

Figure 3.19 Vemurafenib treatment modulates spare respiration capacity in Melmet5. **A.** Data from the representative experiment (shown in figure 3.13), where the OCR values were normalized to the basal OCR in each sample. **B.** Spare respiration capacity after FCCP injection in Melmet5 treated with 1μM and 4μM vemurafenib for 24h. Error bars show SEM in three separate experiments. *- significant. p≤0.0005; unpaired t-test.

Everolimus effect on aerobic glycolysis and oxygen consumption in Melmet5 cells

mTORC1 has been cited as a regulator of glycolysis in several contexts. However, its role in metabolic alterations in melanoma remains poorly understood. Here we investigated the effect of everolimus on oxygen consumption and lactate production in the Melmet5 cells. The cells were treated with 5nM everolimus for 24 hours prior to running the Seahorse™ assay. We found that OCR was reduced, similarly to the effect observed after treatment with vemurafenib. ECAR levels, however, were almost unchanged (figure 3.20), suggesting that everolimus has a stronger influence on mitochondrial activity than glycolysis.

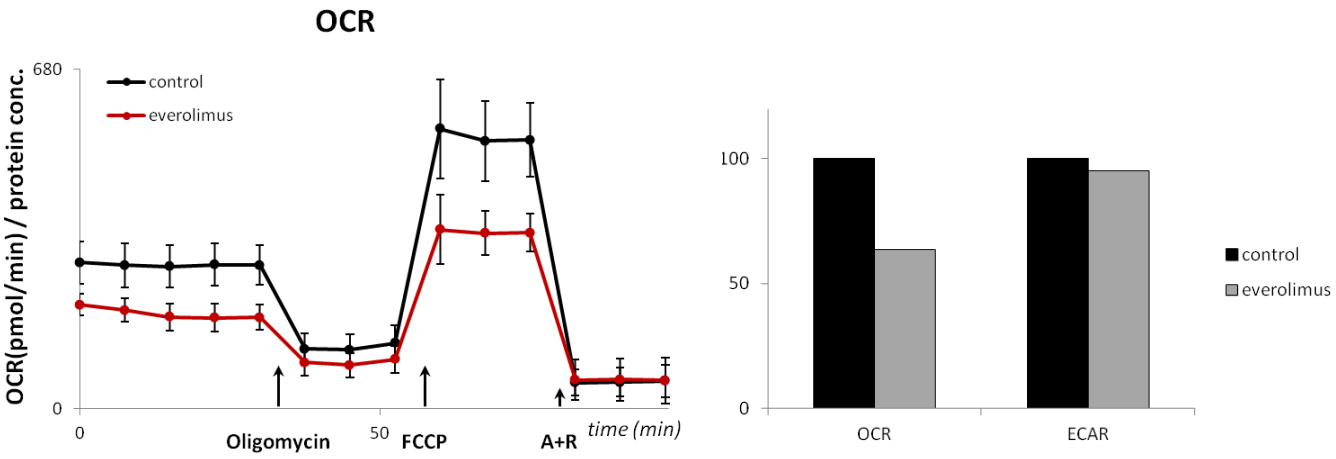

Figure 3.20 Everolimus treatment modulates oxygen consumption rate in Melmet5. **A.** OCR in Melmet5, which were treated with 5nM everolimus for 24 hours prior to the test. **B.** OCR and ECAR basal levels (5th measurement, prior to the injection of oligomycin) in the everolimus-treated samples compared to untreated controls. Data from 4 technical parallels in a single experiment.

Discussion

Stroma-mediated vemurafenib resistance in melanoma

Discovery of the targeted therapy against kinases of the MAPK pathway has been a huge step forward in the treatment of metastatic melanoma. However, MAPK inhibition, although efficient, is almost never long-lasting. Research in the field of malignant melanoma has since focused on the nature of the drug resistance and the role of the intricate cross-talk between the cancer cells and the microenvironment.

Here we show that stromal fibroblasts potently protect melanoma cells from vemurafenib enhancing the survival of treated cancer cells. This goes in concert with several of the previous reports showing stromal role in protection against vemurafenib and other targeted agents [45, 84]. These studies have implicated stroma-secreted soluble factors in this protection. Confirming these findings, we show that concentrated conditioned media derived from the fibroblasts does elicit a degree of protection on the HM8 melanoma cells. However, direct proximity of the tumor and stromal cells appeared to be a more important requirement as the absence of the intercellular contacts almost completely abolished the protective effect. Supported by the evidence that adhesion to the other cells and the extracellular matrix is important for survival and proliferation, this finding pointed towards cell-cell connections as a possible mechanism for vemurafenib resistance. Cell contacts between the cancer and the stromal cells have been shown to be important for every step of the disease progression [19, 22, 23] and here we show that they continue to be important for cancer cell survival after treatment.

The mechanism of the cell contact-mediated protection remains not fully understood, however. Gap junctions have been previously described as mediators of protection against chemothepary in melanoma brain metastasis [20, 21]. Here, we could not find the evidence of their involvement in our model system, though our data does not exclude this possibility completely. Other studies where inhibition of gap-junctions resulted in reduced SMDR, used higher concentrations of inhibitors (i.e. 100µM CBX [20, 21]), that in our hands were severely toxic for the melanoma and the stromal cells alike. We therefore had to use a smaller dose (50µM CBX) which induced only a partial gap-junction blockade. This might be the reason

why we could not see a reduction in the stroma-mediated protection. The other explanation is that the gap-junctions are not involved in SMDR, while other proteins, for instance integrins, coordinate pro-survival signaling between the stromal cells and the cancer cells enabling protection. Indeed, integrins and integrin-related signaling were shown to be involved in the tumor-stroma crosstalk [85]. A recent publication by Eishu Hirata and colleagues demonstrated that the fibroblast-mediated protection of the melanoma cells against vemurafenib is maintained via β1-integrins and that inhibition of β1-integrins abolishes such protection [86]. It would therefore be interesting to investigate the role of integrins in our model.

Fibroblasts induce mTORC1 activation

We found that in mono-cultures that are sensitive to vemurafenib, S6 phosphorylation was significantly reduced, suggesting diminished mTORC1 activity after the treatment. This corresponds to other studies which showed that the vemurafenib-sensitive cells suppress mTORC1 activation under the influence of vemurafenib treatment [55]. However, as others in the group have demonstrated, this suppression was significantly impaired in the co-cultures, leading to higher levels of pS6 as a direct consequence of mTORC1 activity in the presence of fibroblasts. Here we also show that pS6 level remains low if the treatment is performed in the trans-well setup. Based on these results we propose that the stroma-mediated protection is mediated through mTORC1 activation triggered by cell connections to the fibroblasts.

There are multiple cascades, converging on mTORC1 [87], which functions as a sensor for diverse intracellular events. In the context of melanoma, mTORC1 activation may be induced by at least two upstream regulators: pERK, or an alternative PI3K-AKT signaling cascade. ERK phosphorylation has been linked to mTORC1 activation [88] and may therefore be the driver of this signaling in the cells influenced by the stroma. pERK, being a member of the MAPK pathway is normally inhibited by vemurafenib; however, as mentioned previously, it may be reactivated in the vemurafenib-resistant cells. At the same time, it is possible that mTORC1 is activated by a different proliferation-related pathway involving PI3K and AKT. Previous studies implicate both mechanisms [88, 89], therefore it is important to further investigate their contributions in our model system.

The notion of mTORC1 involvement was further strengthened in the experiments where inhibition of mTORC1 by everolimus in presence of vemurafenib, reduced stroma-mediated protection. There are two possible explanations for this effect of the everolimus treatment. First, everolimus may eliminate melanoma cell subpopulation that does not respond to vemurafenib due to stromal influence. Secondly, everolimus may sensitize the cells to BRAF inhibition. Interestingly, in mono-cultures the cytotoxic influence of vemurafenib and combination of vemurafenib and everolimus, was the same, indicating that everolimus does not improve the vemurafenib effect in the sensitive population.

Fibroblasts induce a phenotypic shift in melanoma in the contact-based cultures

In this study we found that the presence of fibroblasts stimulates a phenotype shift towards a more aggressive transcriptional state. Fibroblasts stimulated expression of genes characteristic for invasive cells [46], namely AXL, DKK3 and TBS1. Expression of melanocytic lineage-specific genes, MITF and its targets, however, was reduced in co-cultures, consistent with the invasive, vemurafenib resistant phenotype. We did not detect strong differences in expression of those genes in the melanoma cells collected from the trans-well plates, once more proving that cell proximity/adhesion is required for the stroma to influence the cancer cells. This suggests that under the influence of fibroblasts, melanoma cells become more invasive and less differentiated. Furthermore, reduced MITF and elevated AXL expression, which indicates dedifferentiated and invasive phenotype, has recently been linked to vemurafenib insensitive state [57].

These data show that the stromal cells potentiate vemurafenib resistant molecular phenotype in melanoma, likely via direct cell-cell connections. This implies that large area of contact with the stroma predicts low sensitivity to BRAF inhibition in melanoma and may therefore be predicative of the treatment outcome.

The phenotypic shift is accompanied by the alterations in metabolism

Rapidly proliferating melanoma cells tend to utilize aerobic glycolysis for ATP production. This is in part controlled by the down-regulation of MITF expression by the activated MAPK pathway. Low levels of MITF lead to reduced expression of PGC1α and, as a result, decrease of the mitochondrial activity and OxPhos [67]. Considering that low MITF levels are

characteristic of the resistant phenotype and that, as we have shown, the stromal cells encourage this phenotype, it is tempting to suggest that co-culture with the fibroblasts would stimulate a metabolic switch from OxPhos to aerobic glycolysis. Additionally, it is known that one of the mediators of glycolysis is the PI3K-mTORC1 pathway [90-93]. It is possible that mTORC1 activation induced by the stromal cells may also impact metabolism of the cancer cells and therefore contribute to the overall malignant phenotype. However, it appears that mTORC1 activation leads to either up- or down-regulation of aerobic glycolysis depending on the cell type and immediate conditions. Little is known about metabolism regulation by mTORC1 in melanoma.

Unfortunately, testing this hypothesis is technically difficult as measuring lactate levels in co-cultures would not make it possible to distinguish lactate produced by the cancer cells from lactate released by the stroma. However, we indirectly show the stroma-induced metabolic shift by analyzing the gene expression of the melanoma cells separated from fibroblasts by FACS. Melanoma cells from the contact-based co-cultures indeed had depleted PGC1α expression, while also showing increased LDHA, which is involved in glycolysis. Once again, we detected much weaker differences in the trans-well system where direct cell-cell contacts were not permitted. This suggests that the melanoma cells which come in close contact with the fibroblasts undergo transcriptional changes that might result in the shift of metabolic preference towards aerobic glycolysis.

Furthermore, we evaluated effect of the vemurafenib and everolimus on OxPhos and lactate production using the Seahorse™ technology. We discovered a decrease of the oxygen consumption levels shortly after the treatment with either of the drugs, indicating suppressed metabolism. This is consistent with the fact that most drugs that reduce proliferative activity of the cells tend to also decrease their general metabolic activity which manifests itself in reduction of both lactate production and oxygen consumption. The 24-hour treatment period that we have applied in this study may be insufficient for the long-term compensation mechanisms to come into play. Regulation of aerobic glycolysis can be rather abrupt as it often involves attenuation of the enzymatic activity. However, up-regulation of OxPhos calls for increased mitochondrial activity as well as simply more mitochondria, which may take several days. Given a longer treatment period, we may be

able to detect metabolic compensation by up-regulation of OxPhos after treatment with vemurafenib as demonstrated in several previous studies [67, 70].

Taking into account the possibility that stroma induces a metabolic shift, we argued that it may make the melanoma cells more vulnerable to dugs targeting preferred metabolic pathways. We hypothesized that melanoma cells exposed to the fibroblasts grow dependent on the aerobic glycolysis pathway which may make them more sensitive to the drugs that impact glycolysis and/or promote OxPhos. We tested this by using the OxPhos stimulant, DCA. We found a stronger reduction of cancer cell viability and cell cycle arrest in the G2 phase in Melmet5 co-cultures compared to mono-cultures in response to DCA. The other cell line, HM8, however, showed no fibroblast-induced difference in either viability or the cell cycle progression, which correlates with a less prominent shift in the metabolism gene expression. It should be mentioned, however, that applied DCA doses induced cell toxicity in both melanoma cells and fibroblasts, highlighting the need for more specific and efficient metabolic modulators.

Future perspectives

Our data strongly support the idea that fibroblasts in the tumor tissue play an extremely important role, transforming the cancer cells through changes in their signaling, gene expression and metabolism. We also show that the tumor cells need to be physically close to the stromal cells for all of these changes to take place. In the future, it would be interesting to confirm the involvement of integrins in the fibroblast-induced protection in our model system. This would involve labeling these proteins to visualize connections between the cancer cells and the fibroblasts. If present, such connections can then be inhibited to verify their role in the SMDR. Additionally, our data did not fully eliminate the possibility of gap junctions being important for the fibroblast-induced protection. It would therefore be important to draw the final conclusion by using a more specific and less toxic gap-junction inhibitor, if possible.

In addition, results of the current study indicate that efficacy of vemurafenib may be improved by combining it with inhibitors of stroma-induced alterations to tackle resistance. With a growing arsenal of inhibitors and small therapeutic agents available for research, there is an enormous potential for development of more appropriate and effective

treatment strategies. It would therefore be of particular interest to verify the *in vitro* data described here, *in vivo* and to find out whether our findings could have a potential for medical use. In particular, a combination of mTORC1 inhibitor everolimus, and vemurafenib, may lead to a better response and experiments where these two agents are applied together are currently being initiated on the mouse models.

Finally, one of the least well understood questions raised in this study is the role of mTORC1 in control of energy metabolism in the melanoma cells. Further experiments are necessary to draw conclusions on this subject. Specifically, the direct impact on metabolism by mTORC1 activation and inhibition in the melanoma cells has to be evaluated and it would be most convenient to use the Seahorse™ metabolic assays for that purpose.

Conclusions

- Fibroblasts induce partial protection of melanoma cells against treatment with vemurafenib.
- The fibroblasts' influence relies mainly on cell-cell contacts and/or proximity and is mediated through maintained activity of mTORC1 signaling.
- Fibroblasts stimulate melanoma cells to undergo transcriptional reprogramming and acquire vemurafenib resistant phenotype accompanied by the altered expression of metabolism-related genes.
- Altered energy metabolism in the melanoma cells may be exploited as a therapeutic target.
- Vemurafenib and the mTORC1 inhibitor everolimus modulate melanoma cell metabolism and trigger an initial decrease in the metabolic activity.

Further studies are required for better understanding of the precise mechanisms involved in the tumor-stroma interaction which reduces vemurafenib efficacy.

References

1. Lang, D., J.B. Mascarenhas, and C.R. Shea, *Melanocytes, melanocyte stem cells, and melanoma stem cells.* Clin Dermatol, 2013. **31**(2): p. 166-78.

2. Zhang, X.L., et al., *The tumor-stroma ratio is an independent predictor for survival in nasopharyngeal cancer.* Oncol Res Treat, 2014. **37**(9): p. 480-4.

3. Oskarsson, T., E. Batlle, and J. Massague, *Metastatic stem cells: sources, niches, and vital pathways.* Cell Stem Cell, 2014. **14**(3): p. 306-21.

4. Shiozawa, Y., K.J. Pienta, and R.S. Taichman, *Hematopoietic stem cell niche is a potential therapeutic target for bone metastatic tumors.* Clin Cancer Res, 2011. **17**(17): p. 5553-8.

5. Oskarsson, T., et al., *Breast cancer cells produce tenascin C as a metastatic niche component to colonize the lungs.* Nat Med, 2011. **17**(7): p. 867-74.

6. Malanchi, I., *Tumour cells coerce host tissue to cancer spread.* Bonekey Rep, 2013. **2**: p. 371.

7. Rebhun, R.B., et al., *Constitutive expression of the alpha4 integrin correlates with tumorigenicity and lymph node metastasis of the B16 murine melanoma.* Neoplasia, 2010. **12**(2): p. 173-82.

8. Peinado, H., S. Lavotshkin, and D. Lyden, *The secreted factors responsible for pre-metastatic niche formation: old sayings and new thoughts.* Semin Cancer Biol, 2011. **21**(2): p. 139-46.

9. Barcellos-Hoff, M.H., D. Lyden, and T.C. Wang, *The evolution of the cancer niche during multistage carcinogenesis.* Nat Rev Cancer, 2013. **13**(7): p. 511-8.

10. Holohan, C., et al., *Cancer drug resistance: an evolving paradigm.* Nat Rev Cancer, 2013. **13**(10): p. 714-26.

11. Pennacchietti, S., et al., *Microenvironment-derived HGF overcomes genetically determined sensitivity to anti-MET drugs.* Cancer Res, 2014. **74**(22): p. 6598-609.

12. Bewry, N.N., et al., *Stat3 contributes to resistance toward BCR-ABL inhibitors in a bone marrow microenvironment model of drug resistance.* Mol Cancer Ther, 2008. **7**(10): p. 3169-75.

13. Xia, B., et al., *c-Myc plays part in drug resistance mediated by bone marrow stromal cells in acute myeloid leukemia.* Leuk Res, 2015. **39**(1): p. 92-9.

14. Kim, Y.R. and K.S. Eom, *Simultaneous Inhibition of CXCR4 and VLA-4 Exhibits Combinatorial Effect in Overcoming Stroma-Mediated Chemotherapy Resistance in Mantle Cell Lymphoma Cells.* Immune Netw, 2014. **14**(6): p. 296-306.

15. Bhowmick, N.A., E.G. Neilson, and H.L. Moses, *Stromal fibroblasts in cancer initiation and progression.* Nature, 2004. **432**(7015): p. 332-7.

16. *Disruption of epithelial cell-matrix interactions induces apoptosis.* J Cell Biol, 1994. **124**(4): p. 619-26.

17. Krysko, D.V., et al., *Gap junctions and the propagation of cell survival and cell death signals.* Apoptosis, 2005. **10**(3): p. 459-69.

18. Ableser, M.J., et al., *Connexin43 reduces melanoma growth within a keratinocyte microenvironment and during tumorigenesis in vivo.* J Biol Chem, 2014. **289**(3): p. 1592-603.

19. Stoletov, K., et al., *Role of connexins in metastatic breast cancer and melanoma brain colonization.* J Cell Sci, 2013. **126**(Pt 4): p. 904-13.

20. Lin, Q., et al., *Reactive astrocytes protect melanoma cells from chemotherapy by sequestering intracellular calcium through gap junction communication channels.* Neoplasia, 2010. **12**(9): p. 748-54.

21. Kim, S.J., et al., *Astrocytes upregulate survival genes in tumor cells and induce protection from chemotherapy.* Neoplasia, 2011. **13**(3): p. 286-98.

22. Ke, H., et al., *CYLD inhibits melanoma growth and progression through suppression of the JNK/AP-1 and beta1-integrin signaling pathways.* J Invest Dermatol, 2013. **133**(1): p. 221-9.

23. Weidert, E., et al., *Actinomyosin contraction, phosphorylation of VE-cadherin, and actin remodeling enable melanoma-induced endothelial cell-cell junction disassembly.* PLoS One, 2014. **9**(9): p. e108092.

24. Rawles, M.E., *The Development of Melanophores from Embryonic Mouse Tissues Grown in the Coelom of Chick Embryos.* Proc Natl Acad Sci U S A, 1940. **26**(12): p. 673-80.

25. Jimbow, K., et al., *Some aspects of melanin biology: 1950-1975.* J Invest Dermatol, 1976. **67**(1): p. 72-89.

26. Geisler, J., et al., *Malignant melanoma--diagnosis, treatment and follow-up in Norway.* Tidsskr Nor Laegeforen, 2013. **133**(20): p. 2154-9.

27. Mc, G.V., *Melanoblastoma.* Med J Aust, 1952. **1**(5): p. 139-42.

28. Breslow, A., *Tumor thickness, level of invasion and node dissection in stage I cutaneous melanoma.* Ann Surg, 1975. **182**(5): p. 572-5.

29. Barth, A., L.A. Wanek, and D.L. Morton, *Prognostic factors in 1,521 melanoma patients with distant metastases.* J Am Coll Surg, 1995. **181**(3): p. 193-201.

30. Miller, A.J. and M.C. Mihm, Jr., *Melanoma.* N Engl J Med, 2006. **355**(1): p. 51-65.

31. van 't Veer, L.J., et al., *N-ras mutations in human cutaneous melanoma from sun-exposed body sites.* Mol Cell Biol, 1989. **9**(7): p. 3114-6.

32. Albino, A.P., et al., *Analysis of ras oncogenes in malignant melanoma and precursor lesions: correlation of point mutations with differentiation phenotype.* Oncogene, 1989. **4**(11): p. 1363-74.

33. Davies, H., et al., *Mutations of the BRAF gene in human cancer.* Nature, 2002. **417**(6892): p. 949-54.

34. Emuss, V., et al., *Mutations of C-RAF are rare in human cancer because C-RAF has a low basal kinase activity compared with B-RAF.* Cancer Res, 2005. **65**(21): p. 9719-26.

35. Pollock, P.M., et al., *High frequency of BRAF mutations in nevi.* Nat Genet, 2003. **33**(1): p. 19-20.

36. Damsky, W., et al., *mTORC1 activation blocks BrafV600E-induced growth arrest but is insufficient for melanoma formation.* Cancer Cell, 2015. **27**(1): p. 41-56.

37. Chapman, P.B., et al., *Improved survival with vemurafenib in melanoma with BRAF V600E mutation.* N Engl J Med, 2011. **364**(26): p. 2507-16.

38. Corcoran, R.B., et al., *EGFR-mediated re-activation of MAPK signaling contributes to insensitivity of BRAF mutant colorectal cancers to RAF inhibition with vemurafenib.* Cancer Discov, 2012. **2**(3): p. 227-35.

39. Prahallad, A., et al., *Unresponsiveness of colon cancer to BRAF(V600E) inhibition through feedback activation of EGFR.* Nature, 2012. **483**(7387): p. 100-3.

40. Montero-Conde, C., et al., *Relief of feedback inhibition of HER3 transcription by RAF and MEK inhibitors attenuates their antitumor effects in BRAF-mutant thyroid carcinomas.* Cancer Discov, 2013. **3**(5): p. 520-33.

41. Nazarian, R., et al., *Melanomas acquire resistance to B-RAF(V600E) inhibition by RTK or N-RAS upregulation.* Nature, 2010. **468**(7326): p. 973-7.

42. Holderfield, M., et al., *Targeting RAF kinases for cancer therapy: BRAF-mutated melanoma and beyond.* Nat Rev Cancer, 2014. **14**(7): p. 455-67.

43. Shi, H., et al., *Melanoma whole-exome sequencing identifies (V600E)B-RAF amplification-mediated acquired B-RAF inhibitor resistance.* Nat Commun, 2012. **3**: p. 724.

44. Johannessen, C.M., et al., *COT drives resistance to RAF inhibition through MAP kinase pathway reactivation.* Nature, 2010. **468**(7326): p. 968-72.

45. Straussman, R., et al., *Tumour micro-environment elicits innate resistance to RAF inhibitors through HGF secretion.* Nature, 2012. **487**(7408): p. 500-4.

46. Hoek, K.S., et al., *Metastatic potential of melanomas defined by specific gene expression profiles with no BRAF signature.* Pigment Cell Res, 2006. **19**(4): p. 290-302.

47. Long, G.V., et al., *Effects of BRAF inhibitors on human melanoma tissue before treatment, early during treatment, and on progression.* Pigment Cell Melanoma Res, 2013. **26**(4): p. 499-508.

48. Beck, D., et al., *Vemurafenib potently induces endoplasmic reticulum stress-mediated apoptosis in BRAFV600E melanoma cells.* Sci Signal, 2013. **6**(260): p. ra7.

49. Roos, W.P., et al., *B-Raf inhibitor vemurafenib in combination with temozolomide and fotemustine in the killing response of malignant melanoma cells.* Oncotarget, 2014. **5**(24): p. 12607-20.

50. Haferkamp, S., et al., *Vemurafenib induces senescence features in melanoma cells.* J Invest Dermatol, 2013. **133**(6): p. 1601-9.

51. Sun, C., et al., *Reversible and adaptive resistance to BRAF(V600E) inhibition in melanoma.* Nature, 2014. **508**(7494): p. 118-22.

52. Ohanna, M., et al., *SIRT1 promotes proliferation and inhibits the senescence-like phenotype in human melanoma cells.* Oncotarget, 2014. **5**(8): p. 2085-95.

53. Karbowniczek, M., et al., *mTOR is activated in the majority of malignant melanomas.* J Invest Dermatol, 2008. **128**(4): p. 980-7.

54. Romeo, Y., et al., *RSK regulates activated BRAF signalling to mTORC1 and promotes melanoma growth.* Oncogene, 2013. **32**(24): p. 2917-26.

55. Corcoran, R.B., et al., *TORC1 suppression predicts responsiveness to RAF and MEK inhibition in BRAF-mutant melanoma.* Sci Transl Med, 2013. **5**(196): p. 196ra98.

56. Hoek, K.S., et al., *In vivo switching of human melanoma cells between proliferative and invasive states.* Cancer Res, 2008. **68**(3): p. 650-6.

57. Muller, J., et al., *Low MITF/AXL ratio predicts early resistance to multiple targeted drugs in melanoma.* Nat Commun, 2014. **5**: p. 5712.

58. Konieczkowski, D.J., et al., *A melanoma cell state distinction influences sensitivity to MAPK pathway inhibitors.* Cancer Discov, 2014. **4**(7): p. 816-27.

59. Hanahan, D. and R.A. Weinberg, *Hallmarks of cancer: the next generation.* Cell, 2011. **144**(5): p. 646-74.

60. Warburg, O., *On the origin of cancer cells.* Science, 1956. **123**(3191): p. 309-14.

61. Vander Heiden, M.G., L.C. Cantley, and C.B. Thompson, *Understanding the Warburg effect: the metabolic requirements of cell proliferation.* Science, 2009. **324**(5930): p. 1029-33.

62. Ho, J., et al., *Importance of glycolysis and oxidative phosphorylation in advanced melanoma.* Mol Cancer, 2012. **11**: p. 76.

63. Vazquez, A., et al., *Catabolic efficiency of aerobic glycolysis: The Warburg effect revisited.* BMC Syst Biol, 2010. **4**: p. 58.

64. Vaughan, R.A., et al., *beta-alanine suppresses malignant breast epithelial cell aggressiveness through alterations in metabolism and cellular acidity in vitro.* Mol Cancer, 2014. **13**: p. 14.

65. Liu, P.F., et al., *Heterogeneity research in muscle-invasive bladder cancer based on differential protein expression analysis.* Med Oncol, 2014. **31**(9): p. 21.

66. Archetti, M., *Heterogeneity and proliferation of invasive cancer subclones in game theory models of the Warburg effect.* Cell Prolif, 2015. **48**(2): p. 259-69.

67. Haq, R., et al., *Oncogenic BRAF regulates oxidative metabolism via PGC1alpha and MITF.* Cancer Cell, 2013. **23**(3): p. 302-15.

68. Basanta, D., et al., *Evolutionary game theory elucidates the role of glycolysis in glioma progression and invasion.* Cell Prolif, 2008. **41**(6): p. 980-7.

69. Sondergaard, J.N., et al., *Differential sensitivity of melanoma cell lines with BRAFV600E mutation to the specific Raf inhibitor PLX4032.* J Transl Med, 2010. **8**: p. 39.

70. Parmenter, T.J., et al., *Response of BRAF-mutant melanoma to BRAF inhibition is mediated by a network of transcriptional regulators of glycolysis.* Cancer Discov, 2014. **4**(4): p. 423-33.

71. Vazquez, F., et al., *PGC1alpha expression defines a subset of human melanoma tumors with increased mitochondrial capacity and resistance to oxidative stress.* Cancer Cell, 2013. **23**(3): p. 287-301.

72. Michels, J., et al., *PARP and other prospective targets for poisoning cancer cell metabolism.* Biochem Pharmacol, 2014. **92**(1): p. 164-71.

73. Corazao-Rozas, P., et al., *Mitochondrial oxidative stress is the Achille's heel of melanoma cells resistant to Braf-mutant inhibitor.* Oncotarget, 2013. **4**(11): p. 1986-98.

74. Neri, D. and C.T. Supuran, *Interfering with pH regulation in tumours as a therapeutic strategy.* Nat Rev Drug Discov, 2011. **10**(10): p. 767-77.

75. Enerson, B.E. and L.R. Drewes, *Molecular features, regulation, and function of monocarboxylate transporters: implications for drug delivery.* J Pharm Sci, 2003. **92**(8): p. 1531-44.

76. Sun, R.C., et al., *Reversal of the glycolytic phenotype by dichloroacetate inhibits metastatic breast cancer cell growth in vitro and in vivo.* Breast Cancer Res Treat, 2010. **120**(1): p. 253-60.

77. Michelakis, E.D., L. Webster, and J.R. Mackey, *Dichloroacetate (DCA) as a potential metabolic-targeting therapy for cancer.* Br J Cancer, 2008. **99**(7): p. 989-94.

78. Bonnet, S., et al., *A mitochondria-K+ channel axis is suppressed in cancer and its normalization promotes apoptosis and inhibits cancer growth.* Cancer Cell, 2007. **11**(1): p. 37-51.

79. Wong, J.Y.Y., et al., *Dichloroacetate Induces Apoptosis in Endometrial Cancer Cells.* Gynecol Oncol, 2008. **109**(3): p. 394-402.

80. Cairns, R.A., et al., *Metabolic targeting of hypoxia and HIF1 in solid tumors can enhance cytotoxic chemotherapy.* Proc Natl Acad Sci U S A, 2007. **104**(22): p. 9445-50.

81. Dunbar, E.M., et al., *Phase 1 trial of dichloroacetate (DCA) in adults with recurrent malignant brain tumors.* Invest New Drugs, 2014. **32**(3): p. 452-64.

82. Day, C.P., et al., *Lentivirus-mediated bifunctional cell labeling for in vivo melanoma study.* Pigment Cell Melanoma Res, 2009. **22**(3): p. 283-95.

83. Parr, C. and W.G. Jiang, *Expression of hepatocyte growth factor/scatter factor, its activator, inhibitors and the c-Met receptor in human cancer cells.* Int J Oncol, 2001. **19**(4): p. 857-63.

84. Tiago, M., et al., *Fibroblasts Protect Melanoma Cells from the Cytotoxic Effects of Doxorubicin.* Tissue Eng Part A, 2014.

85. Tawil, N.J., et al., *Integrin alpha3beta1 can promote adhesion and spreading of metastatic breast carcinoma cells on the lymph node stroma.* Int J Cancer, 1996. **66**(5): p. 703-10.

86. Hirata, E., et al., *Intravital Imaging Reveals How BRAF Inhibition Generates Drug-Tolerant Microenvironments with High Integrin beta1/FAK Signaling.* Cancer Cell, 2015. **27**(4): p. 574-88.

87. Xu, K., P. Liu, and W. Wei, *mTOR signaling in tumorigenesis.* Biochim Biophys Acta, 2014. **1846**(2): p. 638-54.

88. Gopal, Y.N., et al., *Basal and treatment-induced activation of AKT mediates resistance to cell death by AZD6244 (ARRY-142886) in Braf-mutant human cutaneous melanoma cells.* Cancer Res, 2010. **70**(21): p. 8736-47.

89. Shi, H., et al., *Combinatorial treatments that overcome PDGFRbeta-driven resistance of melanoma cells to V600EB-RAF inhibition.* Cancer Res, 2011. **71**(15): p. 5067-74.

90. Lu, C.L., et al., *Tumor Cells Switch to Mitochondrial Oxidative Phosphorylation under Radiation via mTOR-Mediated Hexokinase II Inhibition - A Warburg-Reversing Effect.* PLoS One, 2015. **10**(3): p. e0121046.

91. Ramanathan, A. and S.L. Schreiber, *Direct control of mitochondrial function by mTOR.* Proc Natl Acad Sci U S A, 2009. **106**(52): p. 22229-32.

92. Liu, C., et al., *mTOR and metabolic regulation of conventional and regulatory T cells.* J Leukoc Biol, 2015.

93. Courtnay, R., et al., *Cancer metabolism and the Warburg effect: the role of HIF-1 and PI3K.* Mol Biol Rep, 2015. **42**(4): p. 841-51.

Supplementary Table

Cell culturing	Producer	Catalogue number
RPMI-1640 medium	Sigma® Life Sciences	R0883
EMEM medium	ATCC	30-2003
L-alanyl-L-glutemine (Glutamax)	Sigma® Life Sciences	G8541
Penicilin - streptavidin	Sigma® Life Sciences	P4458
Fetal Bovine Serum (FBS)	Sigma® Life Sciences	F7524
Tissue culture EasY-flasks	Nunc	157400
Tissue culture plates	Falcon®	353072
24-well trans-well plates	Corning®	3470
6-well trans-well plates	Corning®	3450
Trypan-blue Stain (0.4%)	Gibco life Technologies	15250-061
Countess™automated cell counter	Invitrogen	
Countess™ cell counting chamber slides	Invitrogen	C10283
EDTA (0.02%)	Sigma® Life Sciences	E8008
Trypsin - EDTA	Sigma® Life Sciences	T3924
Dimethyl-sulphoxide-hybri-max (DMSO)	Sigma® Life Sciences	D2650
1420 multilabel counter Victor²	Wallac	
PBS	Sigma® Life Sciences	D8537
White wall 96-well plates for bioluminescence measurement	Corning Costar	3610
Therapeutic drugs	**Producer**	**Catalogue number**
Vemurafenib	Selleckchem	S1267
Everolimus	Novartis	
Virus production	**Producer**	**Catalogue number**
Optimem	Gibco	31985
Lipofectamine 2000	Life technologies	11668027
293HEK cells	ATCC	CRL-1573
Polybrene	Sigma® Life Sciences	AL-118
Antibodies For Western blotting	**Producer**	**Catalogue number**
α-tubulin, mouse monoclonal	EMD Millipore, USA	CP06
phospho-cMet, rabbit monoclonal	Cell Signaling	3077
phospho-S6, rabbit monoclonal	Cell Signaling	4858S
phospho-ERK, p44/42 MAPK	Cell Signaling	4370S
Histone 3	Cell Signaling	4499S
PGC1-α	Cell signaling	2178
c-Met	Cell Signaling	8198
Western blotting Materials and Equipment	**Producer**	**Catalogue number**
Pierce™BCA Protein Assay Kit	Thermo Scientific, USA	23227

4-12% Nu-PAGE Bis-Tris 1.0mm x 12-well gel	Novex for life sciences, Invitrogen	NP0322 BOX
See Blue®Plus 2 prestained standard	Invitrogen	LC5925
Immobilon PVDF transfer membrane	Millipore	IPVH00010
Mini-cell and XCellII™ Blot module	Invitrogen, Novex	92008
MES SDS electrophoresis Running buffer	Invitrogen, USA	NP0002-02
Bovine Serum Albumine (BSA)	Sigma Life Science	A3294
Super Signal® West Dura extended duration substrate	Thermo Scientific, USA	A 34076F
Membrane visualization Chamber G:Box	Syngene	
NaCl	Sigma® Life Sciences	S9888
Tris pH 7.5	Merck	77-86-1
Protease inhibitor	Roche	04693159001
Phosphotase inhibitor	Roche	4906845001
Seahorse® metabolism assay materials	**Producer**	**Catalogue number**
XFe96 analyzer	Seahorse®	
XFe24 analyzer	Seahorse®	
96-well culture plates	Seahorse®	101104-004
24-well culture plates	Seahorse®	101037-004
calibration solution	Seahorse®	102353-100
96-well cartridges	Seahorse®	102416-100
24-well cartridges	Seahorse®	102340-100
DMEM medium	Seahorse®	102353-100
mito-stress kit	Seahorse®	103015-100
glycolysis stress-kit	Seahorse®	103020-100
Additional chemicals and equipment for metabolic assays	**Producer**	**Catalogue number**
D – (+) - glucose	Sigma® Life Sciences	G8270
L - glutamine	Sigma® Life Sciences	G3126
sodium pyruvate	Sigma® Life Sciences	P2256
DCA	Sigma® Life Sciences	347795
pico-green	Life technologies	P11496
nano-drop 2000	Thermo Scientific	
Flow cytometry	**Producer**	**Catalogue number**
Paraformyldehyde (PFA)	Sigma® Life Sciences	P6148
Methanol	Merck Milipore	106009
12 x 75 mm Tube with 35µm Cell Strainer Cap	BD Falcon	352235
Hoechst 33258 pentahydrate	Invitrogen	H3569
Pacific Orange	life technologies	P30014
Cell tracker™ CM-DiL	Invitrogen	C7000
BD LSRII Flow cytometer	Becton Dickinson (BD), USA	

Real time PCR	Producer	Catalogue number
Trizol	life technologies	10296010
qScript™ DNA synthesis kit	Quanta Biosciences	95047-100
Thermo-cycler Gene-amp®	PE Applied Biosystems	9700
Nucleotide-Perfecta® super mix	Quanta Biosciences	84008
Real time PCR CFX-connect™	Bio-RAD	
Primers	**Sequence**	**Universal probe**
MITF	foreward: cattgttatgctggaaatgctaga reverse: tgctaaagtggtagaaaggtactgc	#62
MLANA	left: gagaaaaactgtgaacctgtggt right: gactgttctgcagagagtttctcat	#39
LDHA	left: gtccttggggaacatggag right: ttcagagagacaccagcaaca	#47
PGC1α	left: tgagagggccaagcaaag right: ataaatcacacggcgctctt	#13
YARS	forward: ggattaacaggcagcaaaatg reverse: ccttccgatcaaggagatca	#35

Table S.1 List of materials and reagents used in the study